

**Evaluating the Biomechanics of Tooth Movement induced through Orthodontic Braces using an Integrated Clinical and Mechanical Approach**

by

Arya Subramanian

A thesis submitted in partial fulfillment of the requirements for the degree of

Master of Science

Department of Mechanical Engineering  
University of Alberta

© Arya Subramanian, 2024

# Abstract

Orthodontics is the dental specialization focused on correcting tooth and jaw misalignments. The treatment is known to have positive effects on the quality of life of the public by improving personal aesthetics and oral health. A common fixed treatment option is orthodontic braces, composed of orthodontic brackets bonded on the dental arch and an archwire inserted through the bracket slots. The interaction between the bracket slot and archwire complex causes orthodontic forces/moments to be applied onto the tooth, resulting in dental movement facilitated by alveolar bone remodelling. The relationship between the biomechanical forces and tooth movement occurring over treatment is poorly understood, limiting the predictability of orthodontic treatment and causing possible side effects such as unwanted tooth movements, longer treatment times, and tissue damage from high-magnitude forces. The limited understanding is largely attributed to insufficient research linking longitudinal clinical observations of tooth movement and biomechanical forces produced by braces.

The objectives of this work were to first utilize clinical cases for obtaining bracket position information and measuring clinical tooth movement over orthodontic treatment by collecting digital intraoral scans and applying scan analysis techniques and in-house scripts. Secondly, the collected bracket positions were physically replicated onto an in vitro Orthodontic Simulator (OSIM) using custom-dimensioned jig sets with bonded brackets to measure the generated forces upon archwire insertion at each treatment interval. Lastly, existing trends were analyzed to better understand the relationship between the measured biomechanical forces produced by braces and the resulting clinical tooth movement magnitude, direction, and rate.

The results of this thesis work showed that the developed methodology utilizing clinical scan analysis techniques and in vitro biomechanical experiments could be applied for a preliminary understanding of the longitudinal biomechanical force and tooth movement relationship. For the investigated clinical cases with mild anterior crowding, cases with larger misalignments generally experienced larger forces, tooth movements, and tooth movement rates between the initial intervals of treatment. For a particular archwire size, the initially measured forces were generally greater than the end forces indicating further tooth alignment as treatment progressed. It was also observed that force magnitudes generally increased for a particular treatment interval when a larger archwire was used. The observed trends between initial force and calculated tooth movement were both consistent and inconsistent. For directionally consistent trends, tooth movements and initial forces were measured in the same direction, while inconsistent cases involved initial force and tooth movement measurements in opposing directions. Other inconsistencies observed included force magnitudes lower than the observed tooth movement and vice versa. Inconsistent trends may have resulted from patient-specific characteristics such as tooth root morphology and periodontal tissue differences, and existing interactions between the dental arches or adjacent teeth, affecting the orthodontic force distribution and resulting tooth movements. The frequency of scan collection also limited the evaluation of the intermediate tooth movement sequence over treatment.

The streamlined methodology presented in this thesis focused on the longitudinal tracking of biomechanical forces and clinical outcomes over orthodontic treatment. Potential applications of this work include investigating more complex tooth misalignments, developing patient-specific models for enhancing treatment predictability, and designing future orthodontic appliances for optimal load delivery.

# Preface

This thesis is original work by Arya Subramanian. The pilot study completed in this thesis received research ethics approval from the University of Alberta Research Ethics Board, Title “Biomechanics of Tooth Movement”, ID: Pro00112968. The contents of this thesis have not been previously published.

# Acknowledgements

I would first like to express my greatest appreciation and gratitude to my Supervisor Dr. Dan Romanyk for his immeasurable support from the moment I started in the lab group as a summer student back in 2020. I am so incredibly grateful for the amount of time you invested in this research work. Your efforts and dedication to my personal, academic, and professional growth is why I am the person I've always wanted to become.

I would like to thank my supervisor Dr. Paul Major for his continuous support throughout my program, providing me with clinical expertise, and always providing guidance to the many questions I would ask in meetings. Even with our interactions being online, it was an absolute privilege to collaborate with you and learn so much from you.

Thank you to my incredible current and previous colleagues from the Romanyk Lab group for always providing insightful feedback during group meetings. A special thank you to those who were involved with this research and for dedicating countless hours in assisting me in the lab, I am so grateful.

A special thank you to Dr. Manuel Lagravere, Susan Helwig, and Keith O'Reilly from the Kaye Edmonton Clinic. Thank you for being so welcoming in the clinic and for your support with scan collection and equipment operation.

I would like to thank my mom, dad, and sister for their constant motivation over countless phone calls, believing in my ability to accomplish anything, and emphasizing the importance of persistence and patience. I would also like to thank my friends for their constant encouragement and the laughs shared during this journey.

# Table of Contents

<b>1</b>	<b>Introduction</b>	<b>1</b>
1.1	Thesis Motivation . . . . .	1
1.2	Thesis Objectives . . . . .	4
1.3	Thesis Outline . . . . .	6
1.4	Thesis Contributions . . . . .	7
<b>2</b>	<b>Background</b>	<b>8</b>
2.1	Teeth Anatomy, Function, & Nomenclature . . . . .	8
2.2	Biomechanics of Tooth Movement . . . . .	11
2.2.1	Types of Tooth Movement . . . . .	11
2.2.2	Phases & Theories of Tooth Movement . . . . .	12
2.2.3	Effect of Force Levels on Tooth Movement . . . . .	14
2.3	Understanding the Biomechanics of Braces . . . . .	16
2.3.1	Finite Element Analysis in Literature . . . . .	16
2.3.2	Existing Measurement Devices in Literature . . . . .	19
2.3.3	Introduction to the Orthodontic Simulator (OSIM) . . . . .	22
2.4	Patient Dental Scan Analysis over Orthodontic Treatment . . . . .	24
2.4.1	Coordinate System Establishment for Dental Scan Alignment . . . . .	24
2.4.2	Dental Scan Superimposition . . . . .	25
2.4.3	Measuring Clinical Tooth Movement from Optical Dental Scans . . . . .	29
<b>3</b>	<b>Tracking orthodontic tooth movement and associated biomechanics using an integrated clinical and in vitro mechanical approach</b>	<b>31</b>
3.1	Introduction . . . . .	31
3.2	Methods . . . . .	34
3.2.1	Clinical Data Collection and Analysis . . . . .	34
3.2.2	Mechanical Experimental Data Collection . . . . .	39
3.3	Results . . . . .	41
3.4	Discussion . . . . .	51

3.4.1	Errors in Scan Superimposition and Bracket Position Replication . . .	52
3.4.2	Changes in Force over Treatment . . . . .	53
3.4.3	Force and Tooth Movement Trends when Tooth Movement Magnitudes were >0.5 mm . . . . .	54
3.4.4	Tooth Movement Rates over Treatment . . . . .	57
3.4.5	Limitations . . . . .	59
3.5	Conclusions . . . . .	59
<b>4</b>	<b>Conclusions, Limitations, &amp; Future Work</b>	<b>61</b>
4.1	Conclusions . . . . .	61
4.2	Limitations & Future Work . . . . .	64
	<b>Bibliography</b>	<b>68</b>
	<b>Appendix A: Patient Scan Analysis</b>	<b>85</b>
A.1	Initial Scan Alignment . . . . .	85
A.2	Scan Superimposition . . . . .	93
A.3	Bracket Position Selection . . . . .	99
A.4	Calculating Clinical Tooth Movements . . . . .	108
	<b>Appendix B: Jig Design &amp; Bracket Position Preparation for Experiments</b>	<b>112</b>
B.1	Default Jig Configuration Design in SolidWorks . . . . .	112
B.2	Patient-Specific Jig Set Creation . . . . .	118
B.3	Evaluating Replication Errors . . . . .	129
B.4	Rectifying Jig Position Errors . . . . .	143

# List of Tables

3.1	Patient scan superimposition errors represented by calculated Hausdorff distances (95th percentile reported) . . . . .	43
3.2	Average patient bracket position translation and rotation replication errors in the local OSIM cantilever directions for the patient mandibular arches and maxillary arches . . . . .	44
3.3	Dental arch coordinate system describing positive sign convention for biomechanical force and tooth movement measurements in the Y- and Z-direction .	47
3.4	Directionally consistent and inconsistent initial force and tooth movement cases for each patient over treatment when a tooth movement threshold of 0.5 mm is considered . . . . .	48
3.5	Initial force and tooth movement trend consistency for each patient arch over treatment in Y- and Z-direction and for each archwire size when 0.5 mm tooth movement threshold is considered . . . . .	49
A.1	Selected molar and canine cusp data over 5 selection times for Rater 1 [mm]	91
A.2	Selected molar and canine cusp data over 5 selection times for Rater 2 [mm]	91
A.3	ICC results for intra-rater reliability in molar/canine cusp selection (k=5, n=4)	92
A.4	ICC results for inter-rater reliability in molar/canine cusp selection (k=2, n=12) . . . . .	92
A.5	Advanced registration settings available in Slicer . . . . .	95
A.6	Outline of different model position cases for preliminary testing of advanced registration settings in Slicer . . . . .	96
A.7	Model to Model Distance range for identical scan superimposition cases using four main registration setting combinations, when distance threshold is 0.00001 mm and mean distance is checked . . . . .	97
A.8	Bracket slot midpoint data for random scan 1 [mm] . . . . .	105
A.9	Bracket slot midpoint data for random scan 2 [mm] . . . . .	106
A.10	Bracket slot midpoint data for random scan 3 [mm] . . . . .	107
A.11	ICC results for intra-rater reliability for random scan 1 (k=3, n=12) . . . . .	107

A.12 ICC results for intra-rater reliability for random scan 2 (k=3, n=12) . . . . .	108
A.13 ICC results for intra-rater reliability for random scan 3 (k=3, n=12) . . . . .	108
B.1 Measured OSIM cantilever angles and mounting hole positions using FaroArm measurement device . . . . .	119
B.2 Summary of setting combinations used for retrieving patient jig set dimensions	120
B.3 Translation and rotation replication errors for Patient 1 mandibular jig sets .	133
B.4 Translation and rotation replication errors for Patient 2 mandibular jig sets .	134
B.5 Translation and rotation replication errors for Patient 2 maxillary jig sets . .	135
B.6 Translation and rotation replication errors for Patient 3 mandibular jig sets .	136
B.7 Translation and rotation replication errors for Patient 3 maxillary jig sets . .	137
B.8 Translation and rotation replication errors for Patient 4 mandibular jig sets .	138
B.9 Translation and rotation replication errors for Patient 4 maxillary jig sets . .	139
B.10 Average measured force in Y-direction at 0.5 mm buccal displacement of ca- nine, central incisor, and second premolar teeth during use of 0.014" and 0.016" archwire . . . . .	144

# List of Figures

2.1	Overview of tooth and periodontium anatomy with tooth sections and tissues labelled . . . . .	9
2.2	Occlusal view of a patient mandibular dental arch with labelled dental directional convention . . . . .	11
2.3	Overview of the in vitro electromechanical Orthodontic Simulator (OSIM) for 3D force and moment measurements . . . . .	22
3.1	Intraoral scan collection protocol for recruited patients over orthodontic treatment with treatment intervals (T1-T4) and archwire changes indicated . . .	35
3.2	Summarized workflow for clinical maxillary scan superimposition; a). Time 1 and Time 2 maxillary arch models for sample patient case opened in Slicer software, b). Segmentation and superimposition of Time 2 rugae region onto the full Time 1 model, c). Superimposition of full Time 2 model on Time 1 model by applying transformation matrix from initial rugae superimposition	36
3.3	Summarized workflow for clinical mandibular scan superimposition; a). Time 1 and Time 2 mandibular arch models for sample patient case opened in Slicer software, b). Segmentation and superimposition of Time 2 molars onto segmented Time 1 molars, c). Superimposition of full Time 2 model on full Time 1 model by applying transformation matrix from initial molar superimposition	37
3.4	Retrieval of bracket slot endpoint and midpoint positions from clinical scans; a). Superimposed Time 1 and Time 2 mandibular scans with tooth number labels based on FDI system, b). Manual selection of four points on bracket, MATLAB coordinate transformations applied to manually selected points to obtain slot endpoint locations, and calculation of slot midpoint using slot endpoint coordinates, c). Plot of bracket positions for Time 1 and 2 scans in MATLAB to visualize and calculate tooth movement over two points of treatment . . . . .	38

3.5	Overview of the in vitro Orthodontic Simulator (OSIM); a). Overview of OSIM with dental arch, load cells, and micrometers labelled, b). Schematic of OSIM indicating the constructed local and global coordinate systems utilized for clinical and experimental data collection . . . . .	39
3.6	Summarized workflow for experimental data collection; a). Patient scan in Slicer with plotted slot endpoints/midpoints calculated in MATLAB, b). Mapping of patient bracket positions and cantilever holes in MATLAB for application of transformation matrices to determine jig dimensions, c). Solid-Works assembly of generated sample jig set based on calculated dimensions, d). Printed jig set mounted on OSIM with bonded brackets, e). Archwire inserted through brackets for experimental measurements of biomechanical forces at each bracket . . . . .	40
3.7	Summary of experimental runs for biomechanical force collection of each sample dental arch, where archwire samples of each size were inserted to measure the initial force for the respective time interval and reinserted to measure the end force for the subsequent time interval (jig set) prior to archwire size increase	42
3.8	Orthodontic force and tooth movement results for the anterior teeth of patient mandibular arches (Tooth 3-3 to 4-3) in Y- and Z-direction; a). Patient 1 mandibular arch, b). Patient 2 mandibular arch, c). Patient 3 mandibular arch, d). Patient 4 mandibular arch . . . . .	45
3.9	Orthodontic force and tooth movement results for the anterior teeth of patient maxillary arches (Tooth 2-3 to 1-3) in Y- and Z-direction; a). Patient 2 maxillary arch, b). Patient 3 maxillary arch, c). Patient 4 maxillary arch . . . . .	46
3.10	Orthodontic tooth movement rates (magnitude) over treatment for the anterior teeth of patient mandibular arches (Tooth 3-3 to 4-3) in Y- and Z-direction; a). Patient 1 mandibular arch b). Patient 2 mandibular arch, c). Patient 3 mandibular arch, d). Patient 4 mandibular arch . . . . .	50
3.11	Orthodontic tooth movement rates (magnitude) over treatment for the anterior teeth of patient maxillary arches (Tooth 2-3 to 1-3) in Y- and Z-direction; a). Patient 2 maxillary arch b). Patient 3 maxillary arch, c). Patient 4 maxillary arch . . . . .	51
A.1	Slicer global coordinate system with defined axes . . . . .	86
A.2	Alignment of sample mandibular arch within Slicer software; a). Selected molar and canine cusps on sample T1 scan, b). Established lines on sample T1 scan for translational and rotational alignment . . . . .	86
A.3	Translation of sample patient T1 scan to defined origin point . . . . .	87

A.4	Schematic of 2D rotation alignment steps performed in Slicer for T1 scan . . .	87
A.5	Rotation of patient T1 scan about Slicer R-Axis . . . . .	88
A.6	Rotation of patient T1 scan about Slicer S-Axis . . . . .	88
A.7	Rotation of patient T1 scan about Slicer A-Axis . . . . .	89
A.8	Comparison of original and oriented sample patient mandibular arch scan . .	89
A.9	3D segmentation and model preparation of mandibular molar surfaces in Slicer for superimposition . . . . .	93
A.10	3D segmentation of maxillary third rugae surface in Slicer in preparation for superimposition . . . . .	94
A.11	Example of completed superimposition of patient mandibular T2 scan on T1 scan . . . . .	96
A.12	Patient 1 superimposed scans over treatment . . . . .	97
A.13	Assessing superimposition error in Slicer; a). Visualizing colour map of Model to Model Distance output file, b). Statistics on Model to Model Distance output file retrieved using Mesh Statistics tool . . . . .	98
A.14	Visual summary of retrieving bracket slot positions; a). Manually selected bracket positions below slot, b). Final slot endpoint positions calculated in MATLAB . . . . .	99
A.15	Summary of bracket position selection procedure to retrieve bracket slot end- point locations . . . . .	100
A.16	Summary of 2D coordinate system transformations required for obtaining bracket endpoint positions . . . . .	100
A.17	Calculation of bracket tilt for second coordinate transformation . . . . .	101
B.1	Construction of jig bottom base in SolidWorks; a). Sketch, b). Extruded sketch, c). Completed bottom base part . . . . .	112
B.2	Construction of jig side walls in SolidWorks; a). Sketch, b). Extruded sketch, c). Completed side walls . . . . .	113
B.3	Construction of jig top base in SolidWorks; a). Sketch, b). Extruded sketch, c). Completed top base part . . . . .	113
B.4	Construction lines for mounting jig hole . . . . .	113
B.5	Construction of jig orientation pieces in SolidWorks; a). Sketch, b). Extruded sketch, c). Base Extension . . . . .	114
B.6	Jig cleanup to remove unwanted material; a) Step 1, b). Step 2, c). Step 3 .	115
B.7	Construction of jig tooth in SolidWorks; a). Tooth sketch, b). Tooth slant sketch, c). Completed tooth feature . . . . .	115
B.8	Addition of bolt hole in jig design for mounting onto OSIM . . . . .	116
B.9	Jig bracket placement guide schematic for calculating dimensions . . . . .	117

B.10 Constructing jig bracket placement guides in SolidWorks; a). Jig bracket placement guide sketch, b). Extruded bracket placement guide sketch . . . .	117
B.11 Jig patient arch identification label; a). Tooth and jig set number sketch, b). Patient arch number sketch, c). Final label etched into jig . . . . .	118
B.12 Final jig design with main features labelled . . . . .	118
B.13 Testing different position combinations for OSIM cantilever holes and patient data shift in Jig Dimensions code; a). Example combination with values out of optimal range, b). Example combination with all values within optimal range	120
B.14 SolidWorks design table to create jig configurations; a). Jig feature dimensions, b). Design table interface for pasting jig dimensions calculated in MATLAB, c). Jig configurations created based on design table . . . . .	121
B.15 Example jig set mounted on OSIM model in SolidWorks assembly . . . . .	122
B.16 Minimizing jig interference in SolidWorks assembly prior to printing jig models; a). Before manual trimming with areas of interference identified, b). Minimal interference after manual trimming . . . . .	122
B.17 Summary of features selected for OSIM global coordinate system construction with FaroArm measurement device . . . . .	130
B.18 OSIM global coordinate system creation in FaroArm CAM2 Measure 10 software	130
B.19 Sample .txt file of measured bracket endpoint coordinates exported from FaroArm CAM2 software . . . . .	131
B.20 MATLAB output for bracket position replication errors; a). Plot visually comparing scanned and FaroArm measured bracket slot midpoint positions, b). In-plane global and local discrepancies for each tooth, c). Vertical discrepancies between adjacent teeth . . . . .	132
B.21 Metal mandibular teeth used in sensitivity analysis experiments with wire inserted through brackets . . . . .	144
B.22 Average Y-directional force results at each 0.1 mm displacement increment for canine, central incisor, and second premolar teeth; a). Results for 0.014" archwires, b). Results for 0.016" archwires . . . . .	144
B.23 Excel sheet for calculating updated micrometer positions for a patient jig set	146
B.24 Micrometer setting user interface in OSIM software for manually updating micrometer positions prior to experimentation . . . . .	147

# Abbreviations

**2D** Two-Dimensional.

**3D** Three-Dimensional.

**ANOVA** Analysis of Variance.

**CBCT** Cone-Beam Computed Tomography.

**COR** Center of Resistance.

**CT** Computed Tomography.

**CuNiTi** Copper-Nickel-Titanium.

**FEA** Finite Element Analysis.

**ICC** Intraclass Correlation Coefficient.

**ICP** Iterative Closest Point.

**OIIRR** Orthodontically Induced Inflammatory Root Resorption.

**OSIM** Orthodontic Simulator.

**PDL** Periodontal Ligament.

**RMANOVA** Repeated Measures Analysis of Variance.

# Chapter 1

## Introduction

*This chapter provides an introduction to orthodontic fixed appliances (braces), and the need for enhancing existing biomechanical knowledge to better understand the complex force systems that arise during treatment and its effect on clinical tooth movement. This chapter also covers the thesis objectives, thesis outline, and thesis contributions.*

### 1.1 Thesis Motivation

In Canada alone, \$13.6 billion was spent on dental services in 2015 [1], and it was reported that 75% of Canadians utilized dental services in 2018 [2]. Orthodontic treatment is a dental service that can help correct tooth and jaw misalignments. Undergoing orthodontic treatment has been reported to have positive effects on a patient's quality of life [3]. In terms of aesthetics, orthodontic treatment improves the appearance of a patient's dentition and can potentially increase a patient's self-confidence [4]. Regarding functionality, one's oral health can be substantially improved as misaligned teeth can lead to tooth decay (cavities), periodontal (gum) disease, and possible issues with breathing, chewing, and speech [5]. In addition, the proper alignment of teeth can help prevent premature wearing of the teeth and jaw pain [5].

Various appliances exist for tooth alignment and are categorized as either removable or fixed appliances [6]. Orthodontic braces are a traditional fixed treatment option that involves the bonding of orthodontic brackets onto a dental arch and the engagement of an orthodon-

tic archwire through the bracket slots [7]. Forces and moments arise due to the archwire and bracket slot interaction, inducing tooth movement [8]. Orthodontic tooth movement is achieved through alveolar bone remodelling initiated by the local mechanical state changes in terms of the stress and strain distributions in the periodontal ligament (PDL) from the applied orthodontic loads [9]. As a result of this biological process, the resulting orthodontic tooth movement occurs over three phases known as the initial, lag, and post-lag phase [10].

Understanding the biomechanical relationship between the applied orthodontic force and the resulting tooth movement is crucial to the planning and predictable outcome of orthodontic treatment. However, there continues to be an incomplete understanding of foundational biomechanical knowledge describing the relationship between force and clinical tooth movement [11, 12]. This is greatly attributed to insufficient research linking clinical observations of tooth movement and the biomechanical forces produced by the bracket/archwire interaction in longevity. Additionally, there are patient-related factors including anatomic differences between/within patients and variability in force application (magnitude, direction, duration), which affect the biologic response to orthodontic force systems [6, 9, 13]. This poor understanding can therefore lead to negative treatment effects such as unwanted tooth movements [14, 15], hyalinization in the PDL or root resorption [6, 16], and extended treatment periods for the patient.

Literature has extensively reported the relationship between force magnitude and tooth movement through clinical, numerical, and mechanical experimental approaches. However, the integration of these approaches for validation or correlation between force and tooth movement results has been limited. The incorporation of braces biomechanics was considered in finite element analysis (FEA) studies, in which some literature applied a mechanical experimental approach for validation of the simulation models [17, 18]. Clinical cases were utilized to construct model geometries [17, 18] and, in some works, were used to measure clinical tooth movement for direct comparison with tooth movements or correlation with stress/strain results obtained from FEA simulations over the treatment length [19, 20]. Despite simulation of the full dental arch, these FEA studies generally restricted analysis to

only the teeth of interest and applied prescribed force or displacement conditions for the simulated treatments to retrieve results. However, orthodontic forces and tooth movements can not be assumed in the case of alignment treatments and require evaluation across the dental arch over the treatment duration.

Mechanical experiment studies that used in vitro measurement devices simulated malocclusion scenarios using artificial teeth or models of patients misaligned dentition [17, 21–24]. Most studies were limited to the measurement of biomechanical loads caused by braces for one or two teeth, instead of monitoring the entire dental arch. Additionally, the initial forces/moments present upon archwire insertion were generally measured only at the beginning of a patient’s treatment and not as treatment progressed for comparison with clinical changes [23, 24]. It is critical that the entire dental arch is investigated for biomechanical load measurement to understand the individual force systems at each tooth and its resulting effect on the clinical tooth movement as treatment progresses.

An Orthodontic Simulator (OSIM) was developed at the University of Alberta [15], and this in vitro electromechanical device can perform simultaneous three-dimensional (3D) measurements of forces and moments for a fourteen-tooth arch using individual load cells. The teeth can be independently positioned using the machine’s horizontal and vertical micrometers and are also exchangeable, providing flexibility in assessing both fixed and removable appliances. In terms of studying braces biomechanics, various studies have utilized this device to investigate ligation and archwire types during simulated misalignments [21, 25–27].

Optical scan analysis techniques offer a way of digitally assessing changes in a patient’s dentition over orthodontic treatment. This is useful for the longitudinal tracking of 3D clinical tooth movements occurring over orthodontic treatment intervals. Digital scans retrieved using intraoral scanning technology is an alternative to regular dental impressions which involve physical model storage/durability issues and patient discomfort [28], and cone-beam computed tomography (CBCT) scanning which poses ionizing radiation exposure. The analysis of digital maxillary/mandibular dental models over treatment includes techniques

for model orientation, scan superimposition (alignment), and measuring changes in tooth position. Previous works have utilized anatomical landmarks on the patient scans to achieve orientation within the software interface [29]. Surface registration was a commonly applied method by studies to superimpose pre-treatment and post-treatment scans using reference regions that remained stable over treatment [30]. Various approaches were taken to measure tooth movements, such as comparing tooth landmarks on the superimposed models, using software measurement tools, and individually superimposing pre-treatment teeth onto the post-treatment teeth to retrieve the resulting 3D translation/rotation components [31–33]. Studies had commonly presented or applied scan analysis techniques to investigate changes before and after treatment for patient maxillary arches. It is crucial that clinical tooth movements are monitored throughout the treatment for both the maxillary and mandibular arches. While using existing analysis methods is beneficial, it is also necessary to develop customized techniques applicable to both dental arches that utilize similar scan features (i.e. anatomical and bracket features) to allow for consistent tooth movement analysis over treatment intervals and direct comparison with force system measurements.

Orthodontic force systems must be quantified in 3D alongside the tracking of clinical tooth movements throughout orthodontic treatment to enhance the understanding of the force and tooth movement relationship in longevity. Further advancements in this understanding can assist with sophisticated patient-specific modelling for orthodontic treatment predictability and facilitate future appliance design for optimal load delivery to prevent undesired treatment effects. Therefore, it is necessary to establish a streamlined methodology that utilizes clinical scan analysis techniques and in vitro biomechanical experiments to determine how the biomechanical forces produced from braces affect the magnitude, direction, and rate of tooth movement during treatment.

## 1.2 Thesis Objectives

The overarching objective of this thesis was to better understand the biomechanical force systems present when using braces and the resulting effect on tooth movement over a stan-

standard orthodontic treatment period. This thesis utilized an integrated clinical and in vitro mechanical experimental approach. The first objective was to obtain clinical cases to collect bracket position information and measure in vivo clinical tooth movement over treatment. This was achieved by collecting digital intraoral scans of patient dentition and superimposing the scans using surface registration methods and developing in-house MATLAB scripts to retrieve bracket slot position data and tooth movement measurements at regular time points of a patient's treatment. The second objective of the work was to perform mechanical experiments using an Orthodontic Simulator (OSIM) to measure experimentally resolved forces present due to the patient-specific bracket configurations. This was accomplished by physically replicating the retrieved bracket positions from the first objective onto the OSIM by bonding orthodontic brackets onto additively manufactured jigs that were custom dimensioned through coordinate transformation computations performed in MATLAB. The third objective focused on observing existing trends between the clinical and experimental sets of data collected for sample patient cases to improve the current understanding of the biomechanical forces produced by braces and its effect on the magnitude, direction, and rate of tooth movement over the treatment period. This was achieved by comparing the calculated tooth movements and the measured initial forces over treatment when a conservative tooth movement threshold of 0.5 mm was considered for discussion of measurable cases not influenced by intrinsic and methodological uncertainty. The conservative threshold was determined based on the average methodological errors present prior to experiments. Additionally, the changes in force and tooth movement rate were monitored over treatment for an improved understanding. By employing a streamlined methodology and providing preliminary biomechanical data alongside clinical tooth movement data, this work aims to guide future works in developing patient-specific predictive models for orthodontic tooth movement over treatment to improve overall treatment predictability and prevent undesirable treatment side effects.

## 1.3 Thesis Outline

This thesis is composed of four chapters and two appendices. Chapter 2 provides a literature review on tooth anatomy and function, tooth movement biomechanics, the effects of varying force magnitude on tooth movement, previous works done on investigating the biomechanics of braces through mechanical experiments and finite element analysis, and a summary of previous techniques used for analyzing patient dental scans over orthodontic treatment.

Chapter 3 presents a study for analysis of the force and tooth movement data sets collected for recruited patient clinical cases over orthodontic braces treatment. This study utilizes patient intraoral scan analysis techniques to obtain bracket slot endpoint position data from digital intraoral scans. This information was used to calculate in vivo clinical tooth movement over the treatment time points and to assist with mechanical experiment preparation. Experimental forces arising from the specific patient arch configurations over treatment were measured upon archwire insertion through the brackets, which were individually positioned using custom-dimensioned jigs. The study then explores the changes in force, the existing trends between initial forces and tooth movement, and the tooth movement rates over treatment, while examining the potential patient-specific and methodological factors that may influence the obtained results.

Chapter 4 presents the conclusions of the work. This chapter also discusses the limitations and the use of the current methodology and preliminary results to drive potential future works.

Appendix A provides the details for patient scan analysis as utilized in Chapter 3's study for clinical data collection and also provides the relevant MATLAB algorithms developed. Appendix B provides the details on the design/preparation of the additively manufactured jig sets along with the evaluation and mitigation of bracket position errors for experimental data collection as outlined in Chapter 3. Relevant MATLAB scripts developed for the procedures are also included in this Appendix.

## 1.4 Thesis Contributions

This thesis presents and validates a streamlined methodology of processing patient scans for the direct measurement of clinical and mechanical experimental data to better understand the force systems arising from braces and its effect on tooth movement over orthodontic treatment. These methods involve patient intraoral scan analysis to aid in tooth movement evaluation, and patient bracket position replication using custom additively manufactured jigs for experimental force collection. In addition, this thesis provides a study where preliminary force and tooth movement data was collected and presented for sample maxillary/-mandibular arches, in which observed trends were discussed for improving the understanding of the relationship between biomechanical forces and tooth movement over orthodontic treatment. Therefore, this thesis contributes to the existing knowledge of the biomechanics of braces and will be some of the first to relate foundational biomechanical data and longitudinal clinical outcomes, as previous literature had not explored this form of analysis. The established methodology alongside preliminary data will guide future research in advancing the methodology to study more complex tooth misalignments, develop predictive tooth movement models for clinical cases, and improve orthodontic appliance design. This can help drive improvements in future orthodontic treatment planning and outcome by delivering optimal loads for desirable tooth movements, reducing treatment times, and preventing tissue damage.

# Chapter 2

## Background

*This chapter introduces relevant background information regarding the anatomy, function, and nomenclature of teeth which is fundamental to understanding the contents of this thesis. Relevant literature pertaining to the biomechanics of tooth movement is presented covering the types of clinical tooth movement, relevant tooth movement theories contributing to the cellular-level understanding, and the effects of force levels on tooth movement from a biomechanical perspective. Information regarding the biomechanics of braces and the various literature that have studied this topic through finite element analysis and mechanical experimentation using measurement devices are presented. An introduction to the Orthodontic Simulator discussed in Chapter 3 is provided. Analysis techniques for patient dental scans are also presented in this chapter to understand coordinate system establishment on dental models, superimposition of scans, and how tooth movement has been typically assessed over orthodontic treatment.*

### 2.1 Teeth Anatomy, Function, & Nomenclature

The structure of a tooth, as shown in Figure 2.1, can be divided into two sections, namely, the crown and root [34]. The crown sits above the gingiva (gums), making it exposed in the mouth, while the tooth root sits below the gingival line unexposed [34, 35]. The teeth themselves are made up of four types of tissue: the pulp cavity (soft tissue) and the dentin, cementum, enamel (hard tissues) [34, 35]. The innermost layer is known as the pulp cavity,

and at the crown, this layer is known as the pulp chamber [34, 35]. The pulp cavity consists of connective tissue, blood vessels, and nerves and its chamber extends into the root of the tooth where it becomes the pulp/root canal and ends at the apical foramen [35], which serves as the entrance for the nerves and vessels [34]. Moving outward, the next layer is known as dentin, which provides the separation between the outer and inner tissue layers and makes up the largest part of the tooth [35]. Dentin has a similar matrix composition as bone, but is not cellular [34]. The outermost layer of the crown is occupied by the enamel (which is the hardest layer of tissue composed of calcium phosphate), and the cementum is the outermost layer of the root [34, 35]. The cementum has a similar composition to bone and different from that of enamel, but still plays the role of covering the dentin [34]. Furthermore, this tooth layer also makes up one of the four components of the periodontium.

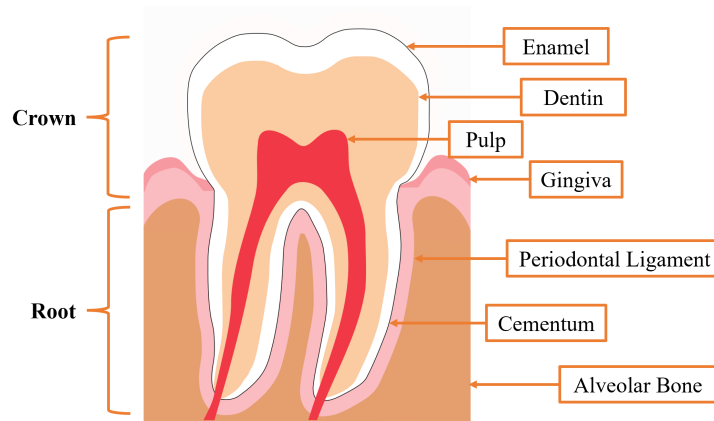


Figure 2.1: Overview of tooth and periodontium anatomy with tooth sections and tissues labelled

The periodontium is made up of four components: the alveolar bone, periodontal ligament (PDL), gingiva, and cementum (these tissues are individually labelled in Figure 2.1) [36–38]. The tooth root sits within the alveolus, which is the bony tooth socket [34, 36]. The periodontium provides the structural support necessary for keeping the tooth intact within the alveolus, in which the PDL provides the main structural connection by connecting the tooth cementum to the alveolar bone inner wall through its collagenous fibres [34, 36–38].

The PDL is a viscoelastic system composed of vascular cellular connective tissue [6, 36, 39]. Along with structural support, the PDL functions as a shock absorber (such as withstanding forces due to mastication [6]), acts as a protective casing for the vessels and nerves, maintains the gingival tissues, and transmits force to bone [36]. Additionally, the PDL plays a vital role in facilitating tooth movement through its biological response to an applied orthodontic force [6]. The alveolar bone provides support to the tooth through the alveolar process, which is the part of the dental arch that make up the tooth sockets [34, 36]. The alveolar bone's structure involves compact and dense cortical bone on the outer layers and spongy trabecular bone in between the cortical layers [36, 39]. Specifically, the compact bone's inner wall in contact with the PDL is commonly referred to as the lamina dura [36]. The gingiva provides a protective barrier from bacteria [34, 36], while also providing direct connection to the tooth through the base of the gingival sulcus called the junctional epithelium [36].

An adult's permanent, or secondary, dentition is composed of 32 teeth, where the upper (maxillary) arch and lower (mandibular) arch each consist of two central incisors, two lateral incisors, two canines, four premolars, and four molars (or six molars if including the wisdom teeth) [34, 35]. Generally, the incisors and canines are single-rooted, while the premolars may have one or two roots and the molars can have up to three roots depending on the arch [34, 35]. The function of human teeth is to assist with the breakdown of food and preparation for digestion during mastication through crushing and cutting food down using the different tooth types [34]. In addition to this direct function, the dentition also supports facial structure, breathing, and speech. Specific teeth of the maxillary and mandibular dental arches can be referenced within four quadrants using the FDI numbering system. Directional convention of the teeth includes the mesial-distal component (front to back of mouth), buccal-lingual component (cheek to tongue), and occlusal-gingival component (tooth surface toward gums) as labelled in Figure 2.2.

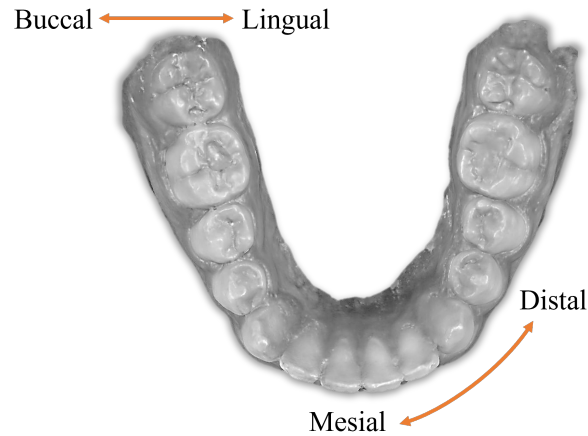


Figure 2.2: Occlusal view of a patient mandibular dental arch with labelled dental directional convention

## 2.2 Biomechanics of Tooth Movement

### 2.2.1 Types of Tooth Movement

When an orthodontic appliance exerts a force system on a tooth, the resulting tooth movement can vary depending on the location and distribution of the applied forces [6]. Commonly, tooth movement can be categorized as pure translation, pure rotation, or a combination of both [40]. Translation or bodily tooth movement occurs when the applied force acts through the center of resistance (COR) [40]. While translation can normally be achieved with a force acting through a free body's center of gravity, the COR presents the analogous location on the restrained tooth [40]. This results in the tooth crown and root to both move in the same direction as well as by the same amount [6, 40, 41]. Rotational movements are a result of the force application at a point other than the COR and this causes a moment to arise inducing rotation of the tooth [40]. More frequently, a combination of the two types of movement occurs [40].

To be able to further classify the main types of tooth movement that can occur over treatment, the incorporation of the center of rotation is considered for discussing tipping, bodily, extrusive and intrusive movements [6, 40]. While the COR varies with each tooth

and provides the location at which pure translation would occur if the force passed through it, the center of rotation is the pivotal location that the tooth rotates about depending on the location of force application [40, 41]. Tipping movements can be either uncontrolled or controlled [40, 41]. In uncontrolled tipping, the center of rotation is normally located between the root apex and COR, and this causes the movement of the root and the crown in opposing directions [40, 41]. In controlled tipping, the center of rotation would be located at the root apex for crown tipping or at the tip of the crown to induce root tipping [40, 41]. When an applied force initiates tooth tipping, the PDL becomes compressed in the tooth root apex region and the alveolar bone crest [6]. For pure translation, the center of rotation would theoretically approach infinity [40, 41]. Tooth translation can include movements in the buccal-lingual, mesial-distal, and occlusal-gingival (extrusion and intrusion) directions [6, 41]. During force application for bodily movements, the compression of the PDL is uniform [6]. In the case of intrusion, the applied force would cause the local compression to be focused on the tooth root apex region [6].

### **2.2.2 Phases & Theories of Tooth Movement**

Orthodontic tooth movement has been categorized into three main phases known as the initial phase, lag phase, and post-lag phase [10, 42]. The initial phase is composed of initial tooth movements after the application of orthodontic force and usually occurs for one to two days [10, 42, 43]. These are fast movements that occur within the periodontal space as a result of the force causing the PDL to become compressed, altering the local mechanical state of the PDL. As the name suggests, the lag phase is comprised of minimal to no tooth movement occurring due to the locally compressed region of the PDL losing its blood supply from the continued applied loads [10, 42–44]. For a large enough force magnitude, a direct result is hyalinization of the PDL where tissue necrosis (cell death) occurs, delaying the tooth movement since cell differentiation can no longer occur in the affected area [10, 42–44]. This dead tissue is removed by phagocytic cells such as macrophages, and this phase of tooth movement can last between 4-20 days [10]. Subsequent to the removal of dead tissue, the

post-lag phase begins (approximately 40 days after the initial application of force), initiating tooth movements at an increasing rate with continuous bone remodelling resuming until the force application ceases [10, 42, 43].

Different types of tooth movements, as described in Section 2.2.1, can be expected from the forces arising during the use of orthodontic appliances. These movements from one position to another are executed through the process of bone remodelling during the phases of tooth movement. When a force is applied to a tooth, the periodontium experiences changes in its mechanical state due to the arising stress and strain distributions, which depends on the surface area of the bone, and the magnitude/distribution of the applied force caused by the orthodontic appliance [9]. The remodelling process is initiated by an inflammatory response and consists of alveolar bone resorption in areas of compression facilitated by osteoclasts and bone deposition/formation in the local areas of tension carried out by osteoblast cells [6, 39]. The detailed biology behind the force conversion to cellular activity is still not fully understood [42, 45], leading to various presented theories to advance the understanding in order to prevent unwanted side effects during orthodontic treatment. The three main orthodontic tooth movement theories presented were the pressure-tension theory, bone-bending theory, and biological electricity theory [10, 42, 45].

In the pressure-tension theory, it was suggested that movement within the periodontal complex is facilitated by the establishment of a pressure and tension side when an orthodontic force is applied [10, 46–48]. On the compressed side, the PDL experiences a decrease in blood flow resulting in lower oxygen levels and hyalinization can occur in this locally affected area [6, 10]. This causes an inflammatory response where chemical messengers are involved with stimulating cellular activity to assist with resorption of the dead tissue [6, 45]. Therefore, it is expected that bone resorption occurs from osteoclast cell activity, while on the tension side, it is expected that bone formation or deposition will occur due to osteoblast activity [6].

In the bone-bending theory, the orthodontic force transmits to near tissues leading to the solid structures of the periodontium (i.e. bone) bending [10, 45, 49]. The bone experiences

bending due to its elastic nature and leads to cellular changes for bone shape/organization modifications [10].

The biological electricity theory can be seen as an extension of the bone-bending theory where the application of an orthodontic force leads to the bending of the alveolar bone, which then causes electrical signals (similar to piezo-electric signals) to be released [6, 10, 50]. These signals then act as cellular messengers to induce bone remodelling for tooth movement [50]. Based on the theories presented, the current understanding of tooth movement has progressed to the extent of recognizing the pressure-tension in the PDL and the biological electricity may both contribute to the tooth movement process [6]. Nonetheless, the summary of existing theories is important to understanding tooth movement at the cellular level.

### **2.2.3 Effect of Force Levels on Tooth Movement**

Within the study of orthodontic biomechanics, the understanding of force magnitude on the resulting tooth movement continues to be a poorly understood relationship. In terms of the general understanding of how applied forces affect tooth movement on a biological level, it was found that low forces may not lead to changes in the PDL, whereas a persistent light force (around 0.25 N [51]) can lead to cell activity over time, commonly through frontal resorption where the adjacent bone can be consistently removed [6]. A clinically relevant orthodontic force can be considered as approximately 0.2 N based on various literature that reported tooth movements occurring with this applied force magnitude [6, 12, 51, 52]. On the other hand, a comparatively high and sustained force (greater than 1.5 N [12]) applied to a tooth can result in the cut off in blood supply in the affected PDL area [6]. This in turn leads to tissue necrosis or hyalinization of the compressed side, requiring removal of dead tissue in the PDL from adjacent cellular PDL regions and from sub adjacent bone marrow spaces before movement can be induced as described previously. As a result, undermining resorption occurs at these high forces for osteoclasts to remove bone for tooth movements to resume [6, 9, 44]. This is a prolonged process since the removal of bone occurs in its underside and not directly adjacent to the compressed PDL area as seen in frontal resorption [6, 44].

In extreme cases where there is high force application, orthodontically induced inflammatory root resorption (OIIRR) is a possible side effect during orthodontic treatment [6, 16, 53]. Essentially, the cell activity responsible for removing hyalinized PDL also results in removal of adjacent cementum [6]. Although the repair of cementum is possible, the continuous removal of this layer without coordinated repair can eventually expose the tooth's dentin layer to the resorption process, permanently affecting the root structure [6, 53].

Previous experimental-based literature attempted to investigate the relationship between force magnitude and resulting tooth movement over various treatment periods using human and animal subjects. Different force magnitudes prescribed by the appliances used were applied on the tooth of interest and the initial tooth displacement was evaluated for human maxillary central incisors [54], and for maxillary molars/incisors in rat subjects [55]. The force application in both studies were short term, resulting in only the investigation of initial tooth displacement instead of considering all phases of orthodontic tooth movement. Other studies have considered a longer treatment time, in which the force application was prolonged, and tooth movements were tracked for 11-22 weeks [56–58]. These studies attempted to measure the tooth movement and its rate, as well as determine whether an optimum force range existed for clinical applicability. One study stated that the rate of tooth movement could be increased if the force magnitude was increased from a low original force, such as when they increased a 10 cN force to 600 cN [57]. Throughout the studies, it was found that differences in individual subjects as well as within the subject itself were major contributors to the differences in results regarding optimal force application ranges [56–58].

In an attempt to summarize existing experimental data, four theoretical models were proposed by Quinn and Yoshikawa [59] to describe the relationship between force and the rate of tooth movement. Although all models showed weak agreement with the available data, the fourth model consisting of an initial linear relationship followed by a plateau region (indicating no rate increase in tooth movement after a certain level of stress magnitude is reached) had greater support from the available data. Similarly, a mathematical model was presented by Ren et al. [60] utilizing past experimental data to represent a generalized rela-

tionship between force and tooth movement rate. The established model could not predict individual cases, and it was suggested that a greater range of data is necessary for further improvement/validation. Ultimately it was found that in addition to patient variation, studies also had varying experimental setup, leading to differences in study length, force magnitude ranges tested, and methods for tooth movement measurement, which would directly affect the results and conclusions presented on what optimal range of force should be used during treatment [11, 12]. Additionally, the experimental approach introduces challenges in calculating the stress and strain distributions within the PDL [11], which is critical information needed for understanding the force's effect on tooth movement at the biomechanical level.

Although an optimum value for orthodontic force has not been agreed upon due to the varying experimental conditions, based on Proffit et al. [6], it was suggested that an optimal force range would be 35-60 gm for tipping, rotation, and extrusion, 70-120 gm for translation, and 10-20 gm for intrusion. From a literature review that summarized experimental studies [12], the generalized force ranges for achieving a particular tooth movement rate were forces less than 100 cN for 0.23-0.44 mm/week, 100-150 cN of force for 0.16-0.47 mm/week, 150-250 cN of force for 0.1-0.46 mm/week, and 250-400 cN of force for 0.34-0.49 mm/week. Despite past literature, the relationship between force magnitude and tooth movement continues to be poorly understood and the relationship itself has not been properly established.

## **2.3 Understanding the Biomechanics of Braces**

### **2.3.1 Finite Element Analysis in Literature**

In addition to the human- and animal-based experimental literature presented in Section 2.2.3, numerical approaches such as finite element analysis (FEA) have been frequently employed to enhance the understanding of the forces and tooth movement occurring over orthodontic treatment. FEA can be advantageous in overcoming limitations that may be encountered during physical experiments (e.g. through complex geometries) [61]. In the context of studying tooth movement biomechanics and general orthodontics, FEA can be

used to simulate user-defined orthodontic forces on anatomically representative or simplified geometries of dentition to study the transfer of loads to the periodontium [62], the arising stress/strain mechanical response of the PDL [61], and its effects on initial/long term tooth movements. Although FEA gives researchers the freedom to define representative geometry, mesh density, material properties, and boundary/loading conditions, this in turn requires assumptions to be made about such values (e.g. material properties) which have a significant impact on simulation results [61, 62].

In earlier literature, FEA involved simplified single-tooth models to investigate the tooth-PDL complex and evaluate the stress and strain distributions within the PDL when loading conditions were applied directly to the tooth, omitting the simulation of orthodontic appliances [63, 64]. The consideration of an orthodontic bracket was included in the FEA models for investigating the bone remodelling theories through inducing different tooth movements including tipping, rotation, and translation using predefined force systems [65, 66]. Investigating optimal loading conditions, estimating the COR/center of rotation location, and evaluating initial tooth displacement were other topics investigated with single-tooth geometries [67–69]. Root resorption was also studied in the context of determining optimal forces to prevent further damage [70]. The complex nonlinear behaviour of the PDL was studied using simplified models and varying material properties to investigate the resulting PDL stress/strain distributions [67, 71–73]. Additional works have specifically studied the isolated bracket and archwire complex to investigate torque generation, bracket slot deformation, and stresses occurring at the bracket base and tooth surface due to the engaged orthodontic archwire [74–76].

More recent research has considered the use of multi-tooth models [77–80], as well as full dental arches [17, 81–88]. With the additional teeth, initially applied orthodontic forces could be further assessed for its effect on the stress/strain distribution occurring in the periodontal complex [77], with the additional consideration of braces where loading conditions were applied onto the archwire [78]. Many of these studies had applied FEA using actual patient scanned dentition models and simulating a variety of orthodontic treatments involving the

bracket-archwire system. One example includes the general arch alignment with continuous archwire insertion where the use of a birth-death method was employed to have control over the contact/interaction between the archwire and bracket elements [17, 79]. Other simulated treatments include distalization (where the posterior teeth are moved distally creating more space at the front of the arch) [86, 87], and retractions/space closures which are commonly achieved with sliding or frictionless mechanics [20, 81, 83–85, 88]. In addition to mimicking clinical treatment by applying defined forces and measuring the resulting tooth movements, some of these studies had also utilized the partial/full dental models to study the effects of fixed-appliance size and material through different archwire and bracket combinations [80, 84, 88, 89].

Long-term tracking of tooth movement biomechanics is another topic that is crucial to improving prediction of tooth movement over orthodontic treatment as investigated in single tooth models [90, 91], and full dental arch geometries [19, 20, 92, 93]. In a study by Chen et al. [20], a bone remodelling algorithm was employed alongside predefined forces to induce maxillary canine retraction. The resulting tooth movements from the simulation were compared with the clinical measurements tracked over a three-month period. Another study had followed a patient’s canine retraction treatment by collecting scans over four treatment intervals to set up the FEA models [19]. Simulations were run to obtain stresses at the tooth root, while the tooth movements were measured by superimposing the collected scans. A developed model utilizing the stress and tooth movement relationship was then established and clinically validated with another sample patient case [19]. Dot et al. [92] had similarly obtained patient scans over treatment intervals to establish a novel approach for constructing geometries and tracking tooth movement over treatment. Scan superimposition for clinical tooth movement measurement was performed for clinical comparison as done in the other works [19, 20]. As a part of the FEA simulations, various mathematical remodelling algorithms were employed such as the spring model [94], hydrostatic pressure-based model [20], and Zener model [92].

Given the applicability of FEA in orthodontic treatment-based research, this approach

is promising to enhance the understanding of the biomechanics of braces and its effect on clinical tooth movement over treatment. The available literature provides useful insight for future analysis of the thesis research, in which FEA can assist with predictive modelling and can be applied to provide validation for the experimental and clinical approaches taken. However, this form of analysis still has its limitations, as various assumptions need to be made regarding the properties of complex tissues (such as the PDL) that are still not fully established, and this can impact the accuracy of results. Additionally, most works lack the long-term force application for measuring tooth movements over longer treatment periods and were restricted to simulating treatments using an orthodontic appliance that delivered a prescribed loading condition. This presents limitations in trying to simulate simple alignment treatments that involve unassumed force conditions caused by the engagement of the archwire in the bracket slots.

### **2.3.2 Existing Measurement Devices in Literature**

Another approach to investigating the biomechanics of braces to understand the generated loads and its effect on tooth movement was through mechanical experimentation. Earlier work was done in measuring force systems through developed in-vivo devices [8, 95, 96]. In Friedrich et al. [8], the in vivo measurement of force and torque was accomplished through a designed apparatus that incorporated a custom-designed orthodontic bracket that allowed for the sensor to measure the isolated force system that would have been applied onto the tooth due to the engaged archwire. In Duyck et al. [95], strain gauges were used to be able to measure the axial force and the moment about the X- and Y-axis during the use of dental implants. Another device consisting of a magnet and eight magnetic sensors was developed, in which the tooth displacement could be measured when a force was applied in vivo [96]. After application of a known force, the magnet's displacement was used to mathematically retrieve the tooth's displacement. Although the presented studies were able to directly measure force systems or initial tooth displacement in vivo, they were limited in terms of design as only one tooth could be investigated at a time.

An abundance of previous attempts was made to understand the biomechanics of braces through the development of various in vitro measurement devices. In an earlier device developed by Kuo et al. [97], four load cells were designed and presented by brass rings mounted at the tooth root that were able to account for horizontal/vertical force and moment measurement. Robotic devices such as the Robot Measurement System (RMS) [24] and Robot Orthodontic Measurement & Simulation System (ROSS) [98] utilized one sensor to measure forces and moments on a single tooth. Some devices utilized two sensors for load measurement of teeth [18, 99, 100]. Other notable devices including the Orthodontic Measurement and Simulation System (OMSS) [101–106], and the Orthodontic Force Tester (OFT)[17, 107, 108] were also designed with two load measurement sensors. The Orthodontic Simulator (OSIM) was a device developed at the University of Alberta which could simultaneously measure the forces and moments acting on anatomically shaped teeth using 14 sensors [15, 21, 25–27, 109]. Later devices such as the FORSED [110, 111] and Orthodontic Force and Moment Sensing Device [22, 112] were similarly designed with 14 sensors, but application of these devices were limited in literature.

Through the various custom in vitro experimental devices, the biomechanical loads during different treatment conditions were measured. Some studies investigated different misalignment cases using artificial teeth models (such as metal or resin) to simulate displacements [15, 21, 22, 102, 110]. Other studies used scanned patient geometry to retrieve patient models to replicate the patient’s arch directly or to modify the existing tooth positions to simulate a particular misalignment [18, 23, 24, 100, 113]. The direct replication of patient dentition could be applied in studies where the device’s sensors were directly attached to the tooth of interest and positioned accordingly [17, 23, 24]. In Fuck et al. [24], the patient’s bracket positions from the scanned dentition were also replicated for experimentation to better reflect the treatment conditions. This study tested different archwire types, measuring the resulting forces by replacing each tooth with the sensor until data for the whole arch was collected. Since only one scan of each patient was replicated, this work primarily concentrated on finding the initially applied force at the start of treatment, instead of tracking

biomechanical loads over the treatment period. In Mencattelli et al. [23], a real patient misalignment case was replicated using a scan that did not include any bonded brackets, therefore, the bonded brackets used for experiments were not based on predefined patient bracket locations. Additionally, only the misaligned portion of the arch was considered for the data collection and only the initial forces after engagement of different archwire sizes were measured (did not investigate the force changes over treatment). The whole patient arch was considered for force measurement in Zhou et al. [17], however, since the device only contained two sensors, experiments were repeated until all data was collected. This paper had also applied an FEA approach, but comparison of simulation and experimental results were limited to the forces/moments occurring at one stage of treatment only.

Within the previous in vitro biomechanical methods, one limitation commonly faced when performing experiments was the device design consisting of less load cells than the number of teeth. When studies considered the whole arch, they were required to repeat experiments to collect data for the complete arch [17, 24]. In other studies, only the force systems of the misaligned tooth were of interest, simplifying the experimental data collection to the investigated tooth or portion of the arch where only the misalignment was located [18, 23, 100, 104, 107]. To better understand the biomechanics of braces, it is necessary to collect data for the entire arch for more clinically representative results to identify the anticipated loading conditions over treatment. Studies that used the OSIM device were capable of achieving this, since each artificial tooth had access to an individual load cell. Although common misalignments were easily tested with this machine, the direct replication of actual patient cases poses a challenge since the machine components are fixed. Another overarching limitation with the studies presented in this section is the lack of comparison of biomechanical loads with clinical tooth movements. Comparison of this is a crucial component to better understanding the relationship between the forces and tooth movement over the treatment period.

### 2.3.3 Introduction to the Orthodontic Simulator (OSIM)

In this thesis, the in vitro Orthodontic Simulator (OSIM) (Figure 2.3), developed at the University of Alberta [15], was used for the measurement of force and moment systems. The OSIM is capable of simultaneously measuring forces and moments in three dimensions for a 14-tooth dental arch using 14 six-axis load cells (Nano17, ATI Industrial Automation). Each tooth is screwed into a metal cantilever arm that extends into a cap, providing connection to the machine's micrometers. Using the horizontal and vertical micrometers consisting of a 10 mm range allows for the tooth positions to be accurately adjusted in the tooth's buccal-lingual and occlusal-gingival direction, respectively. The dentition (manufactured metal pieces representing the tooth's anatomical shape) can be replaced according to the work at hand, giving the OSIM the ability to test various orthodontic appliances, including traditional braces and orthodontic aligners.

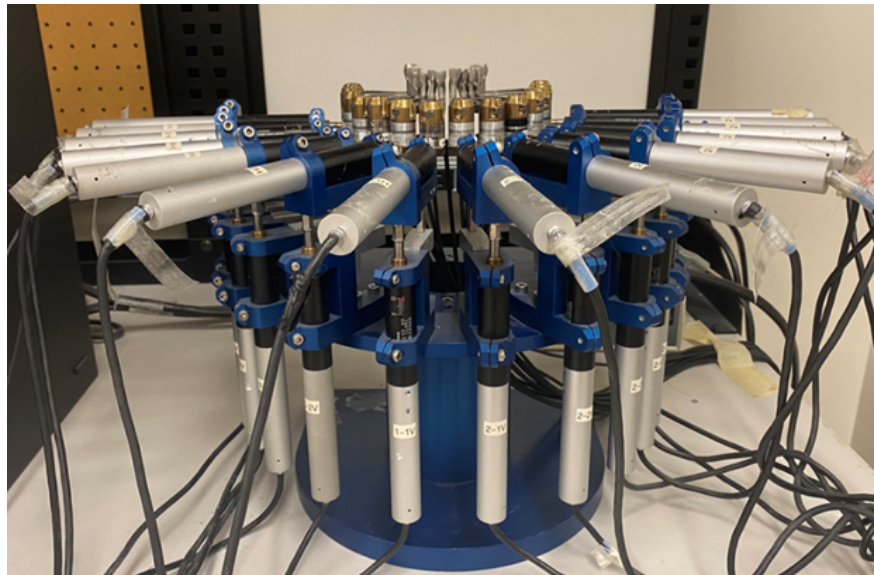


Figure 2.3: Overview of the in vitro electromechanical Orthodontic Simulator (OSIM) for 3D force and moment measurements

Force and moment data is initially collected at each of the load cells and is analogous to a simple cantilever beam system where the load cell represents the fixed end, and the orthodontic loads occurring at the tooth is located at the free end of the cantilever arm. The forces and moments acting at the free end can then be determined at the fixed end

of the system where the load cell is located. Using Jacobian transformation matrices, the data initially collected at the load cells can then be converted to represent the forces and moments at a more relevant point of interest such as the bracket midpoint or the COR of the anatomical teeth.

The in vitro OSIM has been previously utilized in several studies to better understand the force and moment systems developed when using braces. Common tooth misalignments have been simulated to investigate specific topics such as ligation type, archwire type/size, and expansion/retraction procedures. Three studies simulated high canine malocclusions to compare the load results when passive and elastic ligation were used for a maxillary arch [25–27]. Another study also investigated the ligation method and its effects on the force and moment magnitudes along the maxillary arch but for an incisor misalignment in the lingual direction [114]. Misalignments for both the canine and incisor were simulated in another study to investigate the force systems arising from two different lingual fixed appliances (straight and mushroom archwires) [21]. In addition to the straight lingual and mushroom lingual fixed appliances, Kaur et al. [109] also considered a straight labial archwire system to evaluate and compare the measured biomechanical loads when a posterior maxillary arch expansion was investigated. Other uses of the OSIM include the measurement of force during en masse retraction [115], and the use of elastics for Class II malocclusion to investigate its effect on the resulting forces acting on the maxillary canines [116].

Despite the extensive research done using the OSIM, the device has existing limitations that affect the thesis work. Since the device is in vitro, patient intraoral conditions including saliva and supporting structures, such as the PDL and bone, are not considered. In addition, only one arch can be investigated at a time, therefore, the occlusal interactions between the maxillary and mandibular arch expected during actual treatment is absent. The OSIM also presents difficulty in directly replicating patient geometries due to the fixed-nature of the equipment components. Even with the availability of horizontal and vertical micrometers, there is no control over the mesial-distal direction for tooth positioning, which is crucial for replicating patient-specific positions.

## 2.4 Patient Dental Scan Analysis over Orthodontic Treatment

### 2.4.1 Coordinate System Establishment for Dental Scan Alignment

An important step in preparing digital dental models for 3D analysis (such as measuring tooth position changes over orthodontic treatment), is the dental scan alignment with an existing or newly established coordinate system within the software being used. Past literature initially established an origin point for a pre-treatment maxillary model using the intersection of the median palatal raphe and incisive papilla [117, 118]. A plane through the median raphe was constructed and a subsequent combination of rotations and translations were performed to complete the alignment of the model within three established planes, namely, the X-Y transverse plane, X-Z sagittal plane, and Y-Z coronal plane [117]. The same origin point location was defined by other studies [31, 119]. The transverse plane was then established using the origin point and one to two randomly selected points along the mid-palatal suture [31, 119]. After the selection of the first/second premolars and first molar buccal cusps, the occlusal plane was established [119]. The occlusal plane in Choi et al. [31] was established slightly differently by using the origin point and central incisor midpoints in addition to the first molar buccal cusps.

Other literature has established coordinate systems for the investigated maxillary arch model using only two planes, by first fitting a transverse plane after selecting the buccal cusps of the first/second premolars and first molars [29, 120]. The midsagittal plane was then constructed with the two additionally selected points along the palatal suture, and the palatal suture point closest to the first molars (projected on the transverse plane) was the defined origin point [29, 120]. A different approach was taken by Grauer and Proffit [121], where local coordinates systems were established for each tooth in addition to the general coordinate system the model sat within. This was done specifically for retrieving tooth movements, which will be explained in Section 2.4.3. In Hayashi et al. [122], only

the palatal region was used to mathematically establish a flat reference plane. For the establishment of a plane for mandibular arch models, one study placed landmarks on the midpoints of the canines, premolar and molar crowns to create a levelled or “best-fit” plane through the selected midpoints [123]. Another study kept the maxillary and mandibular arches in occlusion and used maxillary landmarks (incisal edges, gingival margin, molar cusps, and medial raphe) to simultaneously orient the mandibular arch [124].

Based on the presented literature, the general process to aligning the scanned pre-treatment or initial dental models involved the definition of an origin point and selection of other supplementary points to establish planes along the X-, Y-, and Z-directions. Since the literature had primarily analyzed maxillary dental models, this results in the need of anatomical features pertaining to the palatal region, which is a limitation when also requiring model alignment for the mandibular dentition. Since this thesis research investigates both maxillary and mandibular models independently, there is a need for a consistent method utilizing anatomical features applicable to both models to later retrieve useful information for clinical and experimental data collection. Additionally, selecting anatomical landmarks such as palatal suture points or tooth midpoints/edges may allow more subjectivity. In this thesis, multiple arches were considered, requiring the use of easily identifiable anatomical landmarks that could be more objectively selected.

## **2.4.2 Dental Scan Superimposition**

Superimposition or registration is a term used to describe the alignment of two scans that were initially in different positions. Alignment of multiple scans for a single patient allows for direct evaluation of the changes occurring between treatment time points, such as tracking clinical tooth movements. Previous literature has explored and applied various methods of superimposition, including point-based registration (landmark-based registration), surface-based registration, and voxel-based registration.

One study tested the point-based superimposition method to align identical models of dentition (one as a computed tomography (CT) scan and the other as a scanned plaster

model) by selecting five points on each model which included the central location between the incisors and the cusps of the first premolar and second molar [125]. These landmarks guided the alignment of the models using the best fit algorithm. Another study had duplicated and randomly positioned sample maxillary models and selected 15 points on the palatal rugae region for an initial superimposition [126]. This was done to improve the subsequent surface registration that utilized the iterative closest point (ICP) algorithm. Some literature only selected 2 points for landmark superimposition: One point on the distal end of the incisive papilla and the other point distal to the first point along the midpalatal raphe [127, 128]. The mucogingival junction region was used in another study with 13 selected landmarks to superimpose two mandibular models of interest to assess dental changes [129]. Some studies that applied landmark-based superimposition simultaneously aligned the maxillary and mandibular arches, since the dental arches were kept in their occlusal positions [124, 130]. In one of these studies, mandibular superimposition was carried out by first positioning the maxillary and mandibular models using three common occlusal contact landmarks [130]. Through the selection of three points along the palatal rugae, simultaneous superimposition of the maxillary and mandibular models was completed, and the maxillary models were then removed to isolate the superimposed mandibular models. Similarly, one study suggested that the superimposition of the mandibular models can be achieved through keeping both arches in occlusion and selecting at least five landmarks on the medial ends of the third rugae and palatal surface region [124].

Surface-based superimposition was investigated through a best-fit approach as reported by Talaat et al. [128], in which the whole model was considered instead of a specific landmark of the dental model. Some papers also utilized available cone-beam computed tomography (CBCT) scans of the patient to integrate a voxel-based superimposition with the mandibular dental models [131]. For example, in Park et al. [132], the pre- and post-treatment models were initially superimposed using a CBCT and dental model by applying the best-fit method. The final output model was then registered by selecting the basal bone as the reference surface. Similarly, in Ioshida et al. [133], the pre- and post-treatment models were first

registered with their CBCT equivalent and were then superimposed with each other using the mucogingival junction as the reference region. One study tested five reference areas around the palatal region of the maxillary model and utilized the iterative closest point (ICP) algorithm [33]. In another study, the maxillary model superimposition was first completed roughly through manually aligning the models and then a finer superimposition was applied using the palatal rugae as the reference area [134]. Based on studies done evaluating the validity of the superimposition methods, it was found that surface-based registration and voxel-based registrations provided more accurate results in comparison to landmark-based superimposition [135]. In the case of the thesis research, surface superimposition will be applied since CBCT scans will not be collected.

In order to apply surface-based superimposition, it is crucial to select an appropriate region or reference area that is stable over treatment and is consistently available on the dental models. Based on earlier literature for maxillary superimposition, it was found that the lateral ends of the first rugae were considered stable [136], and the medial points of the palatal rugae were suitable [137]. Others suggested the use of the medial and lateral points of third rugae [138, 139]. In more recent literature, similar conclusions were reached regarding suitable landmarks, in which the surface across the palatal rugae was used [31, 119, 140]. Two studies selected the palate as a mushroom-shaped region [134, 141]. In Jang et al. [142] and Chen et al. [30], the stable region for superimposition was presented as the medial two-thirds of the third rugae and regional palatal vault. This stable region was then applied by other works [33, 120], and was the recommended region based on a literature review [143].

Literature pertaining to the stable regions of mandibular dental models were less abundant in comparison to the available maxillary-based literature. One study concluded that the mandibular torus was a potential stable area, whereas the buccal and alveolar surfaces near the dentition could not be considered as stable [144]. In Nguyen et al. [145], the chin and symphysis were identified as stable regions, while the third molar showed higher errors. Two studies utilized the mucogingival junction for their superimposition process [129, 133].

Other studies kept the maxillary and mandibular arches in occlusion, eliminating the process required to separately superimpose the mandibular arches, since superimposition techniques were directly applied to the maxillary arches [124, 130]. Schmidt et al. [146] proposed two methods of superimposing digital models by presenting mathematical formulas which utilized the principles of force/moment equilibrium and minimizing the volume of bone remodeling. Despite the potential areas of stability presented in literature, there is a lack of unity regarding the recommended stable region. There are also limitations on what anatomical features are included in the retrieved intraoral scans in the thesis research, which prevents the application of suggestions such as portions of the mandible which would not be available in an intraoral scan. Additionally, due to the ethical concerns arising from unnecessary radiation exposure when obtaining multiple CBCT scans, it is best to avoid this scanning procedure as measurements can still be tracked through intraoral scans.

Orthodontic aligner-based papers were also investigated to broaden the search for recommended regions of stability for the mandibular arches. The posterior teeth were utilized in some studies for superimposing the mandibular scans and were assumed to remain stable despite the observance of slight movement [32, 147]. Other papers that used the stable posterior teeth included the premolars and molars as reference surfaces [148, 149], while one study used all but one tooth that was simulated for movement as “untreated” reference surfaces for superimposition [150]. The use of the untreated molars was applied by another study where the post-treatment molars were segmented and registered onto the full pre-treatment model [151]. One study suggested that the use of stable teeth should only be applied for the cases where only a few teeth were planned to be displaced [152]. Even then, Lombardo et al. [152] explained that there could be collateral effects on the other tooth positions, which was observed in Charalampakis et al. [32]. Based on the available literature, the use of untreated teeth as a reference region for surface superimposition is feasible in the thesis research, being aware of the existing limitations.

### 2.4.3 Measuring Clinical Tooth Movement from Optical Dental Scans

Analysis commonly performed following the alignment of dental scans over treatment time points is the measurement of changes in tooth positions over treatment. A variety of techniques have been employed by previous literature to make these quantitative evaluations to compare pre- and post-treatment dentition. Some of these ways included superimposing the individual tooth of interest from the pre-treatment model to the post-treatment model, manual evaluation using measuring tools within the software, or automatic software-based measurements.

Several studies have applied an individual tooth superimposition approach to measure the three-dimensional tooth movements. Subsequent to the superimposition of the dental models, a local coordinate system (origin at centroid of tooth's crown) was established on each segmented pre-treatment tooth of interest and after superimposition of these individual teeth on the post-treatment teeth, the required movements represented the position changes and were recorded as the local X-, Y-, Z-movements and rotations [33]. In Grauer and Proffit [121], the tooth centroids were considered to measure position changes with respect to individual local tooth coordinate systems. Chen et al. [153] had also applied the same method and calculated the tooth movements using the transformation matrix outputs from the individual tooth superimpositions. Other aligner-based studies investigating treatment efficacy had utilized the same methods and the positions were automatically calculated by the software in the local direction of each tooth [154–156], as opposed to using the general model coordinate system [33].

Other literature previously introduced for coordinate system construction methods had measured movements over various treatments through comparing landmark coordinates within 2D planes. For example, Ashmore et al. [117] studied the movements of molars by using the centroid of selected molar points and Canan and Senisik [118] landmarked the mesio-incisal edge of the incisors and the cusp tips of the canines, first premolars, and first molars. Other papers that made horizontal and vertical measurements of maxillary and

mandibular incisor/molar movements similarly selected the edges of the incisors and the cusp tips of the first molars [31, 119, 144, 157]. Once the required landmarks were selected on the models of interest, the differences in position between the landmarks were calculated within the main model coordinate systems previously established. Some works used a different approach where the tooth movement measurements were made with respect to the helical axis system instead of the rectangular coordinate system to enhance the visualization of positional changes over treatment [158, 159].

Measuring tools used within software were another common way studies measured tooth movements between selected landmarks. Some studies used a ruler tool and Q3DC tool (built-in tool for evaluating distances between selected landmarks) both available within the 3D Slicer software for measuring tooth movement components in each direction [32, 129, 133, 160]. When using these types of tools, the horizontal and vertical displacement components were obtained through the selection of the incisal edges and cusp tips for the canines and premolars/molars on the two models of interest [129, 133]. Kravitz et al. [148] utilized the ToothMeasure software, which automatically provided quantitative measurements for tooth movements.

Despite the extensive work done in evaluating tooth movements, these studies primarily investigated the movements occurring between the start and end of treatment only, obtaining measurements with respect to a general coordinate system or individual tooth coordinate systems. In the case of the present research, multiple scans over treatment will be available for analysis; therefore, the movements need to be recorded in consistent directions so that they can be managed and compared for rates over treatment points as well as used for comparison with the mechanical experimental data.

# Chapter 3

## Tracking orthodontic tooth movement and associated biomechanics using an integrated clinical and in vitro mechanical approach

*This chapter introduces a study where biomechanical force systems and clinical tooth movement were evaluated over orthodontic treatment for patient clinical cases by applying intraoral scan analysis techniques and performing in vitro biomechanical experiments. This study addresses the first and second objectives of the thesis by developing a streamlined methodology using patient clinical cases to drive clinical tooth movement and biomechanical data collection. The third objective of the thesis was also addressed through comparing the tooth movement and force pilot data to observe and discuss existing trends to better understand the effect of biomechanical forces on clinical tooth movement over orthodontic braces treatment.*

### 3.1 Introduction

Orthodontic treatment is a dental service known for its positive effects on the quality of life by improving personal aesthetics and oral health [3], as misaligned teeth can lead to tooth decay, periodontal disease, and issues with breathing, chewing, and speech [5]. Orthodontic braces are a common fixed-appliance treatment for straightening misaligned teeth in patients by applying forces/moments through the bracket and archwire interaction to cause dental

movement [7, 8]. Bone remodelling allows for tooth movement to occur due to changes in the periodontal complex, in which bone resorption is conducted by osteoclasts and bone formation is conducted by osteoblasts [6]. The extent of tooth movement is governed by the changes in the local mechanical state as a result of the stresses and strains arising in the periodontal ligament (PDL) from the application of an orthodontic force [9]. Higher orthodontic forces can lead to tissue necrosis in the PDL due to the highly compressed area losing blood supply, resulting in tooth movement delays until undermining resorption occurs [6, 9]. An incomplete understanding of the biomechanical force systems produced during orthodontic treatment and its effect on tooth movement leads to treatment outcome unpredictability, which may result in undesirable tooth movements [14, 15], possible tissue damage such as PDL hyalinization or orthodontically induced inflammatory root resorption (OIIRR) instigated by high force application [6, 8, 16], and longer treatment times due to inefficiency in applied forces.

Experimental studies have investigated the relationship of force levels on tooth movement by applying predefined loading conditions on teeth of human and animal subjects and measuring the initial tooth displacements under the applied force [54, 55]. Other studies considered a longitudinal approach to take account of all phases of orthodontic tooth movement by prolonging the force application time [9, 57, 58]. Further, collected data from clinical/experimental studies were used to establish theoretical models [59] and mathematical models [60] to describe the relationship between force and tooth movement. Despite the many experimental studies performed, differences in experimental setup, variations within and between subjects, and variables pertaining to study length and tooth measurement methods ultimately led to different results for tooth movement rate and recommended optimal load ranges [11, 12]. In addition, these studies were limited to particular teeth under assumed loading conditions instead of tracking actual patient misalignments with unknown initial orthodontic forces acting upon the whole dental arch.

Numerical studies utilizing finite element analysis (FEA) have been used to study the relationship between force and tooth movement. A combination of early and recent studies

applied predefined loading conditions in varying directions on simplified single tooth models to investigate initial tooth displacement/mobility and the stress/strain arising within the PDL complex [63, 64, 66–68, 90], optimal loading conditions [67, 90], and root resorption [70]. Later literature considered multi-tooth models and included orthodontic appliances [78, 80]. Using scans of the patient dentition, common clinical treatments including retractions/space closures and distalization were simulated [20, 81–88, 161, 162], while some others investigated different appliance dimensions and archwire/bracket combinations [80, 84, 88, 89]. Canales et al. [79] studied the initial force transfer on a four-tooth model upon continuous archwire insertion by utilizing the element birth-death technique in simulations; Zhou et al. [17] also incorporated this technique in similar work but for a full dental arch.

In an attempt to predict orthodontic tooth movement over treatment in longevity, recent studies implemented algorithms or developed models alongside the performed FEA for comparability/applicability to clinical data. Likitmongkolsakul et al. [19] followed a sample patient clinical treatment to retrieve dentition scans over treatment intervals, driving numerical analysis to establish a tooth movement prediction model that was then clinically validated using another patient case. Chen et al. [20] and Dot et al. [92] also retrieved patient clinical scans over treatment and utilized FEA modelling algorithms to retrieve tooth movements that were then compared with the clinically measured tooth movements. Despite the extensive numerical analysis available, the general requirement for an assumed force or displacement condition within the simulation model limits the investigation of patient alignment treatment, where the orthodontic force and tooth movements are unassumed and need to both be evaluated over treatment.

The biomechanics of braces has been extensively studied in a mechanical experimental approach through developing various measurement systems including in vivo devices [8, 95, 96], and numerous in vitro devices [15, 22–24, 99, 101, 107, 110]. Common misalignment cases were investigated by simulating displacement of artificial teeth [27, 104, 110, 114], replicating/digitally modifying models of scanned patient geometry [17, 23, 24, 100, 113], and replicating patient bracket positions [24], to measure the biomechanical loads that occur

for various treatment conditions. Due to measurement limitations in many in vitro devices, studies often considered only part of the arch where the misalignment was located [23, 100], or had repeated experiments to obtain data across the whole arch [17, 24]. In addition to most studies performing experiments based on simulated misalignments, those that did consider patient cases mainly involved the collection of biomechanical information at the start of treatment, which in turn lacked the long-term tracking of forces and comparison to clinical tooth movements.

Despite a significant body of work studying orthodontic biomechanics, there remains a lack of investigations that longitudinally compare clinical tooth movement with experimentally measured biomechanical forces. Additionally, studies showed the necessity for assuming an initial applied force or tooth displacement within the experimental models to drive data collection. This study applies a designed process to replicate bracket positions from patient clinical cases onto an in vitro Orthodontic Simulator (OSIM) [15] to measure forces produced from braces to determine their effect on clinical tooth movement during treatment. This pilot study was undertaken with the following objectives: 1. Collect and superimpose patient intraoral scans using developed registration methods to retrieve clinical tooth movement measurements and bracket positions over treatment; 2. Replicate bracket positions using custom jigs mounted on the OSIM and collect pilot data for sample patient arches by measuring experimentally generated forces; 3. Identify existing trends between the clinical tooth movement and in vitro experimental data to gain insight on how orthodontic forces produced by braces affect the tooth movement over treatment.

## **3.2 Methods**

### **3.2.1 Clinical Data Collection and Analysis**

All clinical aspects of the current study were approved by the University of Alberta's Research Ethics Office (Pro00112968). Patient recruitment criteria included healthy male and female patients with full permanent dentition where possible (not including third molars),

presenting mild anterior crowding (2-4mm) and being treated using orthodontic braces. The maxillary and mandibular arches of four patients (2 male, 2 female) between 11-14 years old were initially considered for the study. The orthodontic appliance components used in treatment were Damon Q2 brackets (slot size 0.022") (Ormco, USA) and three sets of Ormco copper-nickel-titanium (CuNiTi) round archwires (0.014", 0.016", 0.018"). Brackets were bonded on all teeth excluding the second molars. Four scans were collected for each patient arch in approximate 6- to 8-week intervals when archwire sizes were increased following treatment protocol, starting after bracket bonding (Time 1) up until the 0.018" archwires were switched to rectangular wires (Time 4) as summarized in Figure 3.1. Digital scanning was performed using an iTero Element intraoral scanner (Align Technology, San Jose, California) posing no radiation risks to patients. This device utilizes the parallel confocal method (a powder-free method) where a laser light is projected for the collection of image slices, which are then stitched together [28]. Intraoral images were taken to reconstruct 3D models of the patient arches at each treatment time point and exported as .STL files. (Fig. 3.2a, Fig. 3.3a).

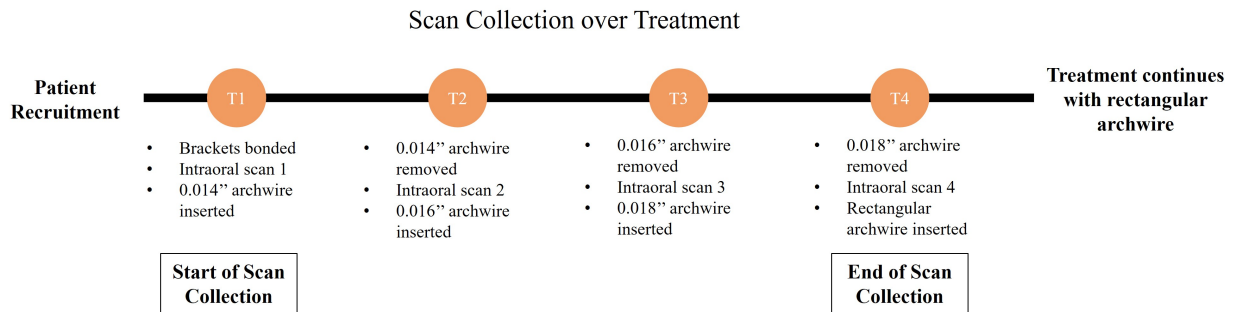


Figure 3.1: Intraoral scan collection protocol for recruited patients over orthodontic treatment with treatment intervals (T1-T4) and archwire changes indicated

3D Slicer (open-source, version 4.11; <https://www.slicer.org/>) [163] was used for scan analysis, where scans over multiple time points for a specific patient arch were aligned to retrieve bracket position data. The Time 1 model was first oriented by selecting the canine and inner anterior first or second molar cusps to establish representative lines for applying translational and rotational transformations (Appendix A.1). Subsequent maxillary scans

were then superimposed onto the Time 1 scan using the medial 2/3rds of the third palatal rugae as a stable region [30, 33, 142]. The rugae surfaces were manually segmented and separated from the rest of the model and were superimposed onto the full T1 model using the Surface Registration tool (Fig. 3.2b) (Appendix A.2). The output transformation from this initial registration was applied for alignment of the entire model (Fig. 3.2c). Errors in superimposing the rugae for maxillary scans were evaluated in 3D Slicer using the Model to Model Distance tool and Mesh Statistics tool to evaluate the Hausdorff distance between the rugae surfaces of interest (Appendix A.2).

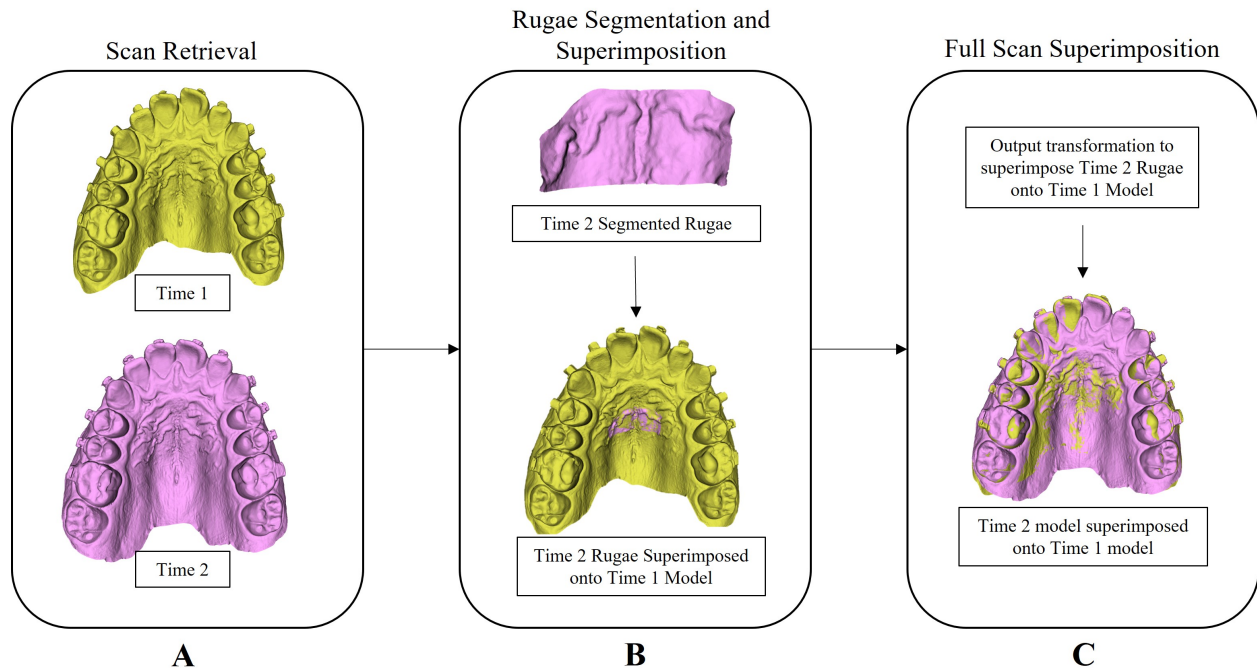


Figure 3.2: Summarized workflow for clinical maxillary scan superimposition; a). Time 1 and Time 2 maxillary arch models for sample patient case opened in Slicer software, b). Segmentation and superimposition of Time 2 rugae region onto the full Time 1 model, c). Superimposition of full Time 2 model on Time 1 model by applying transformation matrix from initial rugae superimposition

Due to the lack of stable landmarks for the mandibular arch, the posterior untreated second molars were used [32, 148, 157, 164]. In cases where the patient arch did not have fully erupted second molars, the first molars were used for superimposition. The molar surfaces were manually segmented and separated from the rest of the model and were initially

superimposed using the Surface Registration tool (Fig. 3.3b) (Appendix A.2). Similar to the maxillary superimposition, the output transformation from this initial registration was then applied for alignment of the entire model (Fig. 3.3c). The Model to Model Distance tool and Mesh Statistics tool were utilized again to evaluate the Hausdorff distance between the T1 molars and subsequent molars of interest in order to evaluate errors in superimposition.

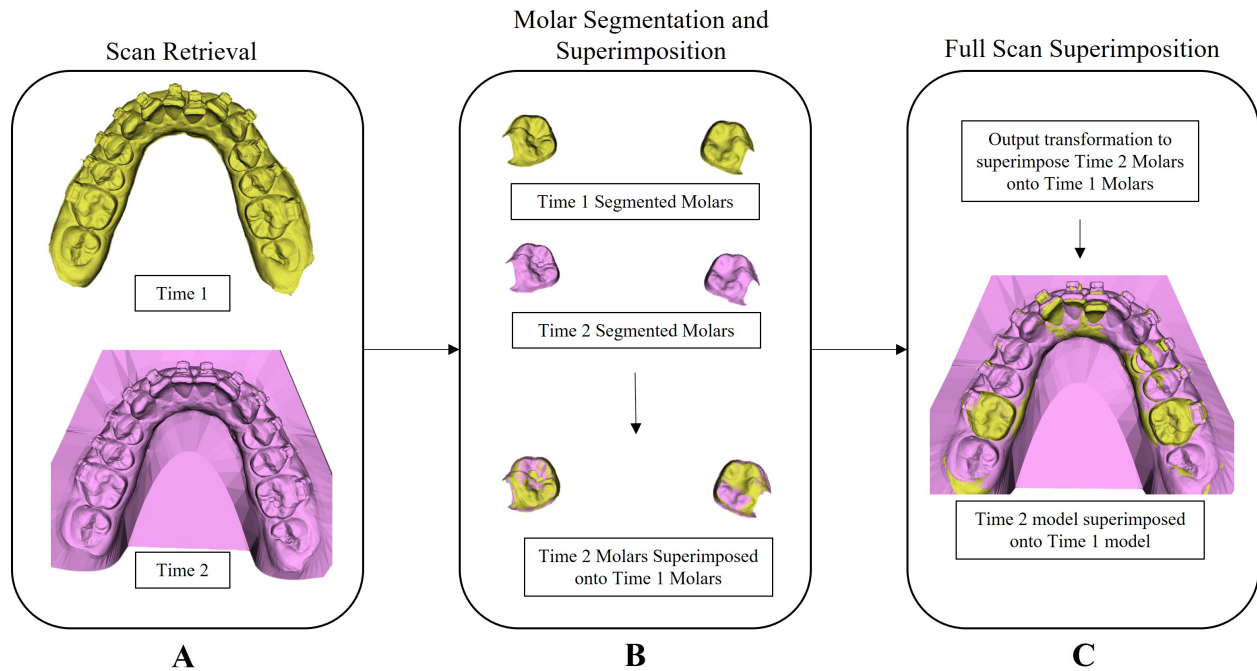


Figure 3.3: Summarized workflow for clinical mandibular scan superimposition; a). Time 1 and Time 2 mandibular arch models for sample patient case opened in Slicer software, b). Segmentation and superimposition of Time 2 molars onto segmented Time 1 molars, c). Superimposition of full Time 2 model on full Time 1 model by applying transformation matrix from initial molar superimposition

For the superimposed scans (Fig. 3.4a), a manual approach was taken to select four points per bracket to remain consistent despite varying scanning conditions (e.g. namely, bracket gates open or closed). The first two points were selected at the outer front edges below the slot of the scanned brackets and another two points were selected directly underneath as a way of determining individual bracket orientation within the scan (Fig. 3.4b). Intra-rater reliability for manual selection was assessed using three random mandibular scans and three bracket position selection times, each evaluated approximately one week apart by the oper-

ator (Appendix A.3). Final midpoint position coordinates were compared across selection times by applying the Repeated Measures ANOVA (RMANOVA) test for each scan separately. ICC values were calculated using the equation provided in [165] and the calculated values were  $> 0.998$ . The collection of points for each arch was imported to an in-house developed code in MATLAB (MathWorks, Natick, USA) to retrieve the bracket slot positions (Fig. 3.4b) (Appendix A.3). Code calculations to retrieve bracket slot endpoint positions involved the application of coordinate transformations and nominal bracket dimensions on the first pair of initially selected points (Fig. 3.4b). The bracket slot position data was imported to another in-house developed MATLAB code to calculate orthodontic tooth movements between two time points of treatment through the positional changes in the slot midpoints (Fig. 3.4c) (Appendix A.4). The tooth movement component calculations were based on the local coordinate systems as defined by the OSIM micrometer/cantilever arm angles in Figure 3.5. This was done intentionally for consistent comparison between tooth movement and force results over treatment intervals.

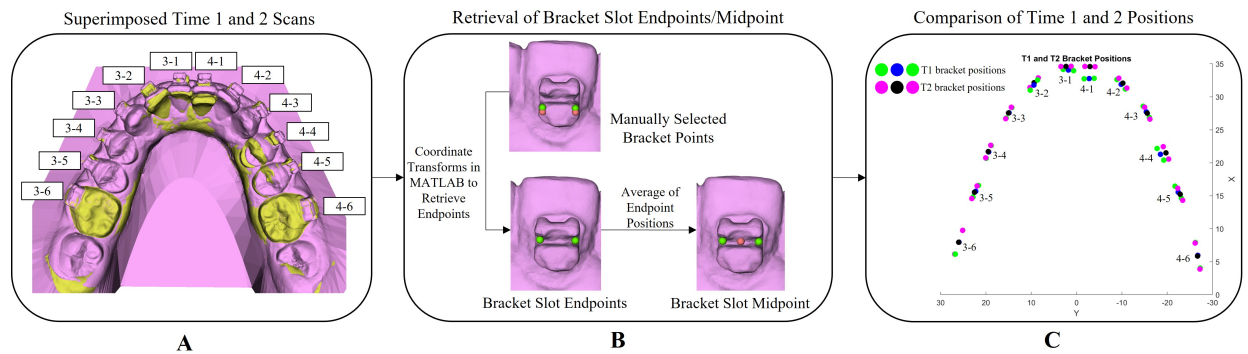


Figure 3.4: Retrieval of bracket slot endpoint and midpoint positions from clinical scans; a). Superimposed Time 1 and Time 2 mandibular scans with tooth number labels based on FDI system, b). Manual selection of four points on bracket, MATLAB coordinate transformations applied to manually selected points to obtain slot endpoint locations, and calculation of slot midpoint using slot endpoint coordinates, c). Plot of bracket positions for Time 1 and 2 scans in MATLAB to visualize and calculate tooth movement over two points of treatment

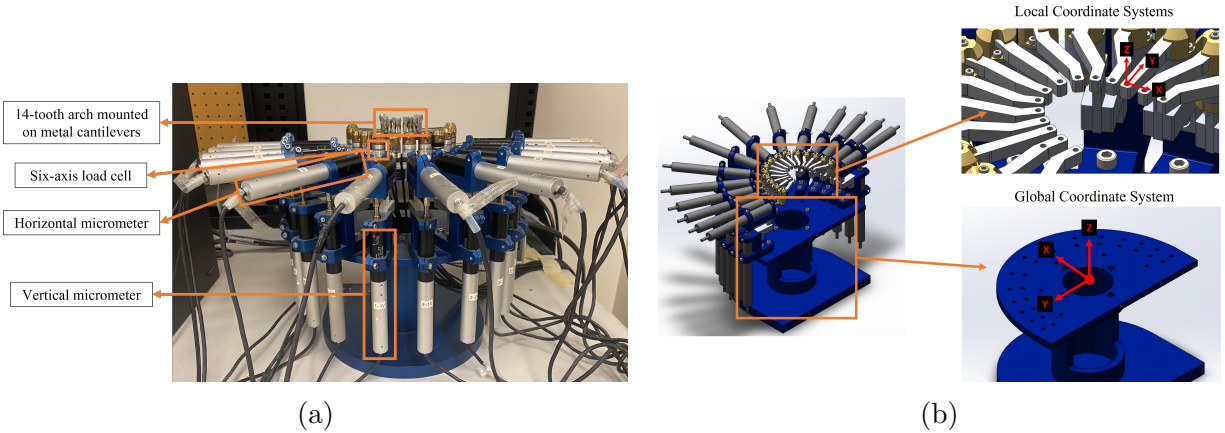


Figure 3.5: Overview of the in vitro Orthodontic Simulator (OSIM); a). Overview of OSIM with dental arch, load cells, and micrometers labelled, b). Schematic of OSIM indicating the constructed local and global coordinate systems utilized for clinical and experimental data collection

### 3.2.2 Mechanical Experimental Data Collection

To measure the biomechanical forces present on the patient arch at different time points of treatment, the bracket midpoint positions calculated for each clinical scan were replicated onto the OSIM. The OSIM (Fig. 3.5), previously described in literature [15, 116], is an in vitro electromechanical system equipped with 14 load cells (Nano17, ATI Industrial Automation) for 3D force and moment measurements, along with horizontal/vertical micrometers for positioning individual teeth for a fourteen-tooth arch (FDI notation used) [15]. Additively manufactured jigs were designed to assist with bracket position replication (Fig. 3.6) to overcome existing OSIM limitations of replicating patient geometries (i.e. micrometer movements only possible in buccal-lingual and occlusal-gingival directions). Jigs were manufactured using the Formlabs Form 3 SLA 3D printer (Formlabs, Massachusetts, USA) using standard grey resin material and a layer height resolution of 25 microns. A default jig configuration was designed in SolidWorks 2022 (Dassault Systemes, Massachusetts, USA) allowing for unique jig sets for each treatment interval to be created by measuring global and local positional differences between the scanned bracket positions and OSIM's tooth mounting hole positions in MATLAB to obtain the unique jig dimensions (Fig. 3.6b-

c) (Appendix B.1, B.2). The same bracket type used in the patient’s treatment was bonded to the individual jigs using light cured Transbond XT (3MT Unitek) and mounted onto the OSIM (Fig. 3.6d). Bracket sets exclusively used for in vitro experiments were cleaned using a micro abrasive sand blaster (Vaniman Manufacturing Co., Murrieta, USA) and reused for each time point to ensure they remained consistent throughout experiments, mimicking patient clinical treatment. The bracket’s positional and rotational replication accuracy was evaluated for every jig set using a FaroArm coordinate measurement device (Faro Technologies, Lake Mary, USA) (Appendix B.3). After establishing the global coordinate system on the OSIM (Fig. 3.5b), the bracket endpoints were measured and compared with the scanned bracket positions. The local Y-direction and Z-direction errors were remedied by moving the OSIM’s respective micrometers (Appendix B.4), while local X-directional errors remained unchanged due to the micrometer’s inability to control that movement.

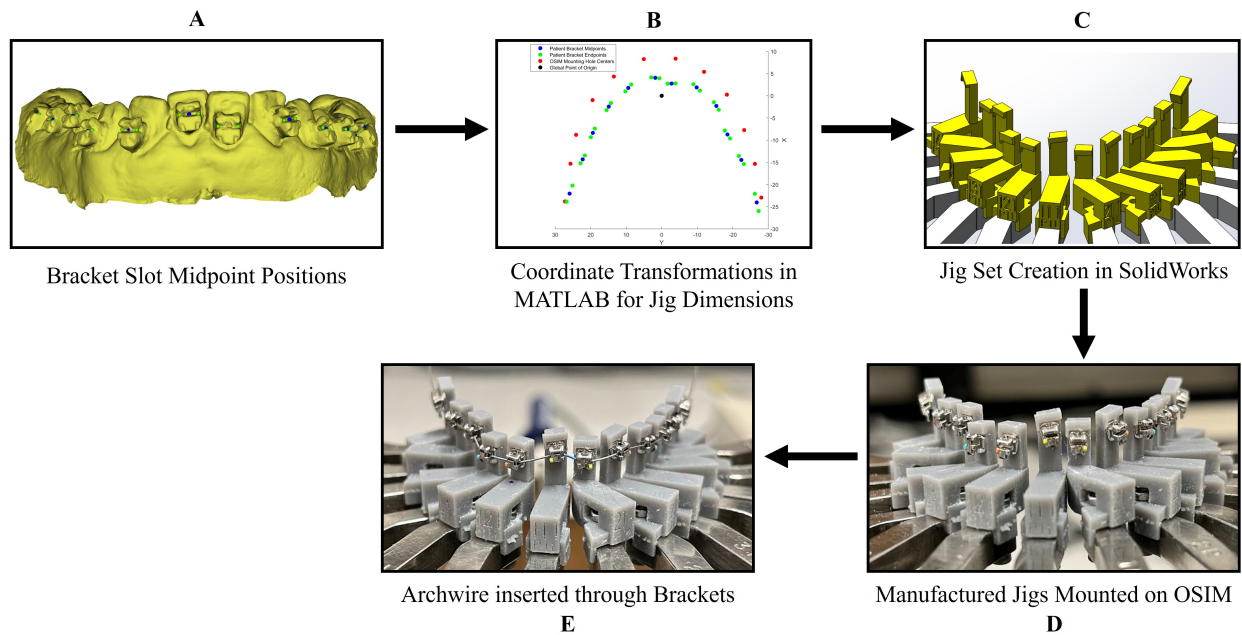


Figure 3.6: Summarized workflow for experimental data collection; a). Patient scan in Slicer with plotted slot endpoints/midpoints calculated in MATLAB, b). Mapping of patient bracket positions and cantilever holes in MATLAB for application of transformation matrices to determine jig dimensions, c). SolidWorks assembly of generated sample jig set based on calculated dimensions, d). Printed jig set mounted on OSIM with bonded brackets, e). Archwire inserted through brackets for experimental measurements of biomechanical forces at each bracket

A heating chamber maintained at 37°C was placed over the OSIM and all archwires to be tested 1.5 hrs prior to starting experiments to simulate intraoral temperature conditions. For the bracket positions at each time interval of treatment, the corresponding jig set was secured onto the OSIM and biomechanical force collection was completed as outlined in Figure 3.7. A sample size of five archwires per archwire size was used to measure the average initial and final forces at each tooth upon archwire insertion through the brackets. At T1, the 0.014” sized CuNiTi archwires were inserted to measure initial forces and reinserted for the T2 jig set to measure the end forces. Similarly, the 0.016” archwires were inserted for the T2 jig set to measure initial forces and T3 jig set to measure end forces, while the 0.018” archwires were inserted into the T3 and T4 jig set for initial and end force measurement, respectively. Forces were originally measured at the load cell and transformed to the bracket slot midpoint by first measuring the location of the bracket midpoint with respect to the load cell by selecting points with the FaroArm. Coordinate systems were constructed at both locations within the FaroArm software to then generate the Jacobian transformation matrices between these two locations. The directional components of force occurring at the bracket midpoint were measured with respect to the OSIM local coordinate systems.

### 3.3 Results

For the sample patient arches considered in this work, Patient 1’s maxillary arch was excluded due to the absence of required palate surface features on the intraoral scan for surface-based superimposition. Therefore, four mandibular arches ( $n=4$ ) and three maxillary arches ( $m=3$ ) were considered for further analysis. The Hausdorff distances, representing superimposition errors to align the Time 2-4 segmented surfaces with the Time 1 surfaces, are provided in Table 3.1. The errors reported are the absolute 95th percentile, where the average superimposition error across all samples was 0.19 mm. The average replication errors of all bracket positions on the OSIM in comparison to the scan positions is presented in Table 3.2 for each patient. Across all arches, an average local X-direction error of 0.60 mm, local Y-direction error of 0.44 mm, and Z-direction error of 0.19 mm were measured, leading to

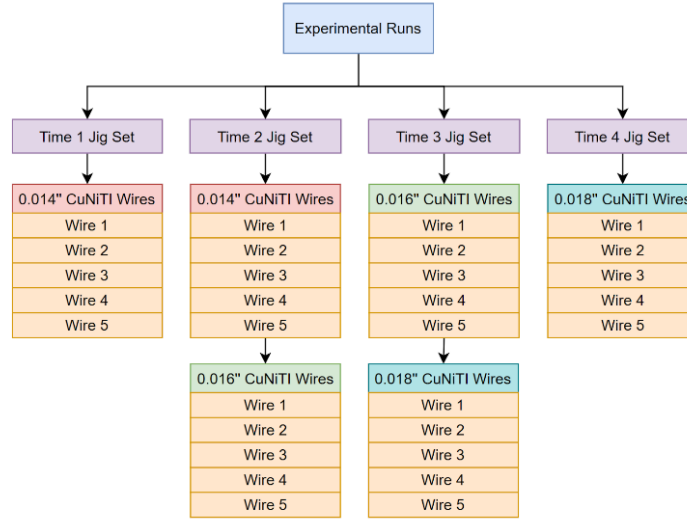


Figure 3.7: Summary of experimental runs for biomechanical force collection of each sample dental arch, where archwire samples of each size were inserted to measure the initial force for the respective time interval and reinserted to measure the end force for the subsequent time interval (jig set) prior to archwire size increase

an average error of 0.41 mm across directions. Positional errors in the local Y-direction and vertical direction were mitigated through post-hoc micrometer movements to correct errors in those directions, simplifying the remaining average error to 0.60 mm in-plane prior to experiments. Rotational errors were also evaluated, and the average bracket and tooth rotation error was  $3.24^\circ$  and  $5.86^\circ$ , respectively.

Figures 3.8-3.9 present the measured average start and end forces along with the calculated orthodontic tooth movements in 3D (see Table 3.3 for sign convention) over treatment for the mandibular arches and maxillary arches, respectively. It is noted that Patient 2's mandibular treatment was only followed to T3 due to a missing bracket in the T4 scan that prevented necessary analysis. The force and tooth movement analysis in this study was limited to the six anterior teeth (Tooth 2-3 to 1-3 for maxillary arches and Tooth 3-3 to 4-3 for mandibular arches) given the clinical focus surrounded mild anterior crowding. Additionally, since mild anterior crowding was treated, the forces in the X-direction were omitted from the presented results as it is generally less prominent in comparison to the other directions. Start force and tooth movement magnitude ranges in the Y-direction were

0.00-1.43 N and 0.03-1.81 mm for Patient 1, 0.02-1.06 N and 0.00-0.63 mm for Patient 2, 0.02-1.18 N and 0.01-0.87 mm for Patient 3, and 0.02-1.30 N and 0.03-1.78 mm for Patient 4 over treatment. In the Z-direction, the magnitude ranges were 0.01-2.17 N and 0.01-1.45 mm for Patient 1, 0.00-0.88 N and 0.01-1.36 mm for Patient 2, 0.02-1.41 N and 0.01-1.45 mm for Patient 3, and 0.02-1.38 N and 0.00-1.24 mm for Patient 4 over treatment. For the purposes of further discussion, a tooth movement threshold of 0.5 mm was set on the data presented in Figures 3.8-3.9 to discuss cases where the observed tooth movements were more probable. The threshold value was determined based on the influential errors present prior to tooth movement and force measurement, in which the average superimposition error was 0.19 mm and the average bracket position replication error across directions was 0.41 mm. To remain conservative, a greater threshold bound of 0.5 mm was chosen.

Table 3.1: Patient scan superimposition errors represented by calculated Hausdorff distances (95th percentile reported)

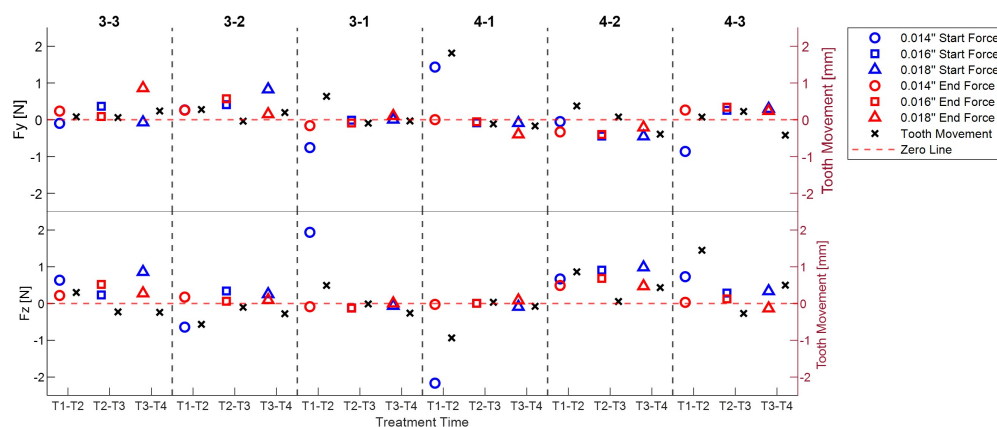
Patient Arch	Superimposition Error (Absolute 95th Percentile) [mm]			
	T2 On T1	T3 On T1	T4 On T1	Average Error
<b>P1 Mandibular</b>	0.160	0.241	0.279	0.227
<b>P2 Maxillary</b>	0.050	0.063	0.158	0.090
<b>P2 Mandibular</b>	0.154	0.220	N/A	0.187
<b>P3 Maxillary</b>	0.110	0.129	0.084	0.108
<b>P3 Mandibular</b>	0.381	0.419	0.420	0.407
<b>P4 Maxillary</b>	0.085	0.067	0.063	0.072
<b>P4 Mandibular</b>	0.176	0.207	0.267	0.217

Note: Reported errors are based on comparison of the molars for mandibular arches and third rugae for maxillary arches

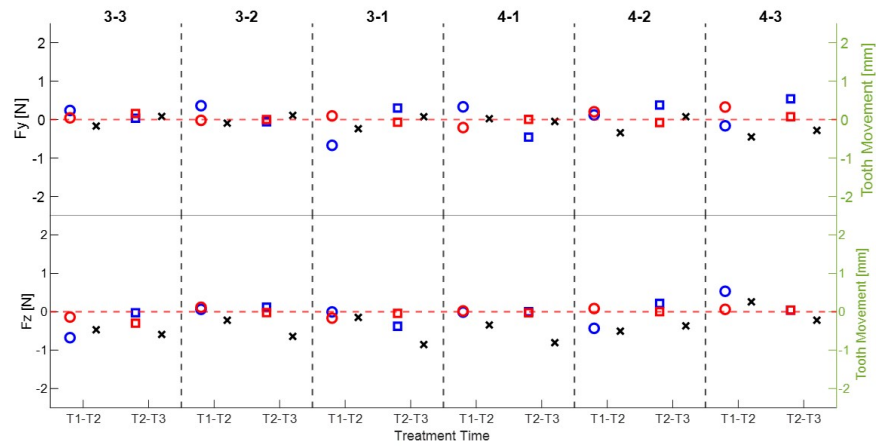
Table 3.2: Average patient bracket position translation and rotation replication errors in the local OSIM cantilever directions for the patient mandibular arches and maxillary arches

Average Replication Error	P1 (n=1, m=0)	P2 (n=1, m=1)	P3 (n=1, m=1)	P4 (n=1, m=1)	Mand arches (n=4)	Max arches (m=3)	Across all arches
Local X-Direction [mm]	0.54	0.61	0.62	0.60	0.59	0.62	0.60
Local Y-Direction [mm]	0.35	0.48	0.46	0.44	0.42	0.47	0.44
Z-Direction [mm]	0.17	0.21	0.21	0.17	0.19	0.19	0.19
Bracket Rotation [°]	2.70	3.68	2.66	3.67	3.39	3.05	3.24
Tooth Rotation [°]	3.73	6.85	6.43	5.35	4.83	7.23	5.86

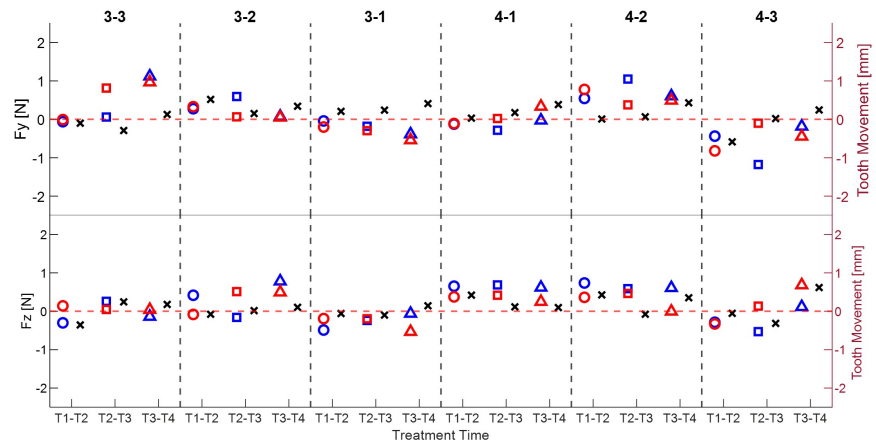
Note: Mand = Mandibular, Max = Maxillary



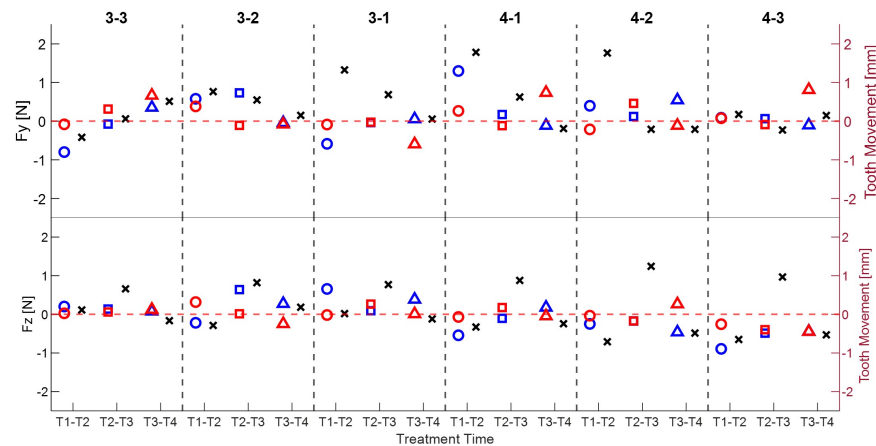
(a)



(b)

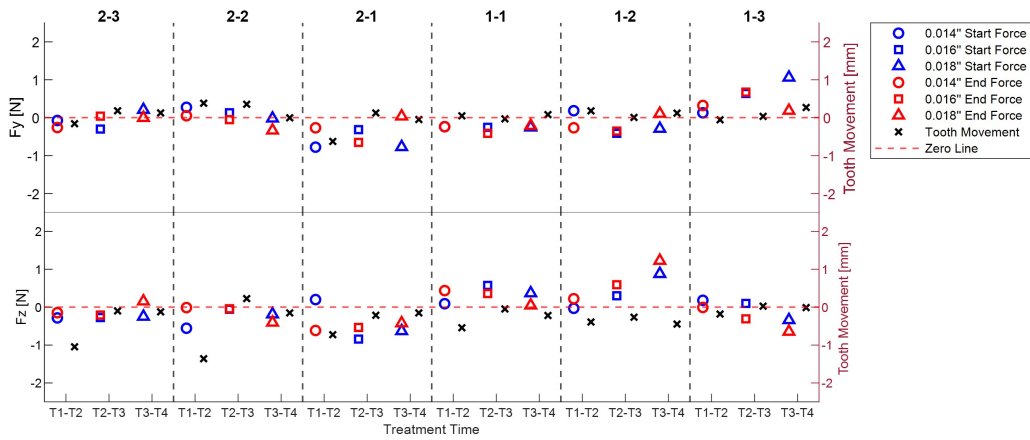


(c)

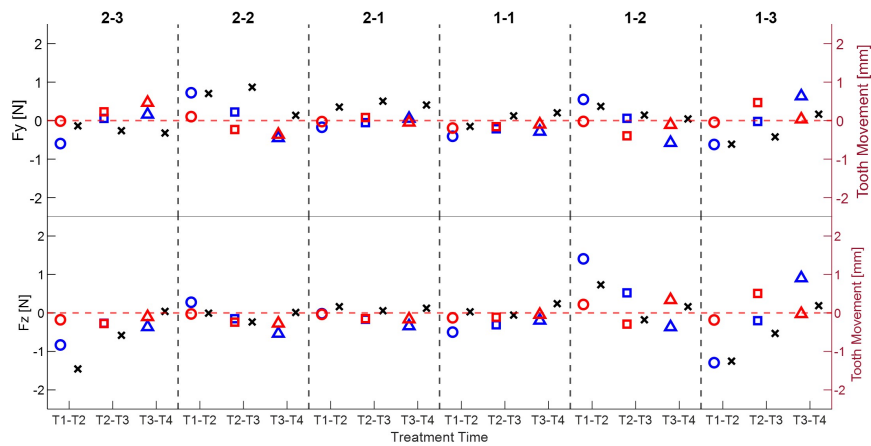


(d)

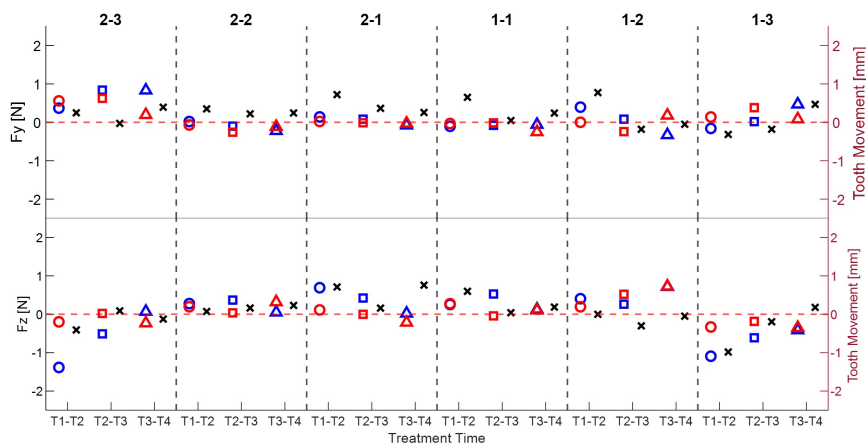
Figure 3.8: Orthodontic force and tooth movement results for the anterior teeth of patient mandibular arches (Tooth 3-3 to 4-3) in Y- and Z-direction; a). Patient 1 mandibular arch, b). Patient 2 mandibular arch, c). Patient 3 mandibular arch, d). Patient 4 mandibular arch



(a)



(b)



(c)

Figure 3.9: Orthodontic force and tooth movement results for the anterior teeth of patient maxillary arches (Tooth 2-3 to 1-3) in Y- and Z-direction; a). Patient 2 maxillary arch, b). Patient 3 maxillary arch, c). Patient 4 maxillary arch

Table 3.3: Dental arch coordinate system describing positive sign convention for biomechanical force and tooth movement measurements in the Y- and Z-direction

<b>Quadrant</b>	<b>Fy</b>	<b>Fz</b>
First Quadrant (Tooth 1-1 to 1-6)	Buccal	Gingival
Second Quadrant (Tooth 2-1 to 2-6)	Buccal	Gingival
Third Quadrant (Tooth 3-1 to 3-6)	Buccal	Occlusal
Fourth Quadrant (Tooth 4-1 to 4-6)	Buccal	Occlusal

Notable consistent trends with the same direction of force and tooth movement were observed for some of the teeth of each patient arch. A trend was considered as directionally consistent for a tooth if the force and tooth movement data were obtained in the same direction, as it would be expected that a force in a particular direction should initiate a tooth movement in the same direction. There were also inconsistent trends where opposing force and tooth movement directions were observed. Table 3.4 provides a full summary of the directionally consistent and inconsistent cases observed across patients when the 0.5 mm tooth movement threshold was considered.

The directional trend consistency for force and tooth movement was evaluated, and a full summary for all arches is provided in Table 3.5. When a tooth movement threshold of 0.5 mm was considered, the average trend consistency based on available cases across patients were 87.14%, 60.19%, and 100.00% for the 0.014" archwire, 0.016" archwire, and 0.018" archwire, and 77.78%, and 82.38% in the Y- and Z-direction, respectively.

Table 3.4: Directionally consistent and inconsistent initial force and tooth movement cases for each patient over treatment when a tooth movement threshold of 0.5 mm is considered

Patient	Directional Trend	Treatment Interval					
		T1-T2		T2-T3		T3-T4	
		Tooth	Dirn	Tooth	Dirn	Tooth	Dirn
1	Consistent	3-2	Z	N/A	N/A	N/A	N/A
		4-1	Y/Z				
		4-2	Z				
		4-3	Z				
	Inconsistent	3-1	Y	N/A	N/A	N/A	N/A
2	Consistent	2-1	Y	3-1	Z	N/A	N/A
		2-2	Z	3-3	Z		
		2-3	Z				
		4-2	Z				
	Inconsistent	1-1	Z	3-2	Z	N/A	N/A
		2-1	Z	4-1	Z		
3	Consistent	1-2	Z	1-3	Z	4-3	Z
		1-3	Y/Z	2-2	Y		
		2-2	Y	2-3	Z		
		2-3	Z				
		3-2	Y				
		4-3	Y				
	Inconsistent	N/A	N/A	2-1	Y	N/A	N/A
4	Consistent	1-1	Z	3-1	Z	2-1	Z
		1-2	Y	3-2	Y/Z	3-3	Y
		1-3	Z	3-3	Z	4-3	Z
		2-1	Y/Z	4-1	Y		
		3-2	Y				
		4-1	Y				
		4-2	Y/Z				
		4-3	Z				
	Inconsistent	1-1	Y	3-1	Y	N/A	N/A
		3-1	Y	4-1	Z		
				4-2	Z		
				4-3	Z		

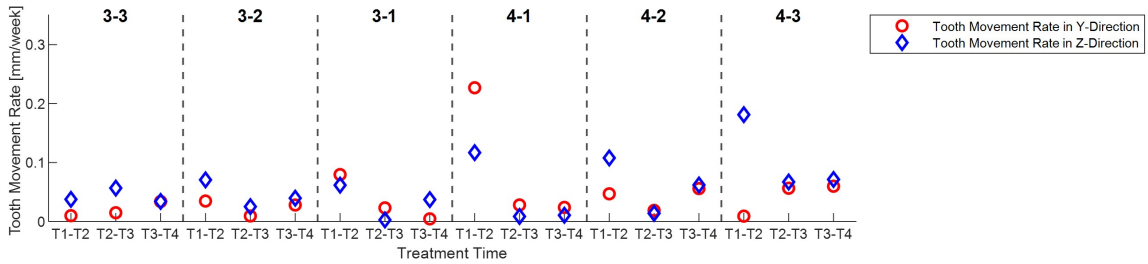
Note: Tooth movement threshold of 0.5 mm was set prior to investigating case trends. N/A entries mean that there were no available cases to analyze after applying the tooth movement threshold.

Table 3.5: Initial force and tooth movement trend consistency for each patient arch over treatment in Y- and Z-direction and for each archwire size when 0.5 mm tooth movement threshold is considered

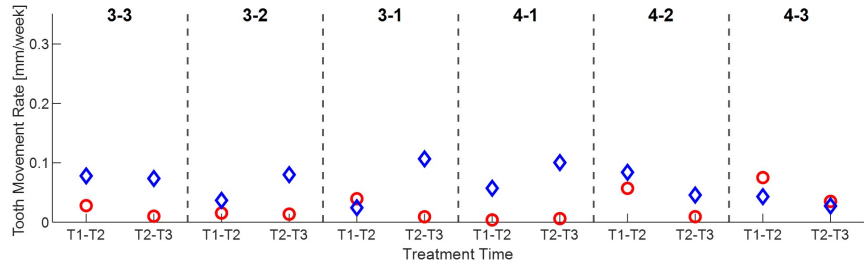
Patient Arch	Trend Consistency with Tooth Movement Threshold [%]				
	Y- Direction	Z- Direction	0.014” Archwire	0.016” Archwire	0.018” Archwire
<b>P1 Mandibular</b>	50.00	100.00	83.33	N/A	N/A
<b>P2 Maxillary</b>	100.00	50.00	60.00	N/A	N/A
<b>P2 Mandibular</b>	N/A	60.00	100.00	50.00	N/A
<b>P3 Maxillary</b>	75.00	100.00	100.00	75.00	N/A
<b>P3 Mandibular</b>	100.00	100.00	100.00	N/A	100.00
<b>P4 Maxillary</b>	66.67	100.00	83.33	N/A	100.00
<b>P4 Mandibular</b>	75.00	66.67	83.33	55.56	100.00
<b>Average</b>	77.78	82.38	87.14	60.19	100.00

Note: Tooth movement threshold of 0.5 mm was set prior to investigating case trends. N/A entries mean that there were no available cases to analyze after applying the tooth movement threshold.

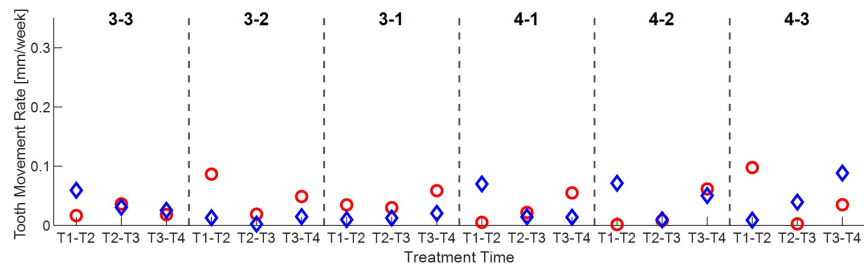
Finally, the magnitude of tooth movement rates over treatment were assessed for the six anterior teeth of each patient arch and are presented in Figures 3.10-3.11. Rates of tooth movement [mm/week] were calculated during the use of each archwire size by dividing the magnitude of calculated tooth movements in the Y- and Z-direction by the length of time between two treatment points (the number of weeks between collected scans/archwire changes, which varied within each patient’s treatment). The range of tooth movement rates in the Y-direction were 0.00-0.23 mm/week for Patient 1, 0.00-0.10 mm/week for Patient 2, 0.00-0.12 mm/week for Patient 3, and 0.00-0.30 mm/week for Patient 4 over treatment. In the Z-direction, the magnitude of rates ranged from 0.00-0.18 mm/week for Patient 1, 0.00-0.23 mm/week for Patient 2, 0.00-0.24 mm/week for Patient 3, and 0.00-0.14 mm/week for Patient 4 over treatment.



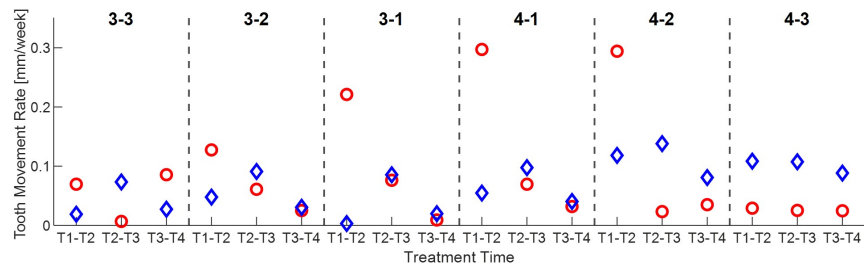
(a)



(b)

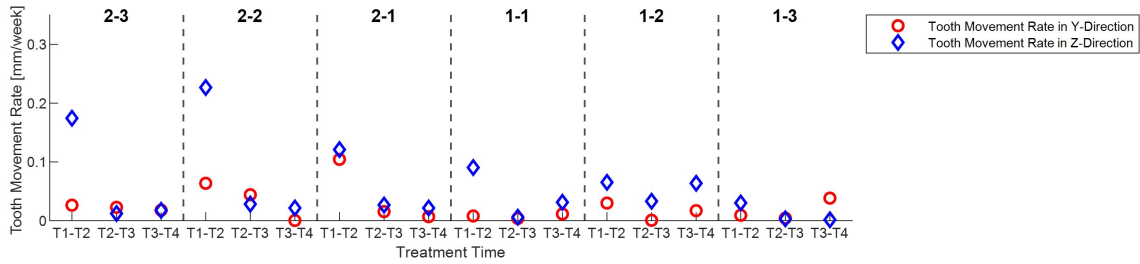


(c)

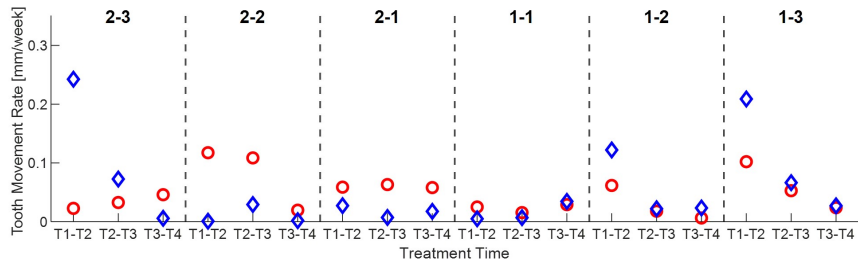


(d)

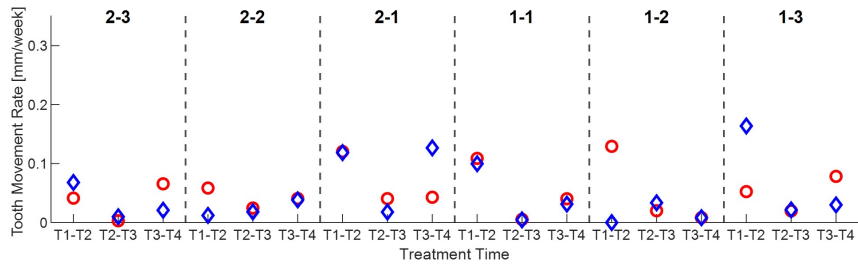
Figure 3.10: Orthodontic tooth movement rates (magnitude) over treatment for the anterior teeth of patient mandibular arches (Tooth 3-3 to 4-3) in Y- and Z-direction; a). Patient 1 mandibular arch b). Patient 2 mandibular arch, c). Patient 3 mandibular arch, d). Patient 4 mandibular arch



(a)



(b)



(c)

Figure 3.11: Orthodontic tooth movement rates (magnitude) over treatment for the anterior teeth of patient maxillary arches (Tooth 2-3 to 1-3) in Y- and Z-direction; a). Patient 2 maxillary arch b). Patient 3 maxillary arch, c). Patient 4 maxillary arch

### 3.4 Discussion

Based on past literature, there is a deficiency in longitudinal collection of biomechanical data. Limited conclusions have been reported from the existing in vivo/in vitro experimental work and numerical work in terms of the relationship between orthodontic force and tooth movement over the full orthodontic treatment period. In this study, pilot data was collected for seven sample arches using a novel approach utilizing clinical cases for tracking orthodontic tooth movement and replication onto the OSIM for measuring biomechanical force systems. Therefore, this work employed a combined clinical and experimental ap-

proach to measure both tooth movement and orthodontic force over treatment using fixed orthodontic appliances. Both force and tooth movement were measured with respect to the local coordinate systems of the in vitro OSIM as presented in Figure 3.5b, to directly compare the two variables over treatment.

### **3.4.1 Errors in Scan Superimposition and Bracket Position Replication**

Scans over treatment were superimposed and compared with the initial T1 scan to evaluate errors in superimposition using the Model to Model Distance tool and Mesh Statistics tool in Slicer. The 95th percentile errors are representative values at which only 5% of the measured distances (point to point distances) between the stable region surfaces are above the reported value. Since the errors can not be evaluated on other parts of the arch due to possible changes over treatment (i.e. orthodontic tooth movement), propagation of alignment error may occur moving farther away from the stable region site. Therefore, these errors will have direct impact on the tooth movement calculations, especially for teeth farthest from the stable region used in surface superimposition. This can then lead to artificially larger tooth movements over treatment intervals if the arches are tilted with respect to each other.

Errors in bracket position replication were evaluated for each jig set used for experiments. Since the measured errors were with respect to the cantilever directions, the applicable micrometers were used to mitigate errors in the controllable Y- and Z-directions prior to experiments. Despite these steps taken to improve errors, the remaining discrepancies in the mesial-distal direction may still affect the measurement of biomechanical forces. Such implications are affected by the resulting differences in inter-bracket distances (length of archwire present between adjacent brackets) between what was replicated and the original scanned positions. Additionally, rotational replication errors could also not be rectified and may contribute to force measurement inaccuracies. Since rotational misalignments will affect how the archwire is positioned within the bracket slot, it is possible that other measured quantities may be impacted [166].

### 3.4.2 Changes in Force over Treatment

Biomechanical experiments were performed to collect initial and end force data, and the change in force over treatment is now discussed. Since three archwire sizes were considered, the initial/end forces for each archwire size were measured and examined over treatment. Generally, the forces would move towards being negligible at the end of the archwire use, which is an expected observation indicating the progress of alignment (or maximum tooth movement) is achieved for a particular treatment interval and this was essentially observed across patients. In some instances, the end force was slightly larger than the start force for a given archwire size. This was seen in cases such as Patient 1's Tooth 3-3 (Y-direction from T3-T4), Patient 2's Tooth 4-3 (Y-direction from T1-T2) and Tooth 1-2 (Z-direction from T2-T4), Patient 3's Tooth 3-3 (Y-direction from T2-T3) and Tooth 1-3 (Y- and Z-direction from T2-T3), and Patient 4's Tooth 4-1 and 4-3 (Y-direction from T3-T4). Although the archwire size was unchanged for initial and end force measurements, the observations could simply be caused by the bracket positions at the particular interval. Since round tripping of teeth is possible during treatment [167, 168], the higher forces at end positions measured for the same archwire size could suggest that some teeth have temporarily moved further out of alignment. The intermediate movements were also not followed, so the detailed sequence of tooth movements could not be determined during the use of each archwire. Additionally, the applied forces will result in varying tooth movements due to different stress/strain distributions, since the periodontal tissues will vary within and across patients [44, 77]. From a methodology perspective, a new customized jig set was used for each time point of treatment, and the bracket position replication errors involved with the specific jig sets may have affected the measured biomechanical forces leading to the observed inconsistencies during a particular archwire size.

Another observation was the force magnitude increases that occurred when a larger archwire was inserted for a particular jig set (treatment interval). In other words, when a larger archwire was used, the measured start force was generally larger than the end force for the

previously sized archwire and these cases can be seen throughout the presented results. This would be expected since the thicker and stiffer archwire would result in larger generated forces applied to the tooth as reported in Major et al. [27], since there is a larger archwire surface area in contact with the bracket slot, increasing the interaction between both components.

Although direct comparison of measured force magnitudes is not possible with other literature, the initial force ranges measured across patients in this study (0.00-1.43 N and 0.01-2.17 N in the Y- and Z-directions, respectively) are in the same order of magnitude as previous studies that performed in vitro mechanical experiments. For example, when the Robot Measurement System (RMS) was used in Fuck et al. [24] to measure the initial forces, the average forces obtained across the arch when using a 0.014" NiTi archwire were 0.44 N and 0.51 N in the Y- and Z-direction, respectively. In Zhou et al. [17], the Orthodontic Force Tester (OFT) was used along with a 0.016" x 0.016" archwire and the magnitude of measured force ranged approximately from 0.1-3.75 N, with the larger forces occurring in regions of increased tooth misalignment. For a partial misaligned arch tested using another in vitro measured device in Mencatelli et al. [23], the force range across the incisor, canine, and premolar were 0.46-0.65 N in the Y-direction and 0.07-0.21 N in Z-direction when using a 0.014" NiTi archwire. It is recognized that since the patient misalignments/geometries and archwire types are different, these force magnitudes can not be directly compared with the results of this work; however, the similarity in force magnitude results supports outcomes from the presented work.

### **3.4.3 Force and Tooth Movement Trends when Tooth Movement Magnitudes were >0.5 mm**

Based on the results for all arches, most of the observable tooth movements for alignment occurred between T1 and T2 of the orthodontic treatment during the use of the 0.014" archwire as shown by the greater number of available cases provided in Table 3.4. Movements from T2-T4 were minimal during the use of the 0.016" and 0.018" archwires, indicating the

progress of the arch alignment over treatment. From a clinical perspective, these observations show that the 0.014" archwire was effective for the level of misalignment investigated. Since changes were minimal in the later intervals, it could be suggested that the 0.014" archwire is directly progressed to the 0.018" archwire, followed by larger rectangular archwires for similar misalignment cases. The initial forces present upon archwire insertion directly impact the movements of teeth from one treatment interval to the next. For the alignment procedures underwent by the patients, it was seen that the arches originally facing larger misalignments (Patient 1 and 4's mandibular arches, and to some extent Patient 2 and 4's maxillary arches), generally experienced overall greater forces and tooth movements over treatment for the misaligned teeth. An obvious example includes the central incisor (4-1) results in the Y-direction from T1-T2 for Patient 1 and 4's mandibular arch. These results are in agreement with other works, such as Owen et al. [21] and Fok et al. [25], that simulated malocclusions and measured the highest forces at the misaligned tooth followed by the adjacent teeth.

Despite the consistent directional trends between force and tooth movement in the sample arches tested, there were instances where the force magnitude was lower than the observed tooth movement, and this was most frequently seen in the Z-direction for the mandibular arches. Examples include some larger tooth movements experienced by Patient 2's Tooth 4-1 through 3-3 and Patient 4's Tooth 4-2 through 3-3 over treatment. Zhou et al. [17] had also reported instances where the orthodontic force magnitude results from the FEA/mechanical experiments were not necessarily larger than the expected tooth movement magnitudes. From a clinical standpoint, potential reasons for these observations could be due to the differences in patient tooth root morphology and alveolar structural support [44]. The results could also be due to less force required for some tooth movements, such as single-rooted teeth undergoing intrusion and extrusion, as suggested by Proffit et al. [6]. Additionally, since multiple scans were not retrieved during the use of each archwire size, the tooth movements were not as frequently tracked. Therefore, interproximal interactions between adjacent teeth and occlusal forces present from maxillary and mandibular arch interactions [13], which can affect the transmitted forces and resulting tooth movements, could not be determined. Other

possible reasons can be attributed to methodological errors. Using the molars for mandibular arch superimposition can cause inevitable error propagation towards the anterior portion of the arch, and the calculated tooth movements may be artificially larger if the superimposed anterior regions were rotationally misaligned. Another factor affecting the observed results could be the replication errors in the local X-direction affecting the inter-bracket distances. If these distances were greater than the scanned positions, there would be a larger segment of archwire present between the brackets, causing a less taut bracket-archwire interaction. Therefore, the larger inter-bracket distance can decrease the force magnitudes measured [6, 169, 170].

The discussed cases up to now were based on a tooth movement threshold, where smaller forces and larger tooth movements occurred. However, the opposite situation was also encountered, in which the original results show instances where force magnitudes indicative of anticipated tooth movements were measured, but the observed tooth movements were low in comparison to other similar scenarios. Some examples include Patient 3's Tooth 3-2, 3-3, and 4-1 and Patient 2's Tooth 2-1 through 1-3 during later treatment intervals. A key clinical factor influencing the lower tooth movements could be the interproximal interactions between adjacent teeth and the occlusal forces present in the patient [13]. Contact and interplay with neighbouring teeth can result in the applied orthodontic forces not being effectively distributed upon the tooth of interest, resulting in smaller than expected tooth movements. Orthodontic tooth movement depends on the local stress and strain distribution within the periodontal complex, and as suggested before, these local mechanical state changes can also vary within and between patients [44]. In terms of methodology, a potential reason for this occurrence could be again due to the replication error affecting the inter-bracket distances. In this case, if the distances between brackets are smaller than the scanned positions, there would be a smaller segment of archwire present between the brackets creating a more prominent bracket-archwire interaction, increasing the measured force magnitudes [6, 169]. In addition to the inter-bracket distances, the rotational replication errors may further impact the bracket placement, leading to greater bracket-archwire misalignment that can impact the

measured forces [166]. Therefore, larger forces could be measured even if the tooth movement calculations were small based on the scan analysis.

In addition to the cases with opposing magnitude extremities for force and tooth movement, there were instances where the directions were also opposite. For example, where there was a positive force, a tooth movement in the opposite direction occurred, and vice versa. These directionally inconsistent cases were previously presented in Table 3.4. It was also observed in some cases that when neighbouring teeth moved in the same direction over treatment intervals, there would be an alternating effect on trend consistency, where a positive force on one tooth created a directionally opposite force reaction on neighbouring teeth. Two notable examples include the directionally opposing forces experienced by Patient 1 and 4's mandibular central incisors (3-1 and 4-1) from T1-T2 when tooth movement of these teeth were both buccal. Similar to the influencing factors explored above, the inconsistency in results can be attributed to the interproximal effects between neighbouring teeth, as this interaction was not modelled on the in vitro OSIM for force measurement. It is also recognized that the sequence of tooth movements occurring in the patient's mouth is not resolvable based on the frequency of scan collection, and this may play an influential role in the contradicting trends. The positional bracket replication errors are another probable factor for this occurring, affecting the forces being measured.

### **3.4.4 Tooth Movement Rates over Treatment**

Based on the results presented for magnitudes of tooth movement rate experienced over each patient's treatment, it was observed that the arches with greater misalignments generally experienced greater tooth movement rates during the initial intervals of treatment. As previously discussed in Section 3.4.3, Tooth 4-1 for both Patient 1 and 4, experienced greater initial applied forces and resulting tooth movement. With greater amounts of tooth movement occurring at the beginning of treatment based on the measured initial forces, these examples showed that there was a higher rate of tooth movement between these initial treatment intervals compared to later intervals (T2-T4), where recorded forces and tooth

movements were minimal. Similar trends in decreasing tooth movement rates were seen in cases such as Patient 1's Tooth 3-1 (Y-direction), Patient 2's Tooth 4-2 and 2-1 (Y- and Z-direction), Patient 3's Tooth 4-1 (Z-direction) and Tooth 1-3 (Y- and Z-direction), and Patient 4's Tooth 3-1 and 1-2 (Y-direction). Clinically, these observed trends may be an indication of the arch alignment progress, requiring less orthodontic tooth movement in the later treatment intervals.

There were also instances where the magnitude of tooth movement rates fluctuated over treatment intervals, during the use of different archwire sizes. Fluctuations observed included the magnitude decreasing/increasing from the initial interval (T1-T2) and then increasing/decreasing during the final tracked treatment interval (T3-T4). Some example cases of these observations include Patient 1's Tooth 3-2 and 4-2 (Y- and Z-direction), Patient 2's Tooth 1-2 (Y- and Z-direction), Patient 3's Tooth 3-2 (Y-direction) and Tooth 4-2 (Z-direction), and Patient 4's Tooth 3-3 to 3-1 (Z-direction) and Tooth 2-1 to 1-2 (Z-direction). In other instances, the tooth movement rate increased over treatment intervals, as seen for Patient 3's Tooth 4-3 (Z-direction) and Tooth 2-3 (Y-direction) and Patient 4's Tooth 2-2 (Z-direction). The majority of the observed cases involved rates of 0.1 mm/week or less, so experienced tooth movements were already minimal. From a clinical perspective, the fluctuating trends could be a result of possible round tripping, where some of the teeth may require more tooth movement near the end of alignment due to their temporarily misaligned position. As previously discussed, without tracking the intermediate tooth movements, the specific tooth movement sequence is unresolvable. Another potential reason could be due to the neighbouring effects of adjacent teeth restricting movements of certain teeth during a particular treatment interval. Additionally, as a result of orthodontic tooth movement, the PDL space is widened [171–173] and the PDL's elasticity is decreased [64, 173, 174]. This can lead to a greater degree of tooth movement occurring after hyalinization, generally facilitated by direct bone resorption [171, 175]. Therefore, this could provide an explanation for the observed cases where tooth movement rates increased with subsequent force application as treatment progressed. Methodologically, possible rotational misalignment between

superimposed arches can cause larger calculated tooth movements to influence the resulting movement rates. Even though the calculated tooth movement rates can not be directly compared with the results of other literature, the ranges in this work (0.00-0.30 mm/week and 0.00-0.24 mm/week in the Y- and Z-direction, respectively) are in general agreement with a literature review summarizing the tooth movement rates observed at various ranges of force for human-based studies, in which a tooth movement rate range of 0.1-0.47 mm/week was reported for the force range of 0.5-2.5 N [12].

### **3.4.5 Limitations**

This study had limitations including the in vitro OSIM lacking real-life maxillary/-mandibular arch occlusal interactions, interproximal interactions between teeth of each arch, and presence of the periodontal ligament and saliva. The sequence of individual tooth movements occurring in the patient between time points could not be determined due to the frequency of scan collection. These limitations in combination can contribute to the complexities of the inconsistent trends observed in the orthodontic force and tooth movement results. With the current methodology utilized in this study, rotations about any axis could also not be discussed; therefore, analysis of moments were omitted from the presented results. Furthermore, the clinical tooth movements and experimental force were measured with respect to the local OSIM cantilever coordinate systems for consistent and direct comparison of the two data sets over all time points of a patient's treatment. In reality however, the actual local tooth coordinate system would change as the teeth moved over treatment, resulting in multiple coordinate systems per tooth for each patient and thus, altering the magnitudes of the presented force and tooth movement data.

## **3.5 Conclusions**

In this pilot study, a streamlined process was developed to measure clinical tooth movement and force systems for recruited patients over orthodontic alignment treatment using a combined clinical and experimental approach. Despite all teeth being tracked for clinical and

experimental data collection, this investigation focused on the Y- and Z-directional forces and tooth movements occurring at the anterior region of the arch for its primary location of crowding. The average superimposition error was 0.19 mm and the average bracket replication error across all directions was 0.41 mm. For all arches, an inclusive initial force and tooth movement range of 0.00-1.43 N and 0.01-1.81 mm was observed in the Y-direction, and a range of 0.01-2.17 N and 0.00-1.45 mm was observed in the Z-direction. Tooth movement rates over treatment ranged from 0.00-0.30 mm/week in the Y-direction and 0.00-0.24 mm/week in the Z-direction across all patients. Over treatment, a combination of consistent and contradicting trends between force and tooth movement was observed for all patient arches. The directional consistency in trends was  $> 60\%$  when a 0.5 mm tooth movement threshold was considered. For the arches that experienced greater initial misalignment, larger initial forces, tooth movements, and tooth movement rates were generally observed from T1 to T2 during the use of the initial 0.014" archwire. Over treatment, the end forces were generally lower than the start forces for a particular archwire size and when a larger archwire size was inserted, there was a force magnitude increase in comparison to the previous archwire's measured end force. These preliminary findings provide an initial understanding of the existing biomechanical force systems and its effect on tooth movements during orthodontic braces treatment, as well as the potential patient specific characteristics and methodological factors influencing observed trends. This will facilitate future work in refining the current methodology and collecting an expanded data set for establishing fundamental relationships between force systems and clinical tooth movement. The larger data set will then be utilized to formulate patient-specific predictive models for tooth movement over treatment. Acquiring this enhanced knowledge will help identify optimal biomechanics to improve orthodontic treatment predictability and prevent undesired effects. Therefore, further investigation with additional data and sophisticated analysis methods is necessary.

# Chapter 4

## Conclusions, Limitations, & Future Work

*This chapter provides the conclusions of the thesis work involving the streamlined methodology developed and the pilot study conducted. The limitations of the work are also discussed along with the recommendations for future work.*

### 4.1 Conclusions

The objectives of this thesis were to gain an advanced understanding of the biomechanics of braces and how the forces arising over orthodontic fixed-appliance treatment affect the clinically observed tooth movement. This was achieved by applying a combined clinical and in vitro experimental approach. A streamlined methodology was developed to collect orthodontic bracket position information from patient clinical scans to measure tooth movements and to replicate on a physical orthodontic simulator for in vitro biomechanical experiments measuring 3D forces. A pilot study was performed using the established methodology to draw preliminary conclusions on the relationship between biomechanical force systems and clinical tooth movement, along with the method/patient-related factors that limit the current assessment of this relationship.

Patient intraoral scan analysis methods were developed to align scans over treatment for each patient arch to obtain bracket position information. Scans were collected using the iTero intraoral scanner and saved as .STL files. The method involved alignment of the first

scan of each patient arch with the Slicer coordinate system, followed by the superimposition of subsequent scans onto the initial scan through segmenting/isolating the stable region of the maxillary/mandibular arch for initial superimposition. The registration step to align the full arch models was completed through applying the transformation matrix output from the initial superimposition. Brackets were manually landmarked on all scans with four points placed on the outer front corners below each bracket slot. The positional information was then exported for quantitative analysis. An in-house developed script applied coordinate system transformations and nominal bracket dimensions on the manually landmarked positions to retrieve the expected bracket slot endpoint coordinates for each investigated scan. Through averaging the slot endpoint coordinates, the midpoint coordinates were obtained for further use in clinical and experimental data collection. Clinical tooth movements were calculated by measuring the difference between midpoints over two time points of treatment.

Experimental methods were established to measure the force systems present for each patient arch using custom jigs. A default design was created, and unique jig sets were dimensioned according to the previously retrieved bracket slot endpoint/midpoint coordinates. Dimension calculations were conducted in an in-house script to position the bracket with respect to the physical OSIM mounting hole positions. This was completed by first mapping the bracket positions with respect to the cantilever hole locations and calculating the global positional differences between each patient bracket slot midpoint position and respective cantilever hole. In-plane coordinate system transformations were then applied to convert these differences from the OSIM's global X- and Y-axis to the specific local cantilever angles. This was completed to retrieve the unique translation dimensions required for the jig to be secured on the OSIM to reach the necessary bracket location. The first and second order rotational dimensions (rotation about the vertical Z-axis and local Y-axis, respectively) were lastly determined by calculating the angles between each set of bracket endpoints. Jigs were additively manufactured, and orthodontic brackets were bonded to each jig using light curing methods. The jigs were then secured onto the OSIM cantilever arms using a nut and bolt, completing the physical replication of digital bracket positions for the investigated

patient arch to perform biomechanical experiments. Discrepancies in replicating the bracket positions were assessed and used to move micrometers to fix errors where possible prior to experimentation.

A pilot study was conducted for four recruited patients (seven considered arches) between the ages of 11-14 years old experiencing mild anterior crowding, in which four intraoral scans were collected for each patient arch in approximate 6–8-week intervals. For each patient, one set of orthodontic brackets and three round archwire sizes (0.014", 0.016", 0.018") were used in experiments, and archwires were sized up at each treatment interval according to the treatment protocol. Clinical tooth movement over treatment was retrieved using the established scan analysis methods and measuring the difference in bracket midpoint positions between two time points of treatment. The established experimental methods were utilized to measure the average initial and end forces upon archwire insertion for each time point of treatment using five sample archwires of each size. Applying this novel methodology provided the preliminary tooth movement and biomechanical force information for the patient arches over orthodontic treatment. It was found that for the arches experiencing greater misalignment, larger tooth movements and tooth movement rates occurred between the first two time points of treatment. Observed tooth movement rates involved decreasing, increasing, and fluctuating trends over treatment. Larger forces were generally observed as the archwire diameter was increased, and the measured end forces were generally less than the initial forces at a given treatment time point. The trends between tooth movement and initial forces were observed as both consistent and inconsistent over treatment, in which the directional trend consistency was  $> 60\%$  when tooth movement cases greater than 0.5 mm were considered. Inconsistency in trends can be attributed to potential clinical factors including the lack of tracking intermediate tooth movements between archwire size changes, and patient-specific features such as tooth root morphology and the interproximal interaction between neighbouring teeth. Current methodological limitations that may also contribute to trend inconsistency include errors associated with the scan superimposition and bracket position replication.

It was concluded that the established methodology could be implemented to gain a preliminary understanding of the tooth movement and biomechanical force relationship, and the findings help contribute to the existing knowledge of this relationship. This direct measurement of clinical tooth movement and biomechanical forces should be applied for a larger sample size for detailed statistical analysis. This will then assist with developing and implementing patient-specific models for optimizing biomechanical load delivery for desired tooth movement. As a result, this could improve the overall predictability and delivery of orthodontic braces treatment.

## 4.2 Limitations & Future Work

The methodology developed for this work was successfully applied for the collection of pilot data; however, limitations existed and should be addressed for improvements to be made prior to further data collection and analysis. The scans collected using the iTero scanner had varying quality with issues encountered for distorted bracket slots and closed bracket gates. Therefore, limitations in scan quality would directly affect the accuracy of the retrieved position coordinates and subsequent calculations. For future scan collection, the bracket gates could be kept closed during the scanning procedure, removing the slot feature, and reducing bracket distortion. Despite the use of a code as a workaround for calculating bracket slot positions, multiple points had to be manually landmarked for each bracket. In addition, the nominal bracket slot dimensions were assumed to retrieve the expected endpoint coordinates, even with the possibility that the actual slot dimensions may slightly vary bracket to bracket. For the superimposition of the mandibular scans, the stability of the second molars was assumed over treatment due to the lack of bracket bonding; however, some of the patient arches included in the study did not have fully erupted second molars, resulting in the use of the first molars as the stable region. This is a limitation since the first molars have bonded brackets and may be subject to movement over treatment. Furthermore, some mandibular arches experienced rotational misalignment after superimposition, which could cause the calculated tooth movements to be artificially large. Future works in

improving patient scan analysis methods should include the development of an automated procedure for consistent bracket landmarking on scans to minimize manual input, as well as the advancement of superimposition techniques to overcome stable region limitations and misalignment issues experienced by the mandibular scans.

For the use of the 3D-printed jigs, measuring the bracket dimensions with digital calipers (used to evaluate jig bracket placement guide dimension) and the manual bonding of the brackets on the jig surface were considered as limitations. Rotational replication of the bracket position in the current design was also limited. Third order rotation (rotation about the local X-axis) was not considered as only round archwires were used, minimizing the expected torque in that direction. Additionally, first order rotational replication errors (rotation about the Z-axis) were larger than positional errors, and this can be attributed to the already existent angles on the manufactured brackets. Although the FaroArm probe size used for coordinate measurement could still locate the bracket slot endpoints, a smaller probe size would better assist with the selection process for assessing replication errors. Future works should involve improving the current jig design by applying more sophisticated methods for measuring overall bracket dimensions (including angles) to obtain more accurate/consistent measurements for the bracket placement guide feature. Further jig improvements should be made for the angular replication of the brackets by considering third order rotation and accounting for the manufactured bracket angulation in the jig dimensions code. Additionally, it may be of interest to validate the jig stiffness (particularly for the tooth feature) using finite element analysis and assuming a simple cantilever beam system where the tooth feature represents the beam, and the jig base is considered as the fixed support (since it is fully secured on OSIM).

In the mechanical experiments, an in vitro approach was taken by using the laboratory OSIM, which caused the experimental setup to neglect some intraoral conditions including the consideration of the PDL and bone components, maxillary and mandibular arch interaction, and adjacent teeth interaction occurring in a real patient's dentition. It is recommended that patient-related characteristics should be taken into consideration for future improve-

ments in biomechanical data collection. Although this is challenging with the current OSIM equipment, future work could involve the use of more representative patient dentition models, which incorporates the tooth geometry and components of the periodontium, while also permitting contact between the teeth. However, this would also require additional scanning (i.e. CBCT scans) to obtain the necessary anatomical features. The lack of micrometer movement in the local X-direction limited the extent of replication error mitigation. Minimization of this error can be improved in future works by simply remeasuring the cantilever mounting hole positions to ensure the most updated coordinates are used for evaluating jig dimensions.

The clinical and experimental data were measured at the bracket midpoint with respect to the local cantilever coordinate systems. This is a limitation since the actual patient dentition have local tooth directions that would vary as the teeth move over treatment, resulting in multiple coordinate systems for a single patient tooth. Due to the complexities that would arise from this, the current analysis was simplified to using the local coordinate systems based on the physical angles of the OSIM cantilever arms to allow for direct comparability between clinical and experimental data sets over the patient's treatment. Future works could involve the transformation of data to the actual patient tooth coordinate systems for more sophisticated analysis. It may also be of interest to convert the data from the bracket midpoint to the center of resistance location using advanced techniques for direct clinical application to investigate the types of tooth movement occurring during treatment.

The work produced for this study provided useful preliminary results to better understanding the biomechanics of braces over orthodontic treatment and assisting future works in improving the current methodology. Application of this work could include the expansion of the study presented in this thesis by using a greater sample size for patient arches and increasing the frequency of scan collection to obtain a larger set of data and to better track the sequence of tooth movements over treatment during the use of each archwire. This will allow for more in-depth data analysis for correlating the biomechanical forces with clinical tooth movement to make more informative conclusions. Another application of this work

could include the development of patient-specific models to improve orthodontic treatment planning and outcome, which could further be studied using finite element analysis to provide validation for the experimental and clinical results obtained. Other potential applications of this work can include investigating more complex tooth misalignment cases as well as assisting in the future design of orthodontic appliances to deliver more optimal loading conditions, while preventing undesirable effects during treatment.

# Bibliography

- [1] Canadian Dental Association, “The State of Oral Health in Canada,” Tech. Rep., 2017, pp. 1–30. [Online]. Available: <https://www.cda-adc.ca/stateoforalhealth/{\}files/thestateoforalhealthincanada.pdf>.
- [2] Statistics Canada, “Health Fact Sheets: Dental Care, 2018,” Tech. Rep. 82, 2019, pp. 1–7. [Online]. Available: <https://www150.statcan.gc.ca/n1/en/pub/82-625-x/2019001/article/00010-eng.pdf?st=gz1R8b-W>.
- [3] S. J. Cunningham and N. P. Hunt, “Quality of life and its importance in orthodontics,” *Journal of Orthodontics*, vol. 28, no. 2, pp. 152–158, 2001, ISSN: 14653125. DOI: 10.1093/ortho/28.2.152.
- [4] A. H. Hassan and H. E. S. Amin, “Association of orthodontic treatment needs and oral health-related quality of life in young adults,” *American Journal of Orthodontics and Dentofacial Orthopedics*, vol. 137, no. 1, pp. 42–47, 2010, ISSN: 08895406. DOI: 10.1016/j.ajodo.2008.02.024.
- [5] Institute for Quality and Efficiency in Health Care (IQWiG), *Misaligned teeth and jaws: Overview*, 2020. [Online]. Available: <https://www.ncbi.nlm.nih.gov/books/NBK553375/?report=classic>.
- [6] W. R. Proffit, H. W. Fields, and D. M. Sarver, *Contemporary Orthodontics*, 4th ed. Elsevier, 2006, p. 755, ISBN: 9780323078184. [Online]. Available: <https://ebookcentral.proquest.com/lib/ualberta/detail.action?docID=3008946>.
- [7] A. N. Natali, Ed., *Dental Biomechanics*, 1st. London: CRC Press, 2003, p. 304, ISBN: 9781134400652. DOI: 10.1201/9780203514849. [Online]. Available: <https://www.taylorfrancis.com/books/9781134400652>.
- [8] D. Friedrich, N. Rosarius, G. Rau, and P. Diedrich, “Measuring system for in vivo recording of force systems in orthodontic treatment-concept and analysis of accuracy,” *Journal of Biomechanics*, vol. 32, no. 1, pp. 81–85, 1999, ISSN: 00219290. DOI: 10.1016/S0021-9290(98)00112-2.
- [9] B. Melsen, “Biological reaction of alveolar bone to orthodontic tooth movement,” *The Angle Orthodontist*, vol. 69, no. 2, pp. 151–158, 1999.
- [10] V. Krishnan and Z. Davidovitch, “Cellular, molecular, and tissue-level reactions to orthodontic force,” *American Journal of Orthodontics and Dentofacial Orthopedics*, vol. 129, no. 4, pp. 469.e1–469.e32, 2006, ISSN: 08895406. DOI: 10.1016/j.ajodo.2005.10.007.

- [11] Y. Ren, J. C. Maltha, and A. M. Kuijpers-Jagtman, "Optimum force magnitude for orthodontic tooth movement: A systematic literature review," *Angle Orthodontist*, vol. 73, no. 1, pp. 86–92, 2003, ISSN: 00033219.
- [12] C. I. Theodorou, A. M. Kuijpers-Jagtman, E. M. Bronkhorst, and F. A. Wagener, "Optimal force magnitude for bodily orthodontic tooth movement with fixed appliances: A systematic review," *American Journal of Orthodontics and Dentofacial Orthopedics*, vol. 156, no. 5, pp. 582–592, 2019, ISSN: 08895406. DOI: 10.1016/j.ajodo.2019.05.011.
- [13] A. Dudic, C. Giannopoulou, and S. Kiliaridis, "Factors related to the rate of orthodontically induced tooth movement," *American Journal of Orthodontics and Dentofacial Orthopedics*, vol. 143, no. 5, pp. 616–621, 2013, ISSN: 0889-5406. DOI: 10.1016/j.ajodo.2012.12.009. [Online]. Available: <http://dx.doi.org/10.1016/j.ajodo.2012.12.009>.
- [14] C. J. Burstone and H. A. Koenig, "Force systems from an ideal arch," *American Journal of Orthodontics*, vol. 65, no. 3, pp. 270–289, 1974, ISSN: 00029416. DOI: 10.1016/S0002-9416(74)90332-7.
- [15] H. M. Badawi, R. W. Toogood, J. P. R. Carey, G. Heo, and P. W. Major, "Three-dimensional orthodontic force measurements," *American Journal of Orthodontics and Dentofacial Orthopedics*, vol. 136, no. 4, pp. 518–528, 2009, ISSN: 08895406. DOI: 10.1016/j.ajodo.2009.02.025.
- [16] B. Weltman, K. W. Vig, H. W. Fields, S. Shanker, and E. E. Kaizar, "Root resorption associated with orthodontic tooth movement: A systematic review," *American Journal of Orthodontics and Dentofacial Orthopedics*, vol. 137, no. 4, pp. 462–476, 2010, ISSN: 08895406. DOI: 10.1016/j.ajodo.2009.06.021.
- [17] X. Zhou, Y. Gan, Q. Zhao, J. Xiong, and Z. Xia, "Simulation of orthodontic force of archwire applied to full dentition using virtual bracket displacement method," *International Journal for Numerical Methods in Biomedical Engineering*, vol. 35, no. 5, pp. 1–14, 2019, ISSN: 20407947. DOI: 10.1002/cnm.3189.
- [18] J. Wu, Y. Liu, J. Zhang, W. Peng, and X. Jiang, "Biomechanical investigation of orthodontic treatment planning based on orthodontic force measurement and finite element method before implementation: A case study," *Technology and Health Care*, vol. 26, no. S1, S347–S359, 2018, ISSN: 09287329. DOI: 10.3233/THC-174689.
- [19] U. Likitmongkolsakul, P. Smithmaitrie, B. Samruajbenjakun, and J. Aksornmuang, "Development and Validation of 3D Finite Element Models for Prediction of Orthodontic Tooth Movement," *International Journal of Dentistry*, vol. 2018, pp. 1–7, 2018, ISSN: 16878736. DOI: 10.1155/2018/4927503.
- [20] J. Chen, W. Li, M. V. Swain, M. Ali Darendeliler, and Q. Li, "A periodontal ligament driven remodeling algorithm for orthodontic tooth movement," *Journal of Biomechanics*, vol. 47, no. 7, pp. 1689–1695, 2014, ISSN: 18732380. DOI: 10.1016/j.jbiomech.2014.02.030.

- [21] B. Owen, G. Gullion, G. Heo, J. P. Carey, P. W. Major, and D. L. Romanyk, "Measurement of forces and moments around the maxillary arch for treatment of a simulated lingual incisor and high canine malocclusion using straight and mushroom archwires in fixed lingual appliances," *European Journal of Orthodontics*, vol. 39, no. 6, pp. 665–672, 2017, ISSN: 14602210. DOI: 10.1093/ejo/cjx028.
- [22] K. Shimoda *et al.*, "Development of 6-Axis Orthodontic Force and Moment Sensing Device for Decreasing Accident of Orthodontic Treatment," in *Proceedings of the 2018 40th Annual International Conference of the IEEE Engineering in Medicine and Biology Society, EMBS*, 2018, pp. 1797–1800, ISBN: 9781538636466. DOI: 10.1109/EMBC.2018.8512648.
- [23] M. Mencattelli, E. Donati, M. Cultrone, and C. Stefanini, "Novel universal system for 3-dimensional orthodontic force-moment measurements and its clinical use," *American Journal of Orthodontics and Dentofacial Orthopedics*, vol. 148, no. 1, pp. 174–183, 2015, ISSN: 08895406. DOI: 10.1016/j.ajodo.2015.01.028.
- [24] L. M. Fuck and D. Drescher, "Force Systems in the Initial Phase of Orthodontic Treatment – a Comparison of Different Leveling Archwires," *Journal of Orofacial Orthopedics*, vol. 67, no. 1, pp. 6–18, 2006, ISSN: 14345293. DOI: 10.1007/s00056-006-0521-0.
- [25] J. Fok, R. W. Toogood, H. Badawi, J. P. Carey, and P. W. Major, "Analysis of maxillary arch force/couple systems for a simulated high canine malocclusion: Part 1. Passive ligation," *Angle Orthodontist*, vol. 81, no. 6, pp. 953–959, 2011, ISSN: 00033219. DOI: 10.2319/012011-40.1.
- [26] J. Fok, R. W. Toogood, H. Badawi, J. P. Carey, and P. W. Major, "Analysis of maxillary arch force/couple systems for a simulated high canine malocclusion: Part 2. Elastic ligation," *Angle Orthodontist*, vol. 81, no. 6, pp. 960–965, 2011, ISSN: 00033219. DOI: 10.2319/012011-41.1.
- [27] P. W. Major, R. W. Toogood, H. M. Badawi, J. P. Carey, and S. Seru, "Effect of wire size on maxillary arch force/couple systems for a simulated high canine malocclusion," *Journal of Orthodontics*, vol. 41, no. 4, pp. 285–291, 2014, ISSN: 14653133. DOI: 10.1179/1465313314Y.0000000099.
- [28] N. D. Kravitz, C. Groth, P. E. Jones, J. W. Graham, and W. R. Redmond, "Intraoral Digital Scanners," *Journal of clinical orthodontics*, vol. 48, no. 6, pp. 337–347, 2014, ISSN: 00223875.
- [29] F. F. Dai, T. M. Xu, and G. Shu, "Comparison of achieved and predicted tooth movement of maxillary first molars and central incisors: First premolar extraction treatment with Invisalign," *Angle Orthodontist*, vol. 89, no. 5, pp. 679–687, 2019, ISSN: 19457103. DOI: 10.2319/090418-646.1.
- [30] G. Chen *et al.*, "Stable region for maxillary dental cast superimposition in adults, studied with the aid of stable miniscrews," *Orthodontics and Craniofacial Research*, vol. 14, no. 2, pp. 70–79, 2011, ISSN: 16016335. DOI: 10.1111/j.1601-6343.2011.01510.x.

- [31] J. I. Choi, B. K. Cha, P. G. Jost-Brinkmann, D. S. Choi, and I. S. Jang, “Validity of palatal superimposition of 3-dimensional digital models in cases treated with rapid maxillary expansion and maxillary protraction headgear,” *Korean Journal of Orthodontics*, vol. 42, no. 5, pp. 235–241, 2012, ISSN: 12255610. DOI: 10.4041/kjod.2012.42.5.235.
- [32] O. Charalampakis, A. Iliadi, H. Ueno, D. R. Oliver, and K. B. Kim, “Accuracy of clear aligners: A retrospective study of patients who needed refinement,” *American Journal of Orthodontics and Dentofacial Orthopedics*, vol. 154, no. 1, pp. 47–54, 2018, ISSN: 08895406. DOI: 10.1016/j.ajodo.2017.11.028.
- [33] G. Vasilakos, R. Schilling, D. Halazonetis, and N. Gkantidis, “Assessment of different techniques for 3D superimposition of serial digital maxillary dental casts on palatal structures,” *Scientific Reports*, vol. 7, pp. 1–11, 2017, ISSN: 20452322. DOI: 10.1038/s41598-017-06013-5.
- [34] F. H. Martini, J. L. Nath, and E. F. Bartholomew, *Fundamentals of Anatomy & Physiology*, 10th ed. Pearson, 2014, ISBN: 0321909070.
- [35] Niel S. Norton, “Oral Cavity,” in *Netter’s Head and Neck Anatomy for Dentistry*, 3rd ed., Philadelphia: Elsevier, 2017, ch. 13, pp. 341–397, ISBN: 978-0-323-39228-0. [Online]. Available: <https://www-clinicalkey-com.login.ezproxy.library.ualberta.ca/{\#}!/content/book/3-s2.0-B978032339228000013X>.
- [36] Y. Fiorellini, JP and Kim, D and Chang, “Anatomy, structure, and function of the periodontium,” in *Newman and Carranza’s Clinical Periodontology*, 13th ed., Philadelphia: Elsevier, 2019, ch. 3, pp. 19–49. [Online]. Available: <https://www-clinicalkey-com.login.ezproxy.library.ualberta.ca/{\#}!/content/book/3-s2.0-B978032387887600004X>.
- [37] B. M. Seo, I. S. Song, S. Um, and J. H. Lee, “Periodontal Ligament Stem Cells,” in *Stem Cell Biology and Tissue Engineering in Dental Sciences*, Boston: Academic Press, 2015, ch. 22, pp. 291–296, ISBN: 9780123977786. DOI: 10.1016/B978-0-12-397157-9.00024-2.
- [38] D. A. Reed and T. G. Diekwisch, “Morphogenesis and Wound Healing in the Periodontium,” in *Stem Cell Biology and Tissue Engineering in Dental Sciences*, Boston: Academic Press, 2015, ch. 35, pp. 445–448, ISBN: 9780123977786. DOI: 10.1016/B978-0-12-397157-9.00039-4.
- [39] B. Shroff, Ed., *Biology of orthodontic tooth movement: Current concepts and applications in orthodontic practice*, 1st ed. Springer, 2016, pp. 1–164, ISBN: 9783319266091. DOI: 10.1007/978-3-319-26609-1.
- [40] R. J. Smith and C. J. Burstone, “Mechanics of tooth movement,” *American Journal of Orthodontics*, vol. 85, no. 4, pp. 294–307, 1984, ISSN: 00029416. DOI: 10.1016/0002-9416(84)90187-8.
- [41] M. Upadhyay and R. Nanda, “Biomechanics in Orthodontics,” in *Esthetics and Biomechanics in Orthodontics: Second Edition*, 2nd ed., St. Louis: W.B. Saunders, 2015, ch. 4, pp. 74–89, ISBN: 9781455750856. DOI: 10.1016/B978-1-4557-5085-6.00004-7.

- [42] M. A. Asiry, “Biological aspects of orthodontic tooth movement: A review of literature,” *Saudi Journal of Biological Sciences*, vol. 25, no. 6, pp. 1027–1032, 2018, ISSN: 1319562X. DOI: 10.1016/j.sjbs.2018.03.008.
- [43] G. Isola, G. Matarese, G. Cordasco, and L. Perillo, “Mechanobiology of the tooth movement during orthodontic treatment,” *Minerva Stomatologica*, vol. 65, no. 5, pp. 299–327, 2016.
- [44] B. Melsen, P. M. Cattaneo, M. Dalstra, and D. C. Kraft, “The Importance of Force Levels in Relation to Tooth Movement,” *Seminars in Orthodontics*, vol. 13, no. 4, pp. 220–233, 2007, ISSN: 10738746. DOI: 10.1053/j.sodo.2007.08.004.
- [45] A. Sabane, A. Patil, V. Swami, and P. Nagarajan, “Biology of Tooth Movement,” *British Journal of Medicine and Medical Research*, vol. 16, no. 12, pp. 1–10, 2016. DOI: 10.9734/bjmmr/2016/27019.
- [46] A. Oppenheim, “Tissue changes, particularly of the bone, incident to tooth movement,” *The European Journal of Orthodontics*, vol. 29, no. Supplement 1, pp. i2–i15, 2007, ISSN: 0141-5387. DOI: 10.1093/ejo/cjl105.
- [47] D. Bister and M. C. Meikle, “Re-examination of ‘Einige Beiträge zur Theorie der Zahnregulierung’ (Some contributions to the theory of the regulation of teeth) published in 1904-1905 by Carl Sandstedt,” *European Journal of Orthodontics*, vol. 35, no. 2, pp. 160–168, 2013, ISSN: 01415387. DOI: 10.1093/ejo/cjs007.
- [48] A. M. Schwarz, “Tissue changes incidental to orthodontic tooth movement,” *International Journal of Orthodontia, Oral Surgery and Radiography*, vol. 18, no. 4, pp. 331–352, 1932, ISSN: 00996963. DOI: 10.1016/s0099-6963(32)80074-8.
- [49] J. N. Farrar, *A treatise on the irregularities of the teeth and their correction*. New York: De Vinne Press, 1888, vol. 1, ISBN: 3663537137.
- [50] C. A. L. Bassett and R. O. Becker, “Generation of electric potentials by bone in response to mechanical stress,” *Science*, vol. 137, no. 3535, pp. 1063–1064, 1962. DOI: 10.1126/science.137.3535.1063.
- [51] J. C. Huang, G. King, and S. Kapila, “Biologic Mechanisms in Orthodontic Tooth Movement,” in *Biomechanics and Esthetic Strategies in Clinical Orthodontics*, R. Nanda, Ed., Saint Louis: W.B. Saunders, 2005, ch. 2, pp. 17–37, ISBN: 978-0-7216-0196-0. DOI: <https://doi.org/10.1016/B978-0-7216-0196-0.50007-2>.
- [52] L. R. Iwasaki, Y. Liu, H. Liu, and J. C. Nickel, “Speed of human tooth movement in growers and non-growers: Selection of applied stress matters,” *Orthodontics and Craniofacial Research*, vol. 20, no. Suppl. 1, pp. 63–67, 2017, ISSN: 16016343. DOI: 10.1111/ocr.12161.
- [53] Y. A. Yassir, G. T. McIntyre, and D. R. Bearn, “Orthodontic treatment and root resorption: An overview of systematic reviews,” *European Journal of Orthodontics*, vol. 43, no. 4, pp. 442–456, 2021, ISSN: 14602210. DOI: 10.1093/ejo/cjaa058.
- [54] R. J. Pryputniewicz and C. J. Burstone, “The Effect of Time and Force Magnitude on Orthodontic Tooth Movement,” *Journal of Dental Research*, vol. 58, no. 8, pp. 1754–1764, 1979, ISSN: 15440591. DOI: 10.1177/00220345790580080101.

- [55] G. J. King, S. D. Keeling, E. A. McCoy, and T. H. Ward, "Measuring dental drift and orthodontic tooth movement in response to various initial forces in adult rats," *American Journal of Orthodontics and Dentofacial Orthopedics*, vol. 99, no. 5, pp. 456–465, 1991, ISSN: 08895406. DOI: 10.1016/S0889-5406(05)81579-3.
- [56] B. Melsen, "Tissue reaction to orthodontic tooth movement - a new paradigm," *European Journal of Orthodontics*, vol. 23, no. 6, pp. 671–681, 2001. DOI: 10.1093/ejo/23.6.671.
- [57] E. J. Van Leeuwen, A. M. Kuijpers-Jagtman, J. W. Von den Hoff, F. A. Wagener, and J. C. Maltha, "Rate of orthodontic tooth movement after changing the force magnitude: An experimental study in beagle dogs," *Orthodontics and Craniofacial Research*, vol. 13, no. 4, pp. 238–245, 2010, ISSN: 16016335. DOI: 10.1111/j.1601-6343.2010.01500.x.
- [58] J. J. Pilon, A. M. Kuijpers-Jagtman, and J. C. Maltha, "Magnitude of orthodontic forces and rate of bodily tooth movement. An experimental study," *American journal of orthodontics and dentofacial orthopedics*, vol. 110, no. 1, pp. 16–23, 1996. DOI: 10.1016/s0889-5406(96)70082-3.
- [59] R. S. Quinn and D. K. Yoshikawa, "A reassessment of force magnitude in orthodontics," *American Journal of Orthodontics*, vol. 88, no. 3, pp. 252–260, 1985, ISSN: 00029416. DOI: 10.1016/S0002-9416(85)90220-9.
- [60] Y. Ren, J. C. Maltha, M. A. Van 't Hof, and A. M. Kuijpers-Jagtman, "Optimum force magnitude for orthodontic tooth movement: A mathematic model," *American Journal of Orthodontics and Dentofacial Orthopedics*, vol. 125, no. 1, pp. 71–77, 2004, ISSN: 08895406. DOI: 10.1016/j.ajodo.2003.02.005.
- [61] D. L. Romanyk, B. Vafaeian, O. Addison, and S. Adeeb, "The use of finite element analysis in dentistry and orthodontics: Critical points for model development and interpreting results," *Seminars in Orthodontics*, vol. 26, no. 3, pp. 162–173, 2020, ISSN: 10738746. DOI: 10.1053/j.sodo.2020.06.014.
- [62] P. M. Cattaneo and M. A. Cornelis, "Orthodontic Tooth Movement Studied by Finite Element Analysis: an Update. What Can We Learn from These Simulations?" *Current Osteoporosis Reports*, vol. 19, no. 2, pp. 175–181, 2021, ISSN: 15442241. DOI: 10.1007/s11914-021-00664-0.
- [63] K. Tanne, M. Sakuda, and C. J. Burstone, "Three-dimensional finite element analysis for stress in the periodontal tissue by orthodontic forces," *American Journal of Orthodontics and Dentofacial Orthopedics Dentofacial Orthopedics*, vol. 92, no. 6, pp. 499–505, 1987. DOI: 10.1016/0889-5406(87)90232-0.
- [64] K. Tanne, S. Yoshida, T. Kawata, A. Sasaki, J. Knox, and M. L. Jones, "An evaluation of the biomechanical response of the tooth and periodontium to orthodontic forces in adolescent and adult subjects.," *British journal of orthodontics*, vol. 25, no. 2, pp. 109–115, 1998, ISSN: 0301228X. DOI: 10.1093/ortho/25.2.109.

- [65] C. Bourauel, D. Freudenreich, D. Vollmer, D. Kobe, D. Drescher, and A. Jäger, “Simulation of orthodontic tooth movements: A comparison of numerical models,” *Journal of orofacial orthopedics*, vol. 60, no. 2, pp. 136–151, 1999, ISSN: 14345293. DOI: 10.1007/BF01298963.
- [66] C. Bourauel, D. Vollmer, and A. Jäger, “Application of Bone Remodeling Theories in the Simulation of Orthodontic Tooth Movements,” *Journal of Orofacial Orthopedics*, vol. 61, no. 4, pp. 266–279, 2000, ISSN: 14345293. DOI: 10.1007/s000560050012.
- [67] J. lei Wu, Y. feng Liu, W. Peng, H. yue Dong, and J. xing Zhang, “A biomechanical case study on the optimal orthodontic force on the maxillary canine tooth based on finite element analysis,” *Journal of Zhejiang University: Science B*, vol. 19, no. 7, pp. 535–546, 2018, ISSN: 18621783. DOI: 10.1631/jzus.B1700195.
- [68] S. Meštrović, M. Šljaj, and P. Rajić, “Finite element method analysis of the tooth movement induced by orthodontic forces,” *Collegium Antropologicum*, vol. 27, no. Suppl. 2, pp. 17–21, 2003, ISSN: 03506134.
- [69] R. Savignano, R. F. Vicilli, and U. Oyoyo, “Three-dimensional nonlinear prediction of tooth movement from the force system and root morphology,” *Angle Orthodontist*, vol. 90, no. 6, pp. 811–822, 2020, ISSN: 19457103. DOI: 10.2319/120919-781.1.
- [70] X. Zhang, M.-q. Li, J. Guo, H.-w. Yang, J. Yu, and G.-j. Li, “An analysis of the optimal intrusion force of the maxillary central incisor with root horizontal resorption using the finite element method and curve fitting,” *Computer Methods in Biomechanics and Biomedical Engineering*, vol. 25, no. 13, pp. 1471–1486, 2022. DOI: 10.1080/10255842.2021.2017904.
- [71] M. Z. Su *et al.*, “Modeling viscoelastic behavior of periodontal ligament with nonlinear finite element analysis,” *Journal of Dental Sciences*, vol. 8, no. 2, pp. 121–128, 2013, ISSN: 19917902. DOI: 10.1016/j.jds.2013.01.001.
- [72] M. Hemanth *et al.*, “An Analysis of the Stress induced in the Periodontal Ligament during Extrusion and Rotation Movements— Part II: A Comparison of Linear vs Nonlinear FEM Study,” *Journal of Contemporary Dental Practice*, vol. 16, no. 10, pp. 819–823, 2015, ISSN: 15263711. DOI: 10.5005/JP-JOURNALS-10024-1763.
- [73] J. Wu *et al.*, “Investigation of effective intrusion and extrusion force for maxillary canine using finite element analysis,” *Computer Methods in Biomechanics and Biomedical Engineering*, vol. 22, no. 16, pp. 1294–1302, 2019, ISSN: 14768259. DOI: 10.1080/10255842.2019.1661390.
- [74] S. E. Elsaka, S. M. Hammad, and N. F. Ibrahim, “Evaluation of stresses developed in different bracket-cement-enamel systems using finite element analysis with in vitro bond strength tests,” *Progress in Orthodontics*, vol. 15, no. 1, pp. 1–8, 2014, ISSN: 21961042. DOI: 10.1186/s40510-014-0033-1.
- [75] V. Magesh, P. Harikrishnan, and T. Chandra Sekhar, “Finite element analysis of orthodontic bracket tie wing deformation due to labial crown torque,” *IOP Conference Series: Materials Science and Engineering*, vol. 402, 2018, ISSN: 1757899X. DOI: 10.1088/1757-899X/402/1/012085.

- [76] P. Harikrishnan, V. Magesh, A. M. Ajayan, and D. K. JebaSingh, “Finite element analysis of torque induced orthodontic bracket slot deformation in various bracket-archwire contact assembly,” *Computer Methods and Programs in Biomedicine*, vol. 197, 2020, ISSN: 18727565. DOI: 10.1016/j.cmpb.2020.105748.
- [77] P. M. Cattaneo, M. Dalstra, and B. Melsen, “Strains in periodontal ligament and alveolar bone associated with orthodontic tooth movement analyzed by finite element,” *Orthodontics and Craniofacial Research*, vol. 12, no. 2, pp. 120–128, 2009, ISSN: 16016335. DOI: 10.1111/j.1601-6343.2009.01445.x.
- [78] C. Field *et al.*, “Mechanical responses to orthodontic loading: A 3-dimensional finite element multi-tooth model,” *American Journal of Orthodontics and Dentofacial Orthopedics*, vol. 135, no. 2, pp. 174–181, 2009, ISSN: 08895406. DOI: 10.1016/j.ajodo.2007.03.032.
- [79] C. Canales, M. Larson, D. Grauer, R. Sheats, C. Stevens, and C. C. Ko, “A novel biomechanical model assessing continuous orthodontic archwire activation,” *American Journal of Orthodontics and Dentofacial Orthopedics*, vol. 143, no. 2, pp. 281–290, 2013, ISSN: 08895406. DOI: 10.1016/j.ajodo.2012.06.019.
- [80] S. N. Papageorgiou, L. Keilig, I. Hasan, A. Jäger, and C. Bourauel, “Effect of material variation on the biomechanical behaviour of orthodontic fixed appliances: A finite element analysis,” *European Journal of Orthodontics*, vol. 38, no. 3, pp. 300–307, 2016, ISSN: 14602210. DOI: 10.1093/ejo/cjv050.
- [81] Y. Kojima and H. Fukui, “Numerical simulation of canine retraction by sliding mechanics,” *American Journal of Orthodontics and Dentofacial Orthopedics*, vol. 127, no. 5, pp. 542–551, 2005, ISSN: 08895406. DOI: 10.1016/j.ajodo.2004.12.007.
- [82] Y. Kojima, T. Mizuno, and H. Fukui, “A numerical simulation of tooth movement produced by molar uprighting spring,” *American Journal of Orthodontics and Dentofacial Orthopedics*, vol. 132, no. 5, pp. 630–638, 2007, ISSN: 08895406. DOI: 10.1016/j.ajodo.2005.07.035.
- [83] J. Tominaga *et al.*, “Effect of play between bracket and archwire on anterior tooth movement in sliding mechanics: A three-dimensional finite element study,” *Journal of Dental Biomechanics*, vol. 3, pp. 1–8, 2012, ISSN: 17587360. DOI: 10.1177/1758736012461269.
- [84] H. Tominaga, Jun-yaOzaki *et al.*, “Effect of bracket slot and archwire dimensions on anterior tooth movement during space closure in sliding mechanics: A 3-dimensional finite element study,” *American Journal of Orthodontics and Dentofacial Orthopedics*, vol. 146, no. 2, pp. 166–174, 2014, ISSN: 08895406. DOI: 10.1016/j.ajodo.2014.04.016.
- [85] J. Kawamura and N. Tamaya, “A finite element analysis of the effects of archwire size on orthodontic tooth movement in extraction space closure with miniscrew sliding mechanics,” *Progress in Orthodontics*, vol. 20, no. 3, 2019, ISSN: 21961042. DOI: 10.1186/s40510-018-0255-8.

- [86] J. Kawamura *et al.*, “Biomechanical analysis for total distalization of the maxillary dentition: A finite element study,” *American Journal of Orthodontics and Dentofacial Orthopedics*, vol. 160, no. 2, pp. 259–265, 2021, ISSN: 08895406. DOI: 10.1016/j.ajodo.2020.04.029.
- [87] J. M. Chae, J. H. Park, Y. Kojima, K. Tai, Y. A. Kook, and H. M. Kyung, “Biomechanical analysis for total distalization of the mandibular dentition: A finite element study,” *American Journal of Orthodontics and Dentofacial Orthopedics*, vol. 155, no. 3, pp. 388–397, 2019, ISSN: 08895406. DOI: 10.1016/j.ajodo.2018.05.014.
- [88] T. Sadhunavar, T. Pradhan, S. Deshpande, A. Sethia, and K. M. Keluskar, “A comparative evaluation of canine retraction and anchor loss using ceramic and stainless steel mbt pre-adjusted edgewise brackets using three dimensional finite element method,” *International Journal of Dentistry and Oral Science*, vol. 7, no. 10, pp. 854–859, 2020, ISSN: 23778075. DOI: 10.19070/2377-8075-20000169.
- [89] S. Wang, M. Hu, S. Wang, H. Qi, D. Song, and H. Jiang, “Comparative study of biomechanical effects between two types of  $2 \times 4$  techniques employing a rocking-chair archwire: a three-dimensional finite element analysis,” *Clinical Oral Investigations*, vol. 27, pp. 4617–4631, 2023, ISSN: 14363771. DOI: 10.1007/s00784-023-05088-x.
- [90] J. Schneider, M. Geiger, and F. G. Sander, “Numerical experiments on long-time orthodontic tooth movement,” *American Journal of Orthodontics and Dentofacial Orthopedics*, vol. 121, no. 3, pp. 257–265, 2002, ISSN: 08895406. DOI: 10.1067/mod.2002.121007.
- [91] A. Zargham, A. Geramy, and G. Rouhi, “Evaluation of long-term orthodontic tooth movement considering bone remodeling process and in the presence of alveolar bone loss using finite element method,” *Orthodontic Waves*, vol. 75, no. 4, pp. 85–96, 2016, ISSN: 13440241. DOI: 10.1016/j.odw.2016.09.001.
- [92] G. Dot, R. Licha, F. Goussard, and V. Sansalone, “A new protocol to accurately track long-term orthodontic tooth movement and support patient-specific numerical modeling,” *Journal of Biomechanics*, vol. 129, pp. 1–9, 2021, ISSN: 18732380. DOI: 10.1016/j.jbiomech.2021.110760.
- [93] R. Hamanaka, S. Yamaoka, T. N. Anh, J. ya Tominaga, Y. Koga, and N. Yoshida, “Numeric simulation model for long-term orthodontic tooth movement with contact boundary conditions using the finite element method,” *American Journal of Orthodontics and Dentofacial Orthopedics*, vol. 152, no. 5, pp. 601–612, 2017, ISSN: 08895406. DOI: 10.1016/j.ajodo.2017.03.021.
- [94] S. Yona, O. Medina, R. Sarig, and N. Shvalb, “An Efficient Spring Model for an Integrated Orthodontic Tooth Movement: A Verified Mathematical Model,” *Applied Sciences*, vol. 13, no. 8, 2023, ISSN: 20763417. DOI: 10.3390/app13085013.
- [95] J. Duyck, H. Van Oosterwyck, M. De Cooman, R. Puers, J. Vander Sloten, and I. Naert, “Three-dimensional force measurements on oral implants: A methodological study,” *Journal of Oral Rehabilitation*, vol. 27, no. 9, pp. 744–753, 2000, ISSN: 0305182X. DOI: 10.1046/j.1365-2842.2000.00581.x.

- [96] N. Yoshida, Y. Koga, A. Saimoto, T. Ishimatsu, Y. Yamada, and K. Kobayashi, “Development of a magnetic sensing device for tooth displacement under orthodontic forces,” *IEEE Transactions on Biomedical Engineering*, vol. 48, no. 3, pp. 354–359, 2001, ISSN: 00189294. DOI: 10.1109/10.914799.
- [97] B. Kuo, K. Takakuda, and H. Miyairi, “Development of an orthodontic simulator for measurement of orthodontic forces,” *Journal of Medical and Dental Sciences*, vol. 48, no. 1, pp. 15–21, 2001.
- [98] B. Dotzer, T. Stocker, A. Wichelhaus, M. Janjic Rankovic, and H. Sabbagh, “Biomechanical simulation of forces and moments of initial orthodontic tooth movement in dependence on the used archwire system by ROSS (Robot Orthodontic Measurement & Simulation System),” *Journal of the Mechanical Behavior of Biomedical Materials*, vol. 144, 2023, ISSN: 18780180. DOI: 10.1016/j.jmbbm.2023.105960.
- [99] Y. F. Liu, P. Y. Zhang, Q. F. Zhang, J. X. Zhang, and J. Chen, “Digital design and fabrication of simulation model for measuring orthodontic force,” *Bio-Medical Materials and Engineering*, vol. 24, no. 6, pp. 2265–2271, 2014, ISSN: 18783619. DOI: 10.3233/BME-141039.
- [100] D. Wang, H. Turkkahraman, J. Chen, B. Li, and Y. Liu, “Quantification of orthodontic loads on teeth in the correction of canine overeruption using different archwire designs,” *American Journal of Orthodontics and Dentofacial Orthopedics*, vol. 163, no. 1, e13–e21, 2023, ISSN: 08895406. DOI: 10.1016/j.ajodo.2022.10.016.
- [101] C. Bourauel, D. Drescher, and M. Thier, “An experimental apparatus for the simulation of three-dimensional movements in orthodontics,” *Journal of Biomedical Engineering*, vol. 14, no. 5, pp. 371–378, 1992, ISSN: 01415425. DOI: 10.1016/0141-5425(92)90081-U.
- [102] M. A. Montasser, L. Keilig, T. El-Bialy, S. Reimann, A. Jäger, and C. Bourauel, “Effect of archwire cross-section changes on force levels during complex tooth alignment with conventional and self-ligating brackets,” *American Journal of Orthodontics and Dentofacial Orthopedics*, vol. 147, no. 4, S101–S108, 2015, ISSN: 08895406. DOI: 10.1016/j.ajodo.2014.11.024.
- [103] M. A. Montasser, T. El-Bialy, L. Keilig, S. Reimann, A. Jäger, and C. Bourauel, “Force levels in complex tooth alignment with conventional and self-ligating brackets,” *American Journal of Orthodontics and Dentofacial Orthopedics*, vol. 143, no. 4, pp. 507–514, 2013, ISSN: 08895406. DOI: 10.1016/j.ajodo.2012.11.020.
- [104] M. A. Montasser, L. Keilig, and C. Bourauel, “Archwire diameter effect on tooth alignment with different bracket-archwire combinations,” *American Journal of Orthodontics and Dentofacial Orthopedics*, vol. 149, no. 1, pp. 76–83, 2016, ISSN: 08895406. DOI: 10.1016/j.ajodo.2015.06.026.
- [105] S. Holtmann *et al.*, “Different bracket-archwire combinations for simulated correction of two-dimensional tooth malalignment: Leveling outcomes and initial force systems,” *Journal of Orofacial Orthopedics*, vol. 75, no. 6, pp. 459–470, 2014, ISSN: 14345293. DOI: 10.1007/s00056-014-0238-4.

- [106] A. Alobeid *et al.*, “Comparison of the efficacy of tooth alignment among lingual and labial brackets: An in vitro study,” *European Journal of Orthodontics*, vol. 40, no. 6, pp. 660–665, 2018, ISSN: 14602210. DOI: 10.1093/ejo/cjy005.
- [107] R. L. Shintcovsk, R. S. Da Silva Júnior, L. White, L. P. Martins, and R. P. Martins, “Evaluation of the load system produced by a single intrusion bend in a maxillary lateral incisor bracket with different alloys,” *Angle Orthodontist*, vol. 88, no. 5, pp. 611–616, 2018, ISSN: 19457103. DOI: 10.2319/081717-556.1.
- [108] J. Chen, S. C. Isikbay, and E. J. Brizendine, “Quantification of three-dimensional orthodontic force systems of T-loop archwires,” *Angle Orthodontist*, vol. 80, no. 4, pp. 754–758, 2010, ISSN: 00033219. DOI: 10.2319/082509-484.1.
- [109] H. Kaur *et al.*, “The biomechanics of posterior maxillary arch expansion using fixed labial and lingual appliances,” *Angle Orthodontist*, vol. 90, no. 5, pp. 688–694, 2020, ISSN: 19457103. DOI: 10.2319/010520-859.1.
- [110] Y. Midorikawa *et al.*, “Six-axis orthodontic force and moment sensing system for dentist technique training,” in *Proceedings of the 38th Annual International Conference of the IEEE Engineering in Medicine and Biology Society, EMBS*, Orlando: IEEE, 2016, pp. 2206–2209, ISBN: 9781457702204. DOI: 10.1109/EMBC.2016.7591167.
- [111] W. J. Lai *et al.*, “A new orthodontic force system for moment control utilizing the flexibility of common wires: Evaluation of the effect of contractile force and hook length,” *Journal of the Formosan Medical Association*, vol. 117, no. 1, pp. 71–79, 2018, ISSN: 18760821. DOI: 10.1016/j.jfma.2017.03.002.
- [112] K. Shimoda *et al.*, “Orthodontic force and moment sensing device: Influence of deflection of wire and tooth’s orientation,” in *2019 IEEE International Conference on Systems, Man and Cybernetics*, Bari: IEEE, 2019, pp. 4337–4340, ISBN: 9781728145693. DOI: 10.1109/SMC.2019.8914173.
- [113] J. Wu *et al.*, “Dynamic measurement of orthodontic force using a tooth movement simulation system based on a wax model,” *Technology and Health Care*, vol. 29, no. 3, pp. 457–466, 2021, ISSN: 09287329. DOI: 10.3233/THC-202451.
- [114] S. Seru, D. L. Romanyk, R. W. Toogood, J. P. Carey, and P. W. Major, “Effect of Ligation Method on Maxillary Arch Force/Moment Systems for a Simulated Lingual Incisor Malalignment,” *The Open Biomedical Engineering Journal*, vol. 8, pp. 106–113, 2014, ISSN: 1874-1207. DOI: 10.2174/1874120701408010106.
- [115] D. Lee, G. Heo, T. El-Bialy, J. P. Carey, P. W. Major, and D. L. Romanyk, “Initial forces experienced by the anterior and posterior teeth during dentalanchored or skeletal-anchored en masse retraction in vitro,” *Angle Orthodontist*, vol. 87, no. 4, pp. 549–555, 2017, ISSN: 19457103. DOI: 10.2319/080916-616.1.
- [116] B. Owen *et al.*, “Three-dimensional in vitro measurement of initial forces and moments acting on maxillary canine teeth using various Class II elastic configurations with a straight archwire fixed lingual appliance,” *Orthodontic Waves*, vol. 78, no. 2, pp. 56–62, 2019, ISSN: 13440241. DOI: 10.1016/j.odw.2019.04.005.

- [117] J. L. Ashmore, B. F. Kurland, G. J. King, T. T. Wheeler, J. Ghafari, and D. S. Ramsay, “A 3-dimensional analysis of molar movement during headgear treatment,” *American Journal of Orthodontics and Dentofacial Orthopedics*, vol. 121, no. 1, pp. 18–29, 2002, ISSN: 08895406. DOI: 10.1067/mod.2002.120687.
- [118] S. Canan and N. E. Senisik, “Comparison of the treatment effects of different rapid maxillary expansion devices on the maxilla and the mandible. Part 1: Evaluation of dentoalveolar changes,” *American Journal of Orthodontics and Dentofacial Orthopedics*, vol. 151, no. 6, pp. 1125–1138, 2017. DOI: 10.1016/j.ajodo.2016.11.022.
- [119] B. K. Cha, J. Y. Lee, P. G. Jost-Brinkmann, and N. Yoshida, “Analysis of tooth movement in extraction cases using three-dimensional reverse engineering technology,” *European Journal of Orthodontics*, vol. 29, no. 4, pp. 325–331, 2007, ISSN: 01415387. DOI: 10.1093/ejo/cjm019.
- [120] Y. Pan, X. Wang, F. Dai, G. Chen, and T. Xu, “Accuracy and reliability of maxillary digital model (MDM) superimposition in evaluating teeth movement in adults compared with CBCT maxillary superimposition,” *Scientific Reports*, vol. 10, pp. 1–8, 2020, ISSN: 20452322. DOI: 10.1038/s41598-020-76537-w.
- [121] D. Grauer and W. R. Proffit, “Accuracy in tooth positioning with a fully customized lingual orthodontic appliance,” *American Journal of Orthodontics and Dentofacial Orthopedics*, vol. 140, no. 3, pp. 433–443, 2011, ISSN: 08895406. DOI: 10.1016/j.ajodo.2011.01.020.
- [122] K. Hayashi, J. Uechi, and I. Mizoguchi, “Three-dimensional analysis of dental casts based on a newly defined palatal reference plane,” *Angle Orthodontist*, vol. 73, no. 5, pp. 539–544, 2003, ISSN: 00033219.
- [123] D. Wiechmann, R. Schwestka-Polly, H. Pancherz, and A. Hohoff, “Control of mandibular incisors with the combined Herbst and completely customized lingual appliance - a pilot study,” *Head and Face Medicine*, vol. 6, pp. 4–7, 2010, ISSN: 1746160X. DOI: 10.1186/1746-160X-6-3.
- [124] M. José Viñas, V. Pie de Hierro, and J. M. Ustrell-Torrent, “Superimposition of 3D digital models: A case report,” *International Orthodontics*, vol. 16, no. 2, pp. 304–313, 2018, ISSN: 17617227. DOI: 10.1016/j.ortho.2018.03.017.
- [125] X. Lin, T. Chen, J. Liu, T. Jiang, D. Yu, and S. G. Shen, “Point-based superimposition of a digital dental model on to a three-dimensional computed tomographic skull: An accuracy study in vitro,” *British Journal of Oral and Maxillofacial Surgery*, vol. 53, no. 1, pp. 28–33, 2015, ISSN: 15321940. DOI: 10.1016/j.bjoms.2014.09.007.
- [126] K. Becker, B. Wilmes, C. Grandjean, and D. Drescher, “Impact of manual control point selection accuracy on automated surface matching of digital dental models,” *Clinical Oral Investigations*, vol. 22, pp. 801–810, 2018, ISSN: 14363771. DOI: 10.1007/s00784-017-2155-6.
- [127] S. Talaat *et al.*, “Reliability of linear and angular dental measurements with the OrthoMechanics Sequential Analyzer,” *American Journal of Orthodontics and Dentofacial Orthopedics*, vol. 147, no. 2, pp. 264–269, 2015, ISSN: 08895406. DOI: 10.1016/j.ajodo.2014.07.027.

- [128] S. Talaat, A. Kaboudan, C. Bourauel, N. Ragy, K. Kula, and A. Ghoneima, “Validity and reliability of three-dimensional palatal superimposition of digital dental models,” *European Journal of Orthodontics*, vol. 39, no. 4, pp. 365–370, 2017, ISSN: 14602210. DOI: 10.1093/ejo/cjx008.
- [129] D. Garib *et al.*, “Three-dimensional mandibular dental changes with aging,” *American Journal of Orthodontics and Dentofacial Orthopedics*, vol. 159, no. 2, pp. 184–192, 2021, ISSN: 08895406. DOI: 10.1016/j.ajodo.2019.12.021.
- [130] H. Chen, A. A. Lowe, F. R. de Almeida, M. Wong, J. A. Fleetham, and B. Wang, “Three-dimensional computer-assisted study model analysis of long-term oral-appliance wear. Part 1: Methodology,” *American Journal of Orthodontics and Dentofacial Orthopedics*, vol. 134, no. 3, pp. 393–407, 2008, ISSN: 08895406. DOI: 10.1016/j.ajodo.2006.10.030.
- [131] G. Han, J. Li, S. Wang, L. Wang, Y. Zhou, and Y. Liu, “A comparison of voxel- and surface-based cone-beam computed tomography mandibular superimposition in adult orthodontic patients,” *Journal of International Medical Research*, vol. 49, no. 1, pp. 1–11, 2021, ISSN: 14732300. DOI: 10.1177/0300060520982708.
- [132] T. J. Park, S. H. Lee, and K. S. Lee, “A method for mandibular dental arch superimposition using 3D cone beam CT and orthodontic 3D digital model,” *Korean Journal of Orthodontics*, vol. 42, no. 4, pp. 169–181, 2012, ISSN: 12255610. DOI: 10.4041/kjod.2012.42.4.169.
- [133] M. Ioshida *et al.*, “Accuracy and reliability of mandibular digital model registration with use of the mucogingival junction as the reference,” *Oral Surgery, Oral Medicine, Oral Pathology and Oral Radiology*, vol. 127, no. 4, pp. 351–360, 2019, ISSN: 22124403. DOI: 10.1016/j.oooo.2018.10.003.
- [134] S. Kiliaridis, G. Jonasson, and L. T. Huanca Ghislanzoni, “Functional factors associated with continuous eruption of maxillary incisors in adulthood: A 10-year prospective cohort study,” *International journal of oral implantology (Berlin, Germany)*, vol. 12, no. 3, pp. 329–335, 2019, ISSN: 2631-6439. [Online]. Available: <http://www.ncbi.nlm.nih.gov/pubmed/31535101>.
- [135] A Ghoneima, H Cho, K Farouk, and K Kula, “Accuracy and reliability of landmark-based, surface-based and voxel-based 3D cone-beam computed tomography superimposition methods,” *Orthodontics and Craniofacial Research*, vol. 20, no. 4, pp. 227–236, 2017, ISSN: 16016343. DOI: 10.1111/ocr.12205.
- [136] F. P. van der Linden, “Changes in the position of posterior teeth in relation to ruga points,” *American Journal of Orthodontics*, vol. 74, no. 2, pp. 142–161, 1978, ISSN: 00029416. DOI: 10.1016/0002-9416(78)90081-7.
- [137] M. A. Almeida, C. Phillips, K. Kula, and C. Tulloch, “Stability of the palatal rugae as landmarks for analysis of dental casts,” *The Angle Orthodontist*, vol. 65, no. 1, pp. 43–48, 1995.
- [138] L. J. Bailey, A. Esmailnejad, and M. A. Almeida, “Stability of the palatal rugae as landmarks for analysis of dental casts in extraction and nonextraction cases,” *The Angle Orthodontist*, vol. 66, no. 1, pp. 73–78, 1996.

- [139] B. R. Hoggan and C. Sadowsky, “The use of palatal rugae for the assessment of anteroposterior tooth movements,” *American Journal of Orthodontics and Dentofacial Orthopedics*, vol. 119, no. 5, pp. 482–488, 2001, ISSN: 08895406. DOI: 10.1067/mod.2001.113001.
- [140] V. Lanteri *et al.*, “Assessment of the Stability of the Palatal Rugae in a 3D-3D Superimposition Technique Following Slow Maxillary Expansion (SME),” *Scientific Reports*, vol. 10, pp. 1–7, 2020, ISSN: 20452322. DOI: 10.1038/s41598-020-59637-5.
- [141] B. Thiruvengkatachari, M. Al-Abdallah, N. C. Akram, J. Sandler, and K. O’Brien, “Measuring 3-dimensional tooth movement with a 3-dimensional surface laser scanner,” *American Journal of Orthodontics and Dentofacial Orthopedics*, vol. 135, no. 4, pp. 480–485, 2009, ISSN: 08895406. DOI: 10.1016/j.ajodo.2007.03.040.
- [142] I. Jang *et al.*, “A novel method for the assessment of three-dimensional tooth movement during orthodontic treatment,” *Angle Orthodontist*, vol. 79, no. 3, pp. 447–453, 2009, ISSN: 00033219. DOI: 10.2319/042308-225.1.
- [143] S. Stucki and N. Gkantidis, “Assessment of techniques used for superimposition of maxillary and mandibular 3D surface models to evaluate tooth movement: A systematic review,” *European Journal of Orthodontics*, vol. 42, no. 5, pp. 559–570, 2020, ISSN: 14602210. DOI: 10.1093/ejo/cjz075.
- [144] K. An, I. Jang, D. S. Choi, P. G. Jost-Brinkmann, and B. K. Cha, “Identification of a stable reference area for superimposing mandibular digital models,” *Journal of Orofacial Orthopedics*, vol. 76, no. 6, pp. 508–519, 2015, ISSN: 14345293. DOI: 10.1007/s00056-015-0310-8.
- [145] T. Nguyen, L. Cevidanes, L. Franchi, A. Ruellas, and T. Jackson, “Three-dimensional mandibular regional superimposition in growing patients,” *American Journal of Orthodontics and Dentofacial Orthopedics*, vol. 153, no. 5, pp. 747–754, 2018, ISSN: 08895406. DOI: 10.1016/j.ajodo.2017.07.026.
- [146] F. Schmidt, F. Kilic, N. E. Piro, M. E. Geiger, and B. G. Lapatki, “Novel Method for Superposing 3D Digital Models for Monitoring Orthodontic Tooth Movement,” *Annals of Biomedical Engineering*, vol. 46, no. 8, pp. 1160–1172, 2018, ISSN: 15739686. DOI: 10.1007/s10439-018-2029-3.
- [147] J. R. Chisari, S. P. McGorray, M. Nair, and T. T. Wheeler, “Variables affecting orthodontic tooth movement with clear aligners,” *American Journal of Orthodontics and Dentofacial Orthopedics*, vol. 145, no. 4, pp. 82–91, 2014, ISSN: 08895406. DOI: 10.1016/j.ajodo.2013.10.022.
- [148] N. D. Kravitz, B. Kusnoto, B. Agran, and G. Viana, “Influence of attachments and interproximal reduction on the accuracy of canine rotation with invisalign,” *Angle Orthodontist*, vol. 78, no. 4, pp. 682–687, 2008, ISSN: 00033219. DOI: 10.2319/060107-263.
- [149] N. D. Kravitz, B. Kusnoto, E. BeGole, A. Obrez, and B. Agran, “How well does Invisalign work? A prospective clinical study evaluating the efficacy of tooth movement with Invisalign,” *American Journal of Orthodontics and Dentofacial Orthopedics*, vol. 135, no. 1, pp. 27–35, 2009, ISSN: 08895406. DOI: 10.1016/j.ajodo.2007.05.018.

- [150] M. Simon, L. Keilig, J. Schwarze, B. A. Jung, and C. Bourauel, "Treatment outcome and efficacy of an aligner technique - regarding incisor torque, premolar derotation and molar distalization," *BMC Oral Health*, vol. 14, pp. 1–7, 2014, ISSN: 14726831. DOI: 10.1186/1472-6831-14-68.
- [151] D. Gibelli, D. De Angelis, F. Riboli, C. Dolci, C. Cattaneo, and C. Sforza, "Quantification of odontological differences of the upper first and second molar by 3D-3D superimposition: a novel method to assess anatomical matches," *Forensic Science, Medicine, and Pathology*, vol. 15, pp. 570–573, 2019, ISSN: 1547769X. DOI: 10.1007/s12024-019-00140-3.
- [152] L. Lombardo, A. Arreghini, F. Ramina, L. T. Huanca Ghislanzoni, and G. Siciliani, "Predictability of orthodontic movement with orthodontic aligners: a retrospective study," *Progress in Orthodontics*, vol. 18, pp. 1–12, 2017, ISSN: 21961042. DOI: 10.1186/s40510-017-0190-0.
- [153] J. Chen, S. Li, and S. Fang, "Quantification of tooth displacement from cone-beam computed tomography images," *American Journal of Orthodontics and Dentofacial Orthopedics*, vol. 136, no. 3, pp. 393–400, 2009, ISSN: 0889-5406. DOI: 10.1016/j.ajodo.2007.10.058.
- [154] T. Grünheid, C. Loh, and B. E. Larson, "How accurate is Invisalign in nonextraction cases? Are predicted tooth positions achieved?" *Angle Orthodontist*, vol. 87, no. 6, pp. 809–815, 2017, ISSN: 19457103. DOI: 10.2319/022717-147.1.
- [155] M. Al-Nadawi, N. D. Kravitz, I. Hansa, L. Makki, D. J. Ferguson, and N. R. Vaid, "Effect of clear aligner wear protocol on the efficacy of tooth movement: A randomized clinical trial," *Angle Orthodontist*, vol. 91, no. 2, pp. 157–163, 2021, ISSN: 19457103. DOI: 10.2319/071520-630.1.
- [156] N. Haouili, N. D. Kravitz, N. R. Vaid, D. J. Ferguson, and L. Makki, "Has Invisalign improved? A prospective follow-up study on the efficacy of tooth movement with Invisalign," *American Journal of Orthodontics and Dentofacial Orthopedics*, vol. 158, no. 3, pp. 420–425, 2020, ISSN: 08895406. DOI: 10.1016/j.ajodo.2019.12.015.
- [157] S. J. Lee, S. Y. Jang, Y. S. Chun, and W. H. Lim, "Three-dimensional analysis of tooth movement after intrusion of a supraerupted molar using a mini-implant with partial-fixed orthodontic appliances," *Angle Orthodontist*, vol. 83, no. 2, pp. 274–279, 2013, ISSN: 00033219. DOI: 10.2319/060912-480.1.
- [158] K. Hayashi, Y. Araki, J. Uechi, H. Ohno, and I. Mizoguchi, "A novel method for the three-dimensional (3-D) analysis of orthodontic tooth movement - Calculation of rotation about and translation along the finite helical axis," *Journal of Biomechanics*, vol. 35, no. 1, pp. 45–51, 2002, ISSN: 00219290. DOI: 10.1016/S0021-9290(01)00166-X.
- [159] K. Hayashi, R. DeLong, and I. Mizoguchi, "Comparison of the finite helical axis and the rectangular coordinate system in representing orthodontic tooth movement," *Journal of Biomechanics*, vol. 39, no. 16, pp. 2925–2933, 2006, ISSN: 00219290. DOI: 10.1016/j.jbiomech.2005.10.030.

- [160] A. C. D. O. Ruellas *et al.*, “3D mandibular superimposition: Comparison of regions of reference for voxel-based registration,” *PLOS ONE*, vol. 11, no. 6, pp. 1–13, 2016, ISSN: 19326203. DOI: 10.1371/journal.pone.0157625.
- [161] H. H. Ammar, P. Ngan, R. J. Crout, V. H. Mucino, and O. M. Mukdadi, “Three-dimensional modeling and finite element analysis in treatment planning for orthodontic tooth movement,” *American Journal of Orthodontics and Dentofacial Orthopedics*, vol. 139, no. 1, e59–e71, 2011, ISSN: 08895406. DOI: 10.1016/j.ajodo.2010.09.020.
- [162] D. Wang *et al.*, “Biomechanical analysis of maxillary anterior teeth movements during different retracting methods with a lever arm miniscrew system in double-slot lingual brackets: A finite element method study,” *Orthodontics and Craniofacial Research*, vol. 26, no. 3, pp. 364–370, 2022, ISSN: 16016343. DOI: 10.1111/ocr.12618.
- [163] A. Fedorov *et al.*, “3D Slicer as an image computing platform for the Quantitative Imaging Network,” *Magnetic Resonance Imaging*, vol. 30, no. 9, pp. 1323–1341, 2012, ISSN: 0730-725X. DOI: <https://doi.org/10.1016/j.mri.2012.05.001>.
- [164] W. Jang, Y. J. Choi, S. Hwang, C. J. Chung, and K. H. Kim, “Anchorage loss assessment of the indirect anchor tooth during adjunctive orthodontic treatment,” *American Journal of Orthodontics and Dentofacial Orthopedics*, vol. 155, no. 3, pp. 347–354, 2019, ISSN: 08895406. DOI: 10.1016/j.ajodo.2018.04.027.
- [165] T. K. Koo and M. Y. Li, “A Guideline of Selecting and Reporting Intraclass Correlation Coefficients for Reliability Research,” *Journal of Chiropractic Medicine*, vol. 15, no. 2, pp. 155–163, 2016, ISSN: 15563707. DOI: 10.1016/j.jcm.2016.02.012.
- [166] D. L. Romanyk, A. George, Y. Li, G. Heo, J. P. Carey, and P. W. Major, “Influence of second-order bracket-archwire misalignments on loads generated during third-order archwire rotation in orthodontic treatment,” *Angle Orthodontist*, vol. 86, no. 3, pp. 358–364, 2016, ISSN: 19457103. DOI: 10.2319/052815-365.1.
- [167] R. W. DeShields, “A Study of Root Resorption in Treated Class II, Division I Malocclusions,” *The Angle Orthodontist*, vol. 39, no. 4, pp. 231–245, 1969.
- [168] S. A. Alexander, “Levels of root resorption associated with continuous arch and sectional arch mechanics,” *American Journal of Orthodontics and Dentofacial Orthopedics*, vol. 110, no. 3, pp. 321–324, 1996, ISSN: 08895406. DOI: 10.1016/S0889-5406(96)80017-5.
- [169] G. F. Schudy and F. F. Schudy, “Intrabacket space and interbracket distance: Critical factors in clinical orthodontics,” *American Journal of Orthodontics and Dentofacial Orthopedics*, vol. 96, no. 4, pp. 281–294, 1989, ISSN: 08895406. DOI: 10.1016/0889-5406(89)90347-8.
- [170] A. Kuhlberg and R. Nanda, “Principles of biomechanics,” in *Biomechanics and Esthetic Strategies in Clinical Orthodontics*, Elsevier Inc., 2005, ch. 1, pp. 1–16, ISBN: 9780721601960. DOI: 10.1016/B978-0-7216-0196-0.50006-0. [Online]. Available: <http://dx.doi.org/10.1016/B978-0-7216-0196-0.50006-0>.

- [171] L. W. Graber, R. L. Vanarsdall, K. W. L. Vig, and G. J. Huang, *Orthodontics: Current Principles and Techniques*, 6th ed. Mosby, 2016, ISBN: 9780323444323. [Online]. Available: <https://ebookcentral.proquest.com/lib/ualberta/detail.action?docID=4747157>.
- [172] H. Mortazavi and M. Baharvand, "Review of common conditions associated with periodontal ligament widening," *Imaging Science in Dentistry*, vol. 46, no. 4, pp. 229–237, 2016, ISSN: 22337830. DOI: 10.5624/isd.2016.46.4.229.
- [173] K. Tanne, Y. Inoue, and M. Sakuda, "Biomechanical behavior of the periodontium before and after orthodontic tooth movement," *The Angle Orthodontist*, vol. 65, no. 2, pp. 123–128, 1995.
- [174] K. Tanne and M. Sakuda, "An analytic technique to simulate tooth bone remodeling during orthodontic tooth movement," *Japanese Journal of Oral Biology*, vol. 36, no. 1, pp. 71–76, 1994. DOI: <https://doi.org/10.2330/joralbiosci1965.36.71>.
- [175] E. Tanaka *et al.*, "Longitudinal measurements of tooth mobility during orthodontic treatment using a Periotest," *Angle Orthodontist*, vol. 75, no. 1, pp. 101–105, 2005, ISSN: 00033219.

# Appendix A: Patient Scan Analysis

## A.1 Initial Scan Alignment

### *Procedure for Alignment*

Scan alignment was completed to later obtain the required bracket position data from patient scans for tooth movement measurement and jig dimension calculations. Model alignment allowed for consistent levelling of bracket position data, which in turn helped create appropriately dimensioned jigs for the experimentation completed in this project. For the analyzed scans presented in Chapter 3, the initial T1 scans for all maxillary and mandibular arches were first imported into Slicer as separate files and oriented prior to superimposition of subsequent treatment scans. Both Excel and 3D Slicer were used, in which the developed Excel sheet mathematically solved for the required translation and rotation values for applying transforms within the Slicer coordinate system (Fig. A.1). In the Excel sheet, values were pasted into the required cells and updated accordingly as transformations were applied to accommodate the changing Slicer coordinates.

On the mandibular/maxillary model opened in 3D Slicer, the inner anterior cusps of the second molars (first molars if second molars were not fully erupted) and the cusps of the canines were selected and labelled as M1, M2, C1, C2, as shown in Figure A.2a. The molars were commonly used in literature when establishing the transverse plane [29, 120]. If the inner anterior cusps were dull and flattened, the posterior cusps were selected instead. The canine cusps were used as the other points of interest, as they were an easily identifiable landmark to manually select. When canines contained double peaks, the highest peak was selected for the landmark.

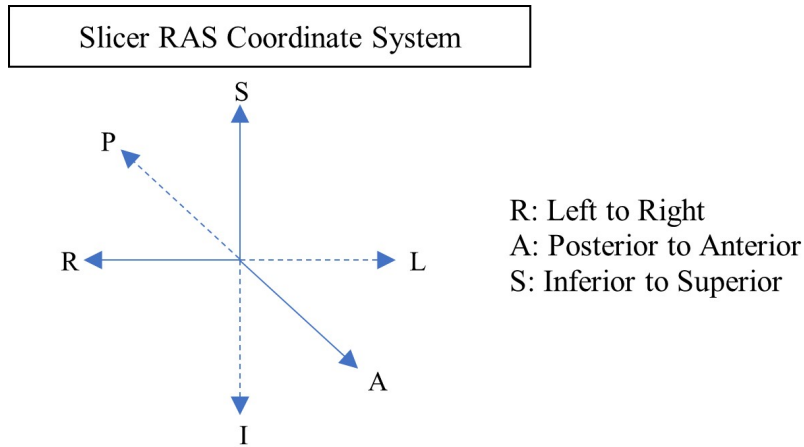


Figure A.1: Slicer global coordinate system with defined axes

After point selection was completed, three lines were established: Molar line, Cuspid line, and Middle line (Fig. A.2b). For the Molar Line, the 3D coordinates of the two selected molar cusps (M1 and M2) were used as the endpoints. For the Cuspid Line, the 3D coordinates of the two selected canine cusps (C1 and C2) were used as endpoints. The Middle Line was established from the Molar Line midpoint to the Cuspid Line midpoint using the 3D coordinates of the calculated Molar Line Center (CM) and the Cuspid Line Center (CC).

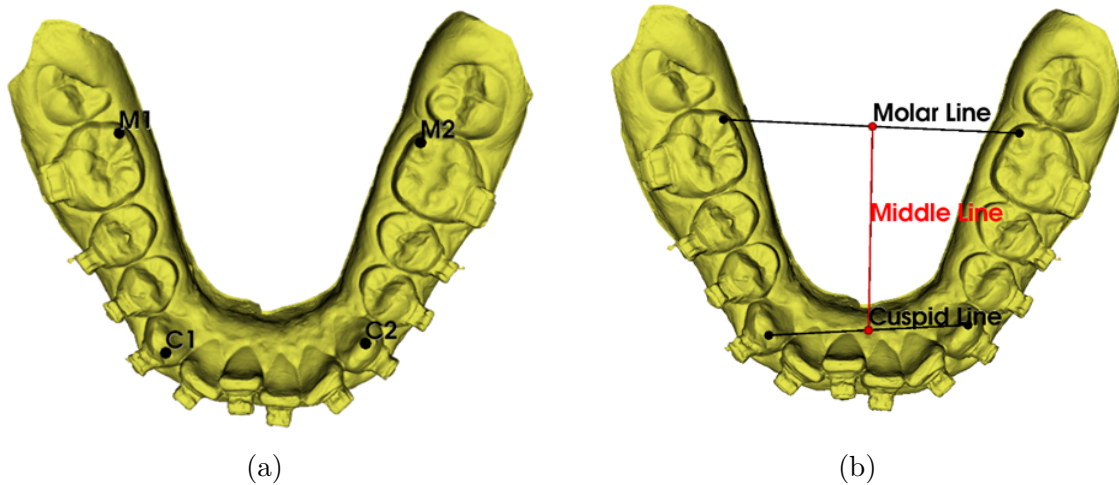


Figure A.2: Alignment of sample mandibular arch within Slicer software; a). Selected molar and canine cusps on sample T1 scan, b). Established lines on sample T1 scan for translational and rotational alignment

The origin point of the model's coordinate system was set to be the Molar Line midpoint

(CM). To ensure that the coordinates of CM were (0,0,0), the entire model (along with the points/lines) was translated by the CM coordinates in the opposite direction (Fig. A.3). The 3D translation was accomplished in Slicer using a new linear transform applied to the model, points, and lines.

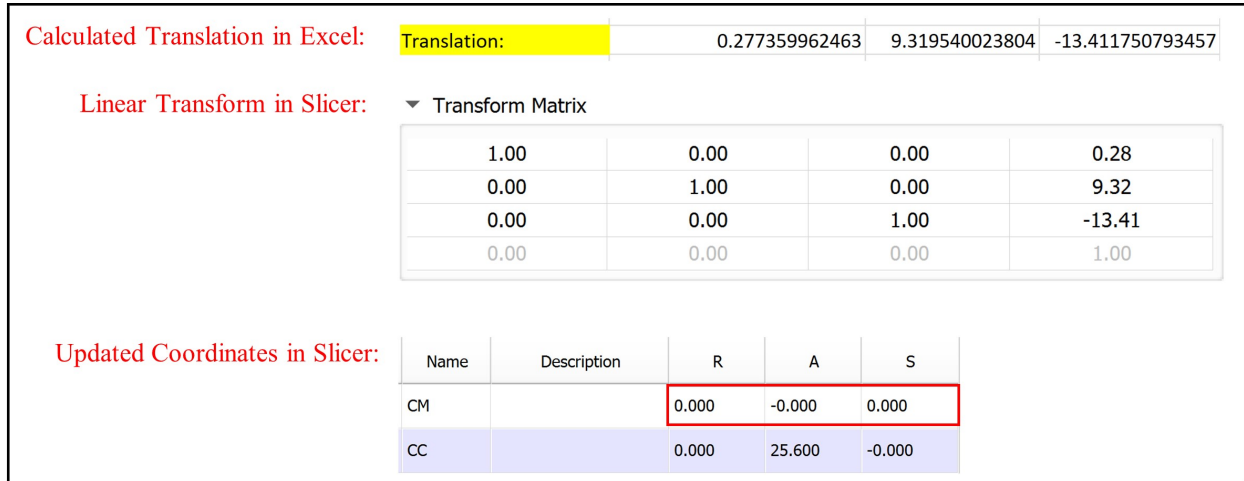


Figure A.3: Translation of sample patient T1 scan to defined origin point

Subsequent alignment steps involved model rotation to align the Middle Line and Molar Line with the Slicer axes. Starting with the R-axis rotation (Figure A.4, Figure A.5), the inverse tangent of the S and A component of CC was calculated in the Excel sheet and applied as a rotational transform in Slicer. After inputting the required angle in the RL transform section in Slicer (leaving other rotations as zero degrees), the transform was applied, and the S coordinate of CC became zero.

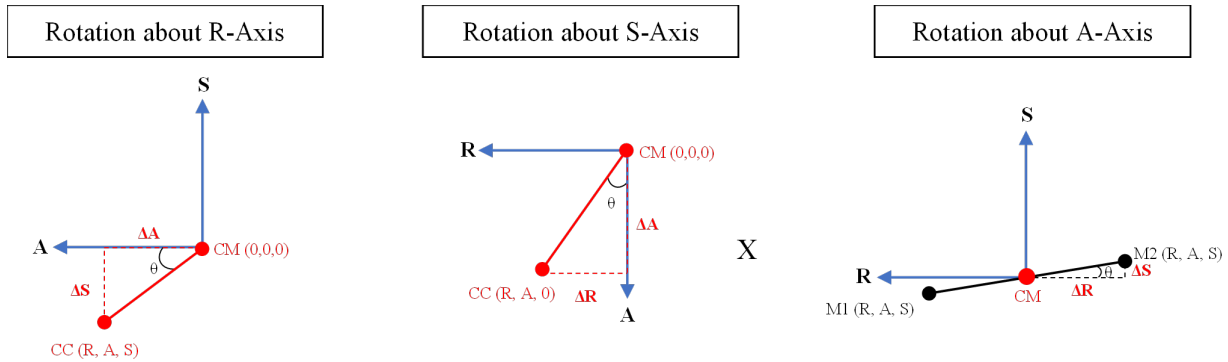


Figure A.4: Schematic of 2D rotation alignment steps performed in Slicer for T1 scan

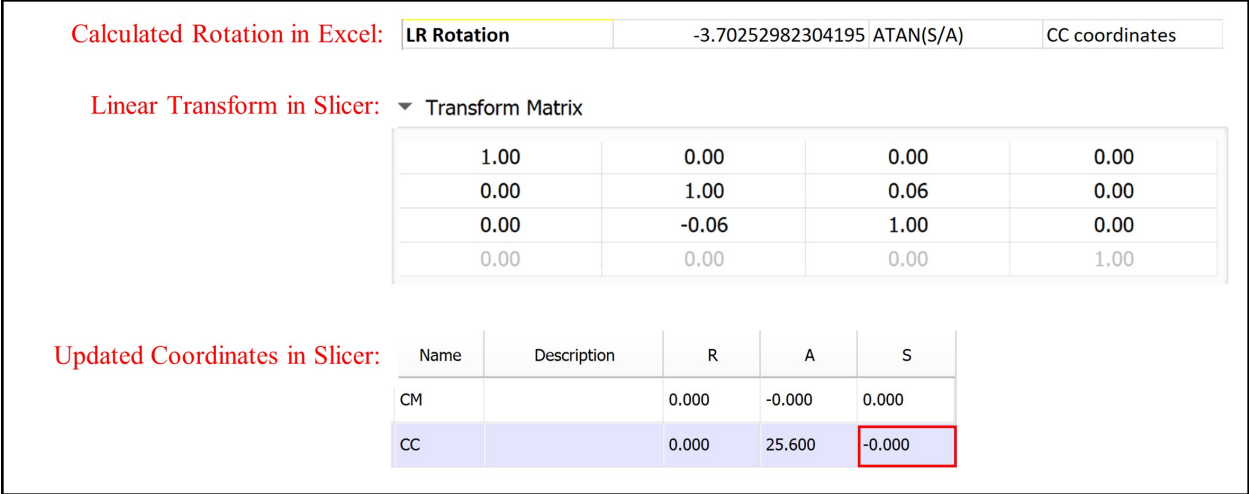


Figure A.5: Rotation of patient T1 scan about Slicer R-Axis

For the S-axis rotation (Figure A.4, Figure A.6), the tan inverse of the R and A component of CC was calculated in Excel and the rotation was achieved with another rotational transform in 3D Slicer. After inputting the required angle in the IS transform section (leave other rotations as zero), the transform was applied, and the R component of CC became zero.

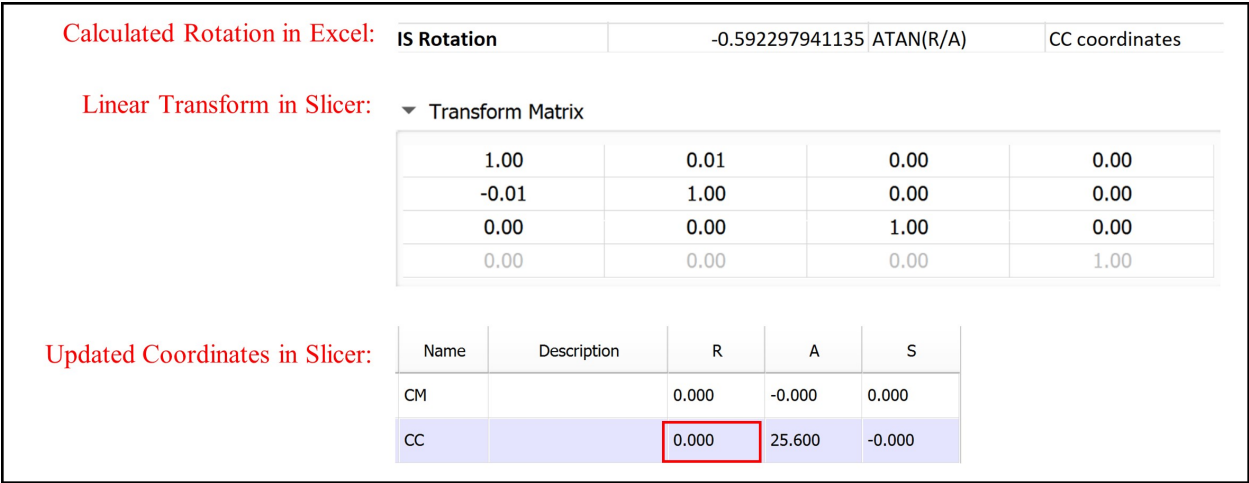


Figure A.6: Rotation of patient T1 scan about Slicer S-Axis

Lastly, the model was rotated about the A-axis (Figure A.4, Figure A.7), in which the tan inverse of M2's S and R component was calculated in the Excel sheet and inputted as another rotational transform in Slicer. After inputting the required angle in the PA section

(leave other rotations as zero), the transform was applied, and the S components of the Molar Line were zero. An example of a properly positioned/aligned T1 scan in comparison to the original import is provided in Figure A.8. For the maxillary arches, an additional 180 degrees was applied about the A-axis to ensure that the teeth were oriented in the occlusal direction (downwards).

**Calculated Rotation in Excel:** PA Rotation      -0.545126261648    ATAN(S/R)    M2 coordinates

**Linear Transform in Slicer:**    Transform Matrix

1.00	0.00	-0.01	0.00
0.00	1.00	0.00	0.00
0.01	0.00	1.00	0.00
0.00	0.00	0.00	1.00

**Updated Coordinates in Slicer:**

Name	Description	R	A	S
M1		18.567	-0.232	-0.000
M2		-18.567	0.232	-0.000

Figure A.7: Rotation of patient T1 scan about Slicer A-Axis

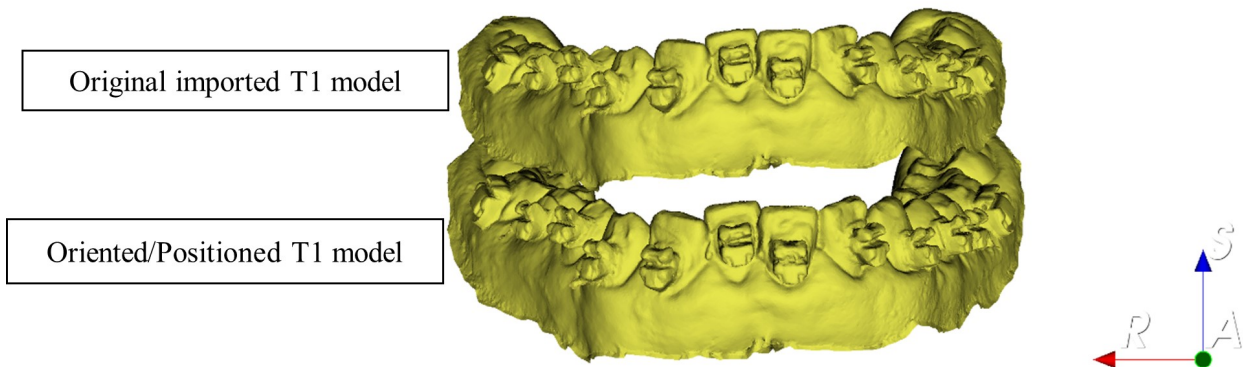


Figure A.8: Comparison of original and oriented sample patient mandibular arch scan

## ***Assessing Intra-Rater and Inter-Rater Reliability for Cusp Selection***

To assess the repeatability of manually selecting the molar and canine cusps, intra-rater reliability and inter-rater reliability were assessed. One sample scan was used, and the four cusps were selected five times by two raters, each selection a day apart. The cusp coordinates were recorded as shown in Table A.1-A.2.

For intra-rater reliability, a repeated measures ANOVA was run in Excel using the Anova: Two-Factor Without Replication option under the Data Analysis tool. Normal distribution and equality of variances were assumed. Future work is recommended to check assumptions and the effect of subject size on the results. The Intraclass Correlation Coefficients (ICCs) were calculated using Equation A.1 originally presented in Koo and Li [165] for the two-way mixed effects model, testing for absolute agreement for a single measurement protocol. The ICC results are presented in Table A.3.

$$ICC = \frac{MS_R - MS_E}{MS_R + (k - 1) MS_E + \frac{k}{n}(MS_C - MS_E)} \quad (A.1)$$

Where,

$MS_R$  = mean square rows

$MS_C$  = mean square columns

$MS_E$  = mean square error

$k$  = no. of observations/raters

$n$  = no. of subjects (no. of points in this context)

For inter-rater reliability, a two-way ANOVA was run in Excel using the Anova: Two-Factor Without Replication option again under the Data Analysis tool. The ICCs were calculated using Equation A.1 for the two-way random effects model this time, testing for absolute agreement for a single rater measurement protocol [165]. The ICC results for each selection time are presented in Table A.4.

Table A.1: Selected molar and canine cusp data over 5 selection times for Rater 1 [mm]

<b>Point</b>	<b>Coordinate</b>	<b>Time 1</b>	<b>Time 2</b>	<b>Time 3</b>	<b>Time 4</b>	<b>Time 5</b>
M1	R	20.8	20.9	21.0	20.8	20.9
	A	-16.3	-16.3	-16.2	-16.2	-16.2
	S	26.8	26.8	26.8	26.8	26.8
M2	R	-19.3	-19.3	-19.3	-19.3	-19.3
	A	-19.0	-19.0	-19.0	-19.0	-19.0
	S	24.3	24.3	24.3	24.3	24.3
C1	R	11.7	11.7	11.7	11.8	11.7
	A	16.1	16.1	16.0	16.0	15.9
	S	30.3	30.3	30.3	30.3	30.3
C2	R	-15.8	-15.8	-15.8	-15.7	-15.7
	A	13.7	13.8	13.8	13.8	13.8
	S	28.4	28.4	28.4	28.4	28.4

Table A.2: Selected molar and canine cusp data over 5 selection times for Rater 2 [mm]

<b>Point</b>	<b>Coordinate</b>	<b>Time 1</b>	<b>Time 2</b>	<b>Time 3</b>	<b>Time 4</b>	<b>Time 5</b>
M1	R	20.8	20.9	21.0	21.3	20.9
	A	-16.3	-16.2	-16.3	-16.3	-16.3
	S	26.8	26.8	26.8	26.7	26.8
M2	R	-19.5	-19.4	-19.3	-19.3	-19.2
	A	-19.2	-19.3	-19.2	-19.3	-19.3
	S	24.3	24.3	24.3	24.2	24.2
C1	R	11.9	11.9	11.6	11.7	11.9
	A	16.1	16.0	16.7	15.9	16.2
	S	30.3	30.3	30.4	30.3	30.3
C2	R	-15.7	-15.7	-15.7	-15.6	-15.7
	A	13.7	13.7	13.8	13.7	13.8
	S	28.4	28.4	28.4	28.4	28.4

Table A.3: ICC results for intra-rater reliability in molar/canine cusp selection (k=5, n=4)

<b>Rater</b>	<b>Coordinate</b>	<b>MS<sub>R</sub></b>	<b>MS<sub>C</sub></b>	<b>MS<sub>E</sub></b>	<b>ICC</b>
Rater 1	R	1986.463	0.001503	0.002026	0.999995
	A	1774.909	0.001249	0.001864	0.999995
	S	32.834	4.07E-05	0.000436	0.999949
Rater 2	R	1997.292	0.018811	0.016428	0.999957
	A	1796.054	0.042554	0.027457	0.999913
	S	32.90482	0.003345	0.001818	0.999666

Table A.4: ICC results for inter-rater reliability in molar/canine cusp selection (k=2, n=12)

<b>Selection Time</b>	<b>MS<sub>R</sub></b>	<b>MS<sub>C</sub></b>	<b>MS<sub>E</sub></b>	<b>ICC</b>
1	808.4386	0.007316	0.007062	0.999982
2	807.5262	0.009818	0.007406	0.999981
3	808.7729	0.012654	0.025469	0.99994
4	807.0374	0.003684	0.012917	0.99997
5	806.7237	0.000861	0.009508	0.999978

## A.2 Scan Superimposition

### *Segmentation of Stable Region*

To analyze the movement of teeth over the various time points of orthodontic treatment as presented in Chapter 3, the patient scans were registered onto the aligned T1 scan in Slicer by first segmenting and isolating the stable surface of each arch. This was done to ensure that the selected region was the only component involved in the superimposition as opposed to the full model where tooth movements were expected over orthodontic treatment. Using the Closed Curve option under the Markups module to select the region of interest, the Curve Cut tool under the Dynamic Modeler module was then applied to separate the area selected from the full model, allowing for the area of interest to become a new separated model.

In the case of the mandibular scans (Figure A.9), the region of interest was the molars as discussed in Chapter 3. However, since each tooth was segmented separately, the Merge Models tool was applied to combine the separately segmented teeth prior to its use in superimposition. For the T1 scan that subsequent scans were superimposed on, the area of interest was 3D segmented and reused for each surface registration.

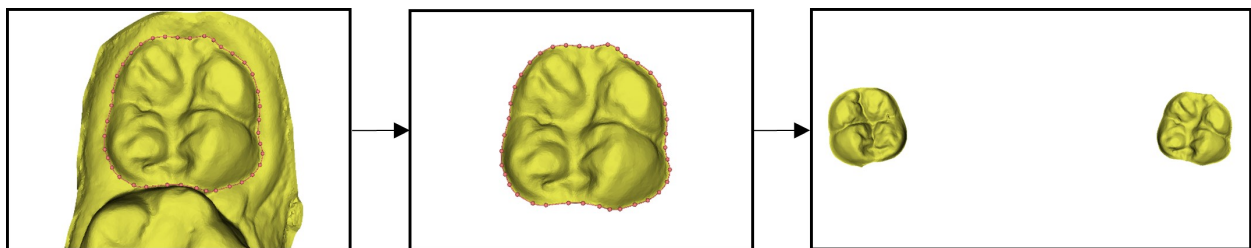


Figure A.9: 3D segmentation and model preparation of mandibular molar surfaces in Slicer for superimposition

The maxillary superimposition had a few notable differences in terms of approach. This includes the T1 rugae region not being segmented. For the selection of subsequent rugae regions (Figure A.10), the entire third rugae was initially traced to calculate the medial 2/3rds and a 5mm region below the rugae was selected using the Open Curve tool. The final region selection was completed with the Closed Curve tool. The rugae was saved as a

separate model by using the Curve Cut tool under the Dynamic Modeler module to separate the selected area from the full model. Since the T1 rugae selection was omitted, an initial manual translation of the subsequent rugae regions also took place to keep the regions as close as possible to the rugae on the T1 full model prior to the registration.

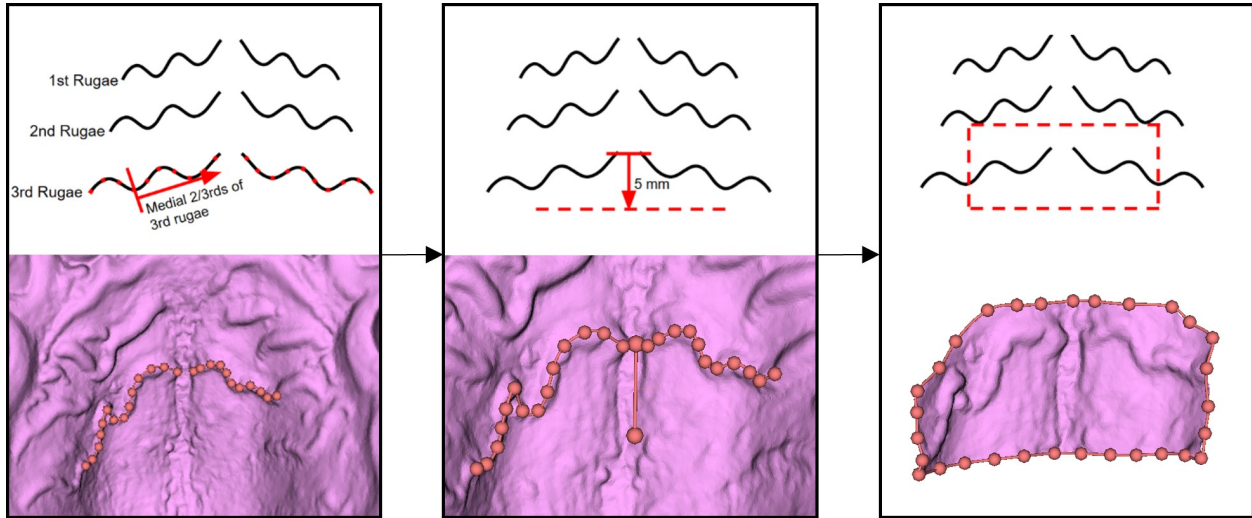


Figure A.10: 3D segmentation of maxillary third rugae surface in Slicer in preparation for superimposition

### *Surface Registration Settings*

Under the CMF Registration module, the Surface Registration option was selected. The fixed model was selected to be the T1 molars (for mandibular arches) and full model (for maxillary arches), and the moving model was selected to be T2/T3/T4 molars (for mandibular arches) or rugae (for maxillary arches). Advanced registration setting options (Table A.5) were also selected after initial research and preliminary trials to better understand which settings greatly affect the superimposition outcome. Preliminary testing as outlined in Table A.6 involved the use of identical models with different starting positions (one model was positioned differently through pure translation, pure rotation, and combined translation/rotation) to test the registration outcomes based on the chosen advanced settings. Settings were varied systematically to determine the most appropriate setting combinations. It was concluded that some settings had more impact on the error than others and Table A.7

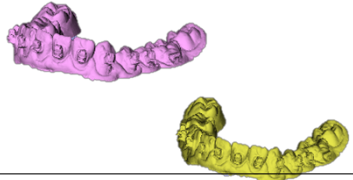
provides example results using the main setting combinations. The same four setting combinations were tested for each scan superimposition completed in Chapter 3, and the trial that provided the smallest range of error (calculated using Model to Model Distance tool explained in the next section) was used to finalize the superimposition.

Table A.5: Advanced registration settings available in Slicer

<b>Check Mean Distance</b>	Force checks distance between model every two iterations
<b>Number of iterations</b>	Manually set algorithm to not continue after this defined number even if mean distance above set threshold (Max number of iterations available: 10,000)
<b>Number of Landmarks</b>	Max number of landmarks on surface used to minimize distance between surfaces (Max number of landmarks available: 2,000)
<b>Maximum of Distance</b>	Distance threshold in which algorithm stops after achieving mean distance below threshold (lowest threshold: 0.00001)

Automatic surface registration was applied to the selected models in which the tool applied the Iterative Closest Point (ICP) algorithm to calculate the linear transformation, for the positional changes to be saved for later use. After the initial superimposition, the full models were superimposed next as they were still in their original unchanged positions. Alignment of the full T2 model onto the T1 model was completed by directly applying the output transformation from the localized registration on the T2 model (Figure A.11). The procedure was repeated for the T3 and T4 scans. Figure A.12 provides an example of superimposed mandibular scans for Patient 1.

Table A.6: Outline of different model position cases for preliminary testing of advanced registration settings in Slicer

Cases to Test for Optimal Advanced Settings Analysis			
<b>Case 1</b>	Movement 1 (IS Axis)	40 mm up	
	Movement 2 (PA Axis)	40 mm front	
	Movement 3 (LR Axis)	40 mm right	
<b>Case 2</b>	Rotation 1 (LR)	20 degrees	
	Rotation 2 (PA)	20 degrees	
	Rotation 3 (IS)	20 degrees	
<b>Case 3</b>	Movement 1 (IS Axis)	40 mm up	
	Movement 2 (PA Axis)	40 mm front	
	Movement 3 (LR Axis)	40 mm right	
	Rotation 1 (LR)	20 degrees	
	Rotation 2 (PA)	20 degrees	
	Rotation 3 (IS)	20 degrees	

Note: Case 1 = pure translation, Case 2 = pure rotation, and Case 3 = combined translation and rotation.

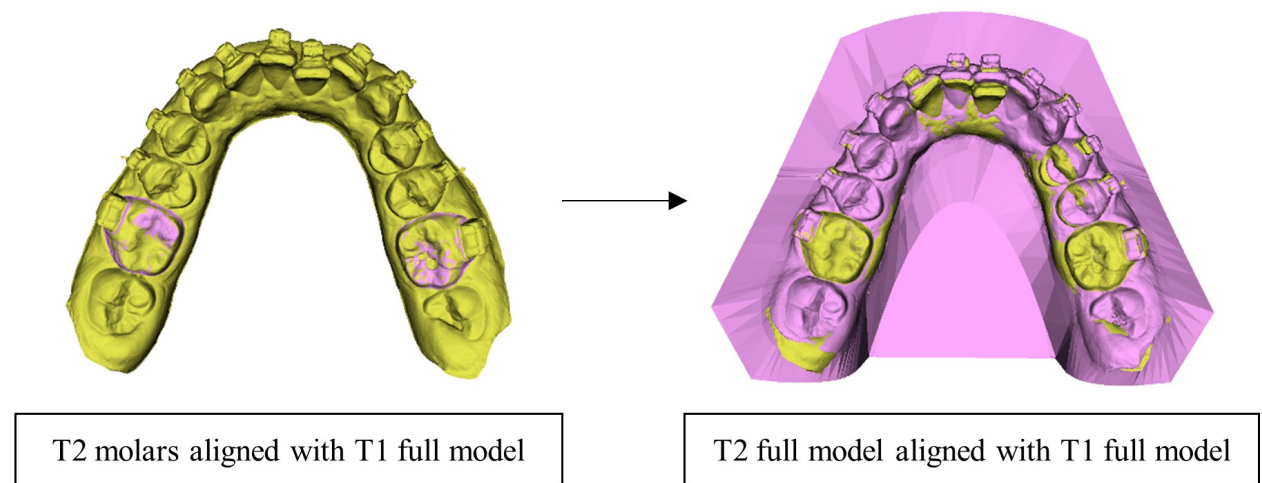


Figure A.11: Example of completed superimposition of patient mandibular T2 scan on T1 scan

Table A.7: Model to Model Distance range for identical scan superimposition cases using four main registration setting combinations, when distance threshold is 0.00001 mm and mean distance is checked

Trial	Iterations	Landmark #	M-to-M Distance Case 1 [mm]	M-to-M Distance Case 2 [mm]	M-to-M Distance Case 3 [mm]
1	1000	200	[-0.000045, 0.0000483]	[-0.00004625, 0.000043]	[-0.0000406, 0.000042]
2	1000	400	[-0.000039, 0.0000396]	[-0.0000479, 0.0000494]	[-0.0000402, 0.0000435]
3	1000	1000	[-0.000042, 0.0000414]	[-0.000043, 0.0000437]	[-0.0000451, 0.000046]
4	1000	2000	[-0.000040, 0.000040]	[-0.0000397, 0.0000401]	[-0.0000422, 0.0000445]

Note: M-to-M Distance = calculated Model to Model Distance, Case 1 = pure translation, Case 2 = pure rotation, and Case 3 = combined translation and rotation.

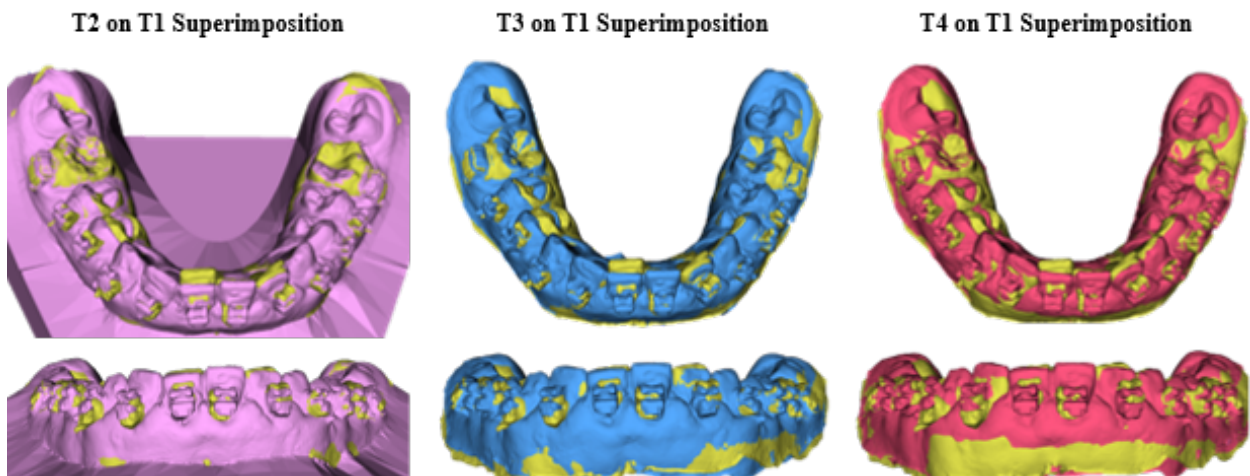


Figure A.12: Patient 1 superimposed scans over treatment

# Assessing Superimposition Error

To assess errors in superimposition, different tools were utilized in Slicer. The Model to Model Distance tool calculated the Hausdorff distance range by measuring the point-by-point distance between the T1 full model and T2-T4 segmented regions. Comparison of the segmented stable region and the full T1 model was performed to avoid unrelated errors from the differences in manual segmentation between the time points. Under the Shape Analysis Module, the Shape Population Viewer tool was used to view the color map of the Model to Model Distance output file (Figure A.13a) to visualize the regions of the output model surface that had higher errors.

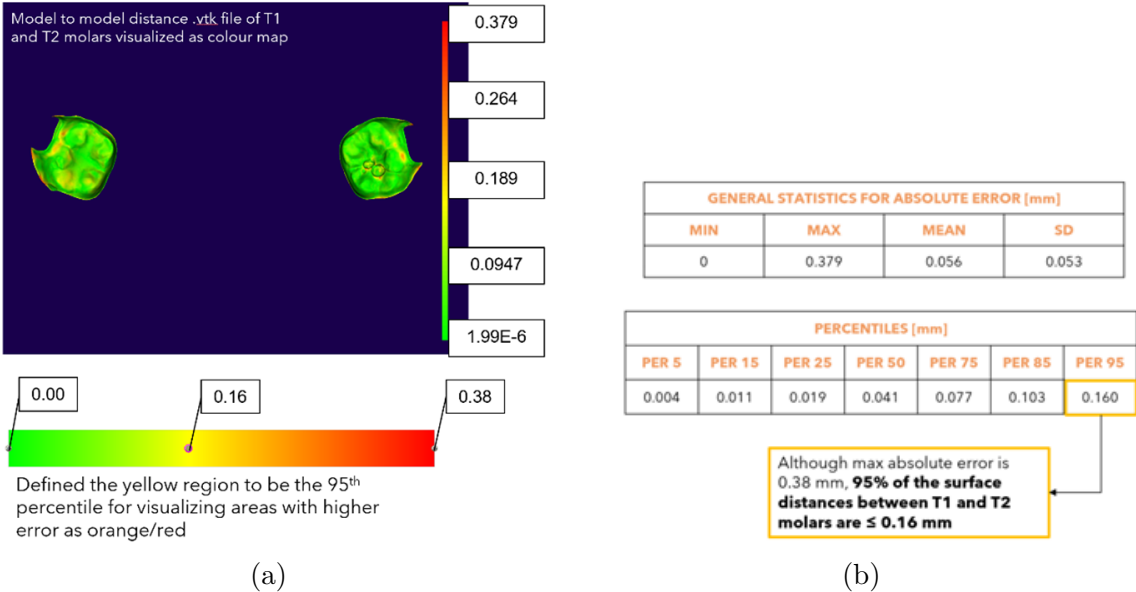


Figure A.13: Assessing superimposition error in Slicer; a). Visualizing colour map of Model to Model Distance output file, b). Statistics on Model to Model Distance output file retrieved using Mesh Statistics tool

Next, the Mesh Statistics tool under the Quantification’s module was used to obtain numerical information on the Model to Model Distance output file. Using this tool, the general statistics for absolute error (min, max, mean, standard deviation) and the absolute percentiles (up to the 95th percentile) were retrieved (Figure A.13b).

## A.3 Bracket Position Selection

### *Procedure for Selecting Bracket Positions*

As presented in Chapter 3’s study, the patient bracket midpoint information was used for driving the fabrication of jig sets used in experiments, as well as the reference feature for measuring clinical tooth movement over treatment. The process involved both the manual selection of points within 3D Slicer and running a MATLAB code to retrieve the final bracket endpoint positions (Figure A.14). Indirect selection of the bracket position was done to avoid areas with possible scan distortion (e.g., the bracket slot) as well as the possibility of bracket gate closure. Therefore, instead of directly selecting points in the slot, the front face of the bracket was the area of interest for placing markers within 3D Slicer. The marker size was set to 0.5588 mm to represent the nominal height of the bracket slot. Two points were placed on either corner of the bracket’s front face, and this was repeated for all the brackets of the investigated arch. Starting at the first bracket again, another set of fiducial points were positioned directly beneath the first set of frontal points. Once four points per bracket were selected (Figure A.14a, Figure A.15), this data was exported into an Excel file to save the bracket position coordinates. This procedure was repeated for the superimposed arches over all time points of treatment.

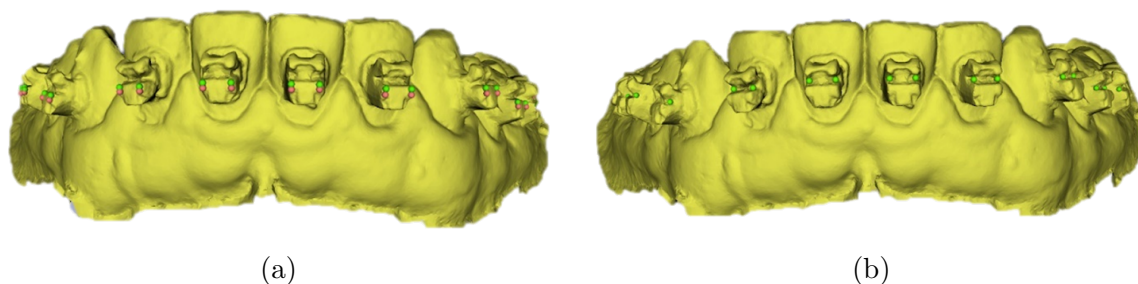


Figure A.14: Visual summary of retrieving bracket slot positions; a). Manually selected bracket positions below slot, b). Final slot endpoint positions calculated in MATLAB

For retrieving the slot endpoint locations (Figure A.14b), the Excel data was imported into the ‘Bracket Slot Endpoint’ MATLAB code (presented within Appendix A.3), which carried out two 2D transformation operations (Figure A.15). These transformations allowed

for the selected points to move with respect to their local bracket coordinate system as summarized in Figure A.16. To complete the second coordinate system transformation, the additional pair of points selected underneath the green points were used to determine the average bracket tilt (Figure A.17).

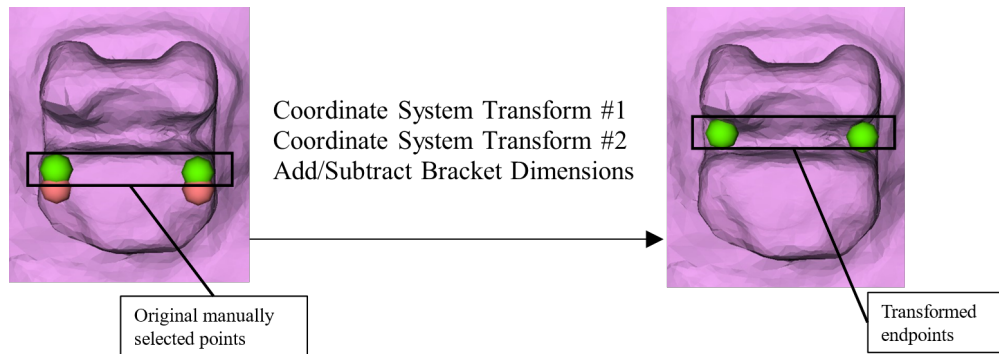


Figure A.15: Summary of bracket position selection procedure to retrieve bracket slot endpoint locations

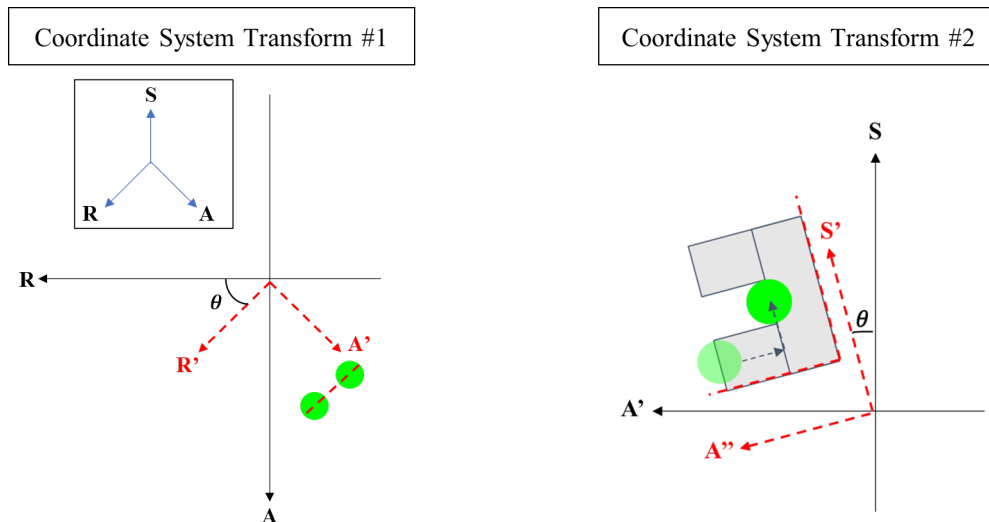


Figure A.16: Summary of 2D coordinate system transformations required for obtaining bracket endpoint positions

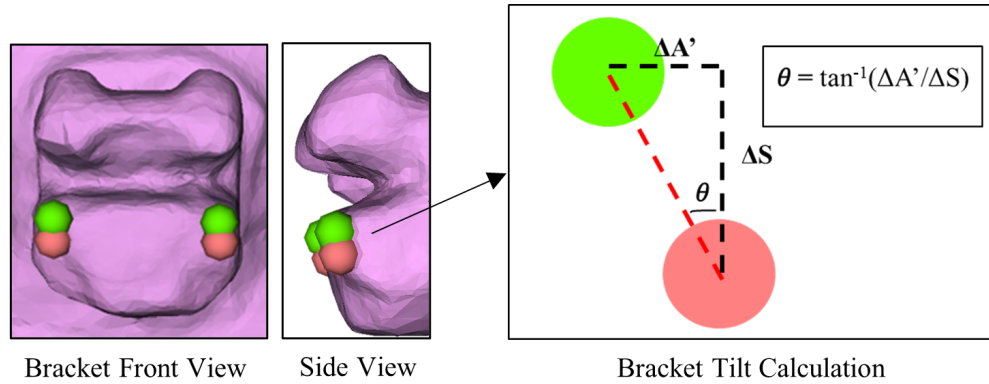


Figure A.17: Calculation of bracket tilt for second coordinate transformation

2D coordinate system transformations were completed using Equation A.2 and altering the variables according to the bracket point coordinates in the Slicer coordinate system. After establishing the specific bracket coordinate system, the nominal bracket dimensions (Slot height dimension: 0.022", Buccal slot dimension: 0.028") were applied to the originally selected points to translate them to the bracket endpoint locations.

$$x' = x \cos \theta + y \sin \theta \quad (\text{A.2a})$$

$$y' = -x \sin \theta + y \cos \theta \quad (\text{A.2b})$$

### ***Bracket Slot Endpoint Code***

The MATLAB script below was created and utilized to transform the originally selected patient bracket positions from scans to their slot endpoint location within the Slicer RAS coordinate system using the nominal bracket dimensions as covered above.

```
% Bracket Slot Endpoint Code

% Import bracket endpoints that were selected at the bracket face and this
% code will provide the mathematical calculations to output the slot
% endpoints

clear
clc

%% STEP 1: Import Endpoint Data
% Upload Excel file with bracket data selected in Slicer
Bracket_Data = 'Bracket_points_Thesis_Data_Maxillary.xlsx';
T1 = readtable(Bracket_Data, 'Sheet', 'P3 T2', 'PreserveVariableNames', true);

% Save R-A-S coordinates from Excel file for Point 1 (P1) and Point 2(P2)
```

```

[P1_R, P1_A, P1_S] = deal(table2array(T1(1:12,2)),table2array(T1(1:12,3)),table2array(T1
(1:12,4)));
[P2_R, P2_A, P2_S] = deal(table2array(T1(1:12,5)),table2array(T1(1:12,6)),table2array(T1
(1:12,7)));

%% STEP 2: Compute the angle produced by the bracket face endpoints
% Solve for the angles
% m1 is the bracket slope in the horizontal plane
m1 = (P2_A - P1_A)./(P2_R - P1_R)
% Solve for angle w.r.t slicer coordinate system
rot_angle = atand(m1)

for i = 1:12
    % If the angle calculated is negative, subtract from 360 degrees
    if rot_angle(i) < 0
        rot_angle(i) = 360 - abs(rot_angle(i));
    end
end

% Display final angle for user
rot_angle

%% STEP 3: Transform Endpoint Data to Local R'A' System
% Transform data to be represented in new CS
% Vertical coordinate 'S' is not affected by CS changes
K = 1;
Num_teeth = 12; %number of teeth considered in arch for patient scans
while K <= Num_teeth
    % Solve for new coordinates of P1
    P1_R_Local(K) = P1_R(K)*cosd(rot_angle(K)) + P1_A(K)*sind(rot_angle(K))
    P1_A_Local(K) = -P1_R(K)*sind(rot_angle(K)) + P1_A(K)*cosd(rot_angle(K))

    % Solve for new coordinates of P2
    P2_R_Local(K) = P2_R(K)*cosd(rot_angle(K)) + P2_A(K)*sind(rot_angle(K))
    P2_A_Local(K) = -P2_R(K)*sind(rot_angle(K)) + P2_A(K)*cosd(rot_angle(K))

    K = K + 1;
end

%% STEP 4: Transform Endpoint Data to Local S'A'' System
% Transform data to be represented in new CS
% Horizontal coordinate 'R' is not affected by new CS changes

% Open points specifically for the calculation of the bracket angle/slant
T2 = readtable(Bracket_Data, 'Sheet', 'P3 T2 Angle Points', 'PreserveVariableNames', true);
[P1_R2, P1_A2, P1_S2] = deal(table2array(T2(1:12,2)),table2array(T2(1:12,3)),table2array(T2
(1:12,4)));
[P2_R2, P2_A2, P2_S2] = deal(table2array(T2(1:12,5)),table2array(T2(1:12,6)),table2array(T2
(1:12,7)));

% Transform these additional points to the same R'A' system as before
K = 1;
Num_teeth = 12;
while K <= Num_teeth
    % Solve for new coordinates of extra P1
    P1_A_Local2(K) = -P1_R2(K)*sind(rot_angle(K)) + P1_A2(K)*cosd(rot_angle(K))
    % Solve for new coordinates of extra P2
    P2_A_Local2(K) = -P2_R2(K)*sind(rot_angle(K)) + P2_A2(K)*cosd(rot_angle(K))

    K = K + 1;
end

% Solve for the bracket angles/slants
% For P1 angles
mP1 = (P1_A_Local - P1_A_Local2)./transpose((P1_S - P1_S2))
% Solve for angle
P1_tilt = atand(mP1)

```

```

% For P2 angles
mP2 = (P2_A_Local - P2_A_Local2)./transpose((P2_S - P2_S2))
% Solve for angle
P2_tilt = atand(mP2)

% Find the average between the angles solved at each end of bracket
bracket_tilt = (P1_tilt + P2_tilt)./2
for i = 1:12
    % If the angle calculated is negative, subtract from 360 degrees
    if bracket_tilt(i) < 0
        bracket_tilt(i) = 360 - abs(bracket_tilt(i));
    end
end
% Display final angle for user
bracket_tilt

% Now knowing the individual bracket slants, transform data to S'A'' CS
K = 1;
Num_teeth = 12;

while K <= Num_teeth
    % Solve for new coordinates of P1
    P1_S_Local(K) = P1_S(K)*cosd(bracket_tilt(K)) + P1_A_Local(K)*sind(bracket_tilt(K))
    P1_A_Local_new(K) = -P1_S(K)*sind(bracket_tilt(K)) + P1_A_Local(K)*cosd(bracket_tilt(K))

    % Solve for new coordinates of P2
    P2_S_Local(K) = P2_S(K)*cosd(bracket_tilt(K)) + P2_A_Local(K)*sind(bracket_tilt(K))
    P2_A_Local_new(K) = -P2_S(K)*sind(bracket_tilt(K)) + P2_A_Local(K)*cosd(bracket_tilt(K))

    K = K + 1;
end

%% STEP 5: Subtract Nominal Slot Distance and Add Slot Height
% Apply nominal bracket dimensions to selected points
% Buccal Slot Dimensions: Apply to local Y-dirn Coord ('A' dirn in Slicer)
NomSlot = 0.7112;
for i = 1:12
    if P1_A_Local_new(i) < 0
        P1_A_NomSlot(i) = P1_A_Local_new(i) + NomSlot;
    else
        P1_A_NomSlot(i) = P1_A_Local_new(i) - NomSlot;
    end
end
P1_A_NomSlot

for i = 1:12
    if P2_A_Local_new(i) < 0
        P2_A_NomSlot(i) = P2_A_Local_new(i) + NomSlot;
    else
        P2_A_NomSlot(i) = P2_A_Local_new(i) - NomSlot;
    end
end
P2_A_NomSlot

% Slot Height Dimensions: Apply to local Z-dirn Coord ('S' dirn in Slicer)
SlotHeight = 0.5588; %% Change this value
P1_S_NomSlot = P1_S_Local + SlotHeight;
P2_S_NomSlot = P2_S_Local + SlotHeight;

%% STEP 6: Convert back to R'A' Slicer Coordinate System
% Resolve for bracket slot endpoint coordinates w.r.t R'A' CS
% Same calculations as before but with negative bracket slant angle
K = 1;
Num_teeth = 12;
while K <= Num_teeth
    % Solve for new coordinates of P1
    P1_S_Global(K) = P1_S_NomSlot(K)*cosd(-bracket_tilt(K)) + P1_A_NomSlot(K)*sind(-bracket_tilt(K));

```

```

P1_A_Local_Last(K) = -P1_S_NomSlot(K)*sind(-bracket_tilt(K)) + P1_A_NomSlot(K)*cosd(-bracket_tilt(K));

% Solve for new coordinates of P2
P2_S_Global(K) = P2_S_NomSlot(K)*cosd(-bracket_tilt(K)) + P2_A_NomSlot(K)*sind(-bracket_tilt(K));
P2_A_Local_Last(K) = -P2_S_NomSlot(K)*sind(-bracket_tilt(K)) + P2_A_NomSlot(K)*cosd(-bracket_tilt(K));

K = K + 1;
end

%% STEP 7: Convert back to RA Slicer Coordinate System
% Resolve for bracket slot endpoint coordinates w.r.t RA CS
% Same calculations as before but with negative bracket horizontal slope
% angle
K = 1;
Num_teeth = 12;
while K <= Num_teeth
    % Solve for new coordinates of P1
    P1_R_Global(K) = P1_R_Local(K)*cosd(-rot_angle(K)) + P1_A_Local_Last(K)*sind(-rot_angle(K));
    P1_A_Global(K) = -P1_R_Local(K)*sind(-rot_angle(K)) + P1_A_Local_Last(K)*cosd(-rot_angle(K));

    % Solve for new coordinates of P2
    P2_R_Global(K) = P2_R_Local(K)*cosd(-rot_angle(K)) + P2_A_Local_Last(K)*sind(-rot_angle(K));
    P2_A_Global(K) = -P2_R_Local(K)*sind(-rot_angle(K)) + P2_A_Local_Last(K)*cosd(-rot_angle(K));

    K = K + 1;
end

%% STEP 8: Save Results in Same Excel File
% Transpose vectors
P1_R_Global = transpose(P1_R_Global)
P1_A_Global = transpose(P1_A_Global)
P1_S_Global = transpose(P1_S_Global)
P2_R_Global = transpose(P2_R_Global)
P2_A_Global = transpose(P2_A_Global)
P2_S_Global = transpose(P2_S_Global)

% Save values in a table
A4 = table(P1_R_Global, P1_A_Global, P1_S_Global, P2_R_Global, P2_A_Global, P2_S_Global);
disp(A4)

% Save values back into same Excel file for later use
writematrix(P1_R_Global, Bracket_Data, 'Sheet', 'P3 T2 Slot Endpoints', 'Range', 'B2')
writematrix(P1_A_Global, Bracket_Data, 'Sheet', 'P3 T2 Slot Endpoints', 'Range', 'C2')
writematrix(P1_S_Global, Bracket_Data, 'Sheet', 'P3 T2 Slot Endpoints', 'Range', 'D2')
writematrix(P2_R_Global, Bracket_Data, 'Sheet', 'P3 T2 Slot Endpoints', 'Range', 'E2')
writematrix(P2_A_Global, Bracket_Data, 'Sheet', 'P3 T2 Slot Endpoints', 'Range', 'F2')
writematrix(P2_S_Global, Bracket_Data, 'Sheet', 'P3 T2 Slot Endpoints', 'Range', 'G2')

% to check consistency of calculations, replot these final coordinates in 3D Slicer
% and visually inspect whether the points line up where we expect them to

```

## *Assessing Intra-Rater Reliability for Manual Bracket Selection*

To assess the repeatability of the manual bracket point selection, intra-rater reliability was assessed. Three mandibular scans were chosen randomly, and the bracket positions were selected three times on each scan by one rater, each selection a week apart. The final calculated slot midpoint coordinates of each bracket were recorded for each scan in Table A.8-A.10.

Table A.8: Bracket slot midpoint data for random scan 1 [mm]

Tooth	Selection Time 1			Selection Time 2			Selection Time 3		
	R	A	S	R	A	S	R	A	S
3-6	-27.5	11.2	-2.3	-27.5	11.2	-2.3	-27.5	11.2	-2.3
3-5	-25.6	20.5	-4.2	-25.6	20.5	-4.2	-25.6	20.5	-4.2
3-4	-21.8	29.0	-4.7	-21.8	29.0	-4.6	-21.7	29.0	-4.7
3-3	-17.6	35.6	-4.1	-17.6	35.6	-4.1	-17.6	35.6	-4.1
3-2	-9.9	41.4	-4.6	-9.9	41.4	-4.6	-9.9	41.3	-4.7
3-1	-3.3	43.4	-4.7	-3.3	43.4	-4.7	-3.3	43.4	-4.7
4-1	3.0	43.2	-4.8	3.0	43.1	-4.8	2.9	43.1	-4.9
4-2	9.5	41.0	-5.3	9.5	41.0	-5.3	9.5	41.0	-5.3
4-3	16.9	36.0	-6.2	16.9	36.0	-6.2	16.9	36.0	-6.2
4-4	21.6	28.0	-5.2	21.6	28.0	-5.2	21.6	28.1	-5.2
4-5	24.3	21.0	-4.9	24.3	21.0	-5.0	24.4	21.1	-4.9
4-6	26.6	12.2	-3.3	26.6	12.2	-3.4	26.6	12.2	-3.3

Table A.9: Bracket slot midpoint data for random scan 2 [mm]

Tooth	Selection Time 1			Selection Time 2			Selection Time 3		
	R	A	S	R	A	S	R	A	S
3-6	-27.5	11.5	-2.5	-27.5	11.5	-2.6	-27.5	11.5	-2.6
3-5	-24.5	19.5	-3.2	-24.5	19.6	-3.3	-24.5	19.6	-3.3
3-4	-21.4	25.6	-3.5	-21.4	25.6	-3.5	-21.4	25.6	-3.5
3-3	-16.3	32.3	-3.7	-16.4	32.3	-3.7	-16.3	32.3	-3.6
3-2	-10.0	37.1	-3.7	-10.0	37.1	-3.7	-10.0	37.1	-3.7
3-1	-3.6	39.3	-3.5	-3.6	39.3	-3.5	-3.6	39.2	-3.5
4-1	2.5	39.5	-3.5	2.5	39.5	-3.5	2.5	39.5	-3.5
4-2	10.0	37.3	-3.5	10.0	37.3	-3.5	10.0	37.4	-3.5
4-3	16.4	32.1	-3.2	16.4	32.1	-3.2	16.4	32.1	-3.2
4-4	20.9	25.9	-3.2	20.9	25.9	-3.2	21.0	25.9	-3.1
4-5	24.2	18.3	-2.5	24.2	18.3	-2.5	24.2	18.3	-2.6
4-6	27.0	10.9	-2.0	27.0	10.9	-2.0	27.0	10.9	-2.0

Table A.10: Bracket slot midpoint data for random scan 3 [mm]

Tooth	Selection Time 1			Selection Time 2			Selection Time 3		
	R	A	S	R	A	S	R	A	S
3-6	-28.1	-1.0	-0.3	-28.1	-1.0	-0.4	-28.1	-1.0	-0.3
3-5	-25.6	8.6	-4.1	-25.7	8.6	-4.0	-25.7	8.6	-4.1
3-4	-22.8	15.5	-4.9	-22.8	15.5	-4.9	-22.7	15.5	-5.1
3-3	-17.2	23.0	-5.3	-17.2	23.1	-5.3	-17.2	23.1	-5.3
3-2	-10.5	27.8	-5.2	-10.5	27.8	-5.2	-10.5	27.8	-5.3
3-1	-3.6	30.2	-5.0	-3.6	30.1	-5.0	-3.5	30.1	-5.0
4-1	2.7	30.1	-4.9	2.8	30.1	-4.9	2.8	30.2	-4.9
4-2	9.4	28.0	-5.2	9.4	27.9	-5.2	9.4	28.0	-5.3
4-3	15.8	23.6	-5.9	15.8	23.6	-5.8	15.9	23.7	-5.8
4-4	21.7	16.1	-5.5	21.6	16.1	-5.5	21.7	16.2	-5.5
4-5	24.2	9.1	-4.6	24.1	9.1	-4.7	24.1	9.1	-4.7
4-6	28.0	-2.5	-2.7	27.9	-2.5	-2.7	28.0	-2.5	-2.7

Using Excel's Two-Factor Without Replication option to run the Repeat Measures ANOVA test, the required mean square variables were obtained to calculate the ICC values using Equation A.1 for each random scan in each direction based on the Slicer coordinate system. The results are presented in Table A.11-A.13.

Table A.11: ICC results for intra-rater reliability for random scan 1 (k=3, n=12)

Coordinate	MS <sub>R</sub>	MS <sub>C</sub>	MS <sub>E</sub>	ICC
R	1214.212	0.000505	0.000475	0.999999
A	413.415	0.000198	0.000423	0.999997
S	2.946	0.000284	0.000278	0.999717

Table A.12: ICC results for intra-rater reliability for random scan 2 (k=3, n=12)

Coordinate	MS <sub>R</sub>	MS <sub>C</sub>	MS <sub>E</sub>	ICC
R	1178.819	0.000579	0.000319	0.999999
A	327.127	0.000485	0.000289	0.999997
S	0.821	0.001076	0.000623	0.997590

Table A.13: ICC results for intra-rater reliability for random scan 3 (k=3, n=12)

Coordinate	MS <sub>R</sub>	MS <sub>C</sub>	MS <sub>E</sub>	ICC
R	1244.600	0.002337	0.000936	0.999997
A	409.312	0.001014	0.000555	0.999996
S	7.073	0.005166	0.002068	0.999014

## A.4 Calculating Clinical Tooth Movements

### *Procedure for Calculating Tooth Movements*

The tooth movements that occur over the various time points of treatment were presented in Chapter 3. The ‘Tooth Movement Calculation’ MATLAB code was developed (presented in the next section of Appendix A.4) to intake the manually selected bracket endpoints from 3D Slicer and calculate the translational movements with respect to the OSIM cantilever directions for direct comparison with biomechanical data.

Bracket position data in the original RAS Slicer coordinate system for two time points of treatment were first imported into MATLAB. Translation changes in the OSIM global coordinate system were calculated using the global X, Y, Z coordinates and subtracting the  $T_i$  midpoint coordinates from the  $T_{i+1}$  midpoint coordinates. Local translation measurements for the X and Y-Directions were evaluated by transforming the global changes to the corresponding local cantilever directions using Equation A.3 below.

$$\Delta x_{Local} = (x_{T_{i+1},global} - x_{T_i,global}) \cos \theta + (y_{T_{i+1},global} - y_{T_i,global}) \sin \theta \quad (\text{A.3a})$$

$$\Delta y_{Local} = -(x_{T_{i+1},global} - x_{T_i,global}) \sin \theta + (y_{T_{i+1},global} - y_{T_i,global}) \cos \theta \quad (\text{A.3b})$$

## Tooth Movement Calculation Code

This MATLAB script was created to calculate patient clinical tooth movement by comparing bracket midpoint positions between two treatment intervals as outlined above.

```
% Tooth Movement Calculation Code

% Calculates tooth movements between two sets of patient points uploaded from
% Excel

%% Import Ti Scan Data
% First import the endpoints selected
% Import patient excel file data
Data = 'Bracket_points_Thesis_Data_Maxillary.xlsx';
T1 = readtable(Data, 'Sheet', 'P2 T3 Slot Endpoints', 'PreserveVariableNames', true);

[R1_R1, R1_A1, R1_S1] = deal(table2array(T1(1:12,2)), table2array(T1(1:12,3)), table2array(T1
(1:12,4)));
[R2_R1, R2_A1, R2_S1] = deal(table2array(T1(1:12,5)), table2array(T1(1:12,6)), table2array(T1
(1:12,7)));

% Solve for the midpoint
% L is the midpoint between slot points, use for landmark
L_R1 = (R1_R1 + R2_R1)/2;
L_A1 = (R1_A1 + R2_A1)/2;
L_S1 = (R1_S1 + R2_S1)/2;

% Convert RAS to XYZ System
% Midpoint
M_X1 = L_A1;
M_Y1 = L_R1*-1;
M_Z1 = L_S1;

% Endpoints
P1_X1 = (R1_A1);
P1_Y1 = (R1_R1*-1);
P1_Z1 = (R1_S1);

P2_X1 = (R2_A1);
P2_Y1 = (R2_R1*-1);
P2_Z1 = (R2_S1);

% Plot the bracket midpoints and endpoints for Ti
figure(1)
point1 = plot3(M_X1, M_Y1, M_Z1, '.', 'Color', 'b', 'MarkerSize', 25);
hold on
point2 = plot3(P1_X1, P1_Y1, P1_Z1, '.', 'Color', 'g', 'MarkerSize', 25);
plot3(P2_X1, P2_Y1, P2_Z1, '.', 'Color', 'g', 'MarkerSize', 25);

% Solve for the angles
% m1 is the real bracket slope for Ti
m1 = (P2_X1 - P1_X1)./(P2_Y1 - P1_Y1);
% Solve for angle w.r.t local cantilever x-axis
rot_angle_T1_v1 = atand(m1)

% Display Ti points
Tooth_num = ['2-6'; '2-5'; '2-4'; '2-3'; '2-2'; '2-1'; '1-1'; '1-2'; '1-3'; '1-4'; '1-5'; '
1-6'];
translation = table(Tooth_num, M_X1, M_Y1, M_Z1, P1_X1, P1_Y1, P1_Z1, P2_X1, P2_Y1, P2_Z1);
translation.Properties.VariableNames = {'Tooth', 'Mid X', 'Mid Y', 'Mid Z', 'P1 X', 'P1 Y',
'P1 Z', 'P2 X', 'P2 Y', 'P2 Z'};
disp('Time 1 Points')
disp(translation)
```

```

%% Import Ti+1 Scan Data
T2 = readtable(Data, 'Sheet', 'P2 T4 Slot Endpoints', 'PreserveVariableNames', true);

%Put RAS coordinates into XYZ
[R1_R2, R1_A2, R1_S2] = deal(table2array(T2(1:12,2)), table2array(T2(1:12,3)), table2array(T2(1:12,4)));
[R2_R2, R2_A2, R2_S2] = deal(table2array(T2(1:12,5)), table2array(T2(1:12,6)), table2array(T2(1:12,7)));

% Solve for the midpoint
% L is the midpoint between slot points, use for landmark
L_R2 = (R1_R2 + R2_R2)/2;
L_A2 = (R1_A2 + R2_A2)/2;
L_S2 = (R1_S2 + R2_S2)/2;

% Convert RAS to XYZ System for Mandibular
% Midpoint
M_X2 = L_A2;
M_Y2 = L_R2*-1;
M_Z2 = L_S2;

% Endpoints
P1_X2 = (R1_A2);
P1_Y2 = (R1_R2*-1);
P1_Z2 = (R1_S2);

P2_X2 = (R2_A2);
P2_Y2 = (R2_R2*-1);
P2_Z2 = (R2_S2);

point3 = plot3(M_X2, M_Y2, M_Z2, '.', 'Color', 'black', 'MarkerSize', 25);
point4 = plot3(P1_X2, P1_Y2, P1_Z2, '.', 'Color', 'magenta', 'MarkerSize', 25);
plot3(P2_X2, P2_Y2, P2_Z2, '.', 'Color', 'magenta', 'MarkerSize', 25);
xlabel('X'); ylabel('Y'); zlabel('Z')
title('T1 and T2 Bracket Positions')
h = [point1(1); point2(1); point3(1); point4(1)];
% Label names according to order of plotting
legend(h, 'T1 Bracket Midpoint', 'T1 Bracket Endpoint', 'T2 Bracket Midpoint', 'T2 Bracket Endpoint');

% Solve for the bracket angles
% m1 is the real bracket slope for Ti+1
m2 = (P2_X2 - P1_X2)./(P2_Y2 - P1_Y2);
% Solve for angle w.r.t local cantilever x-axis
rot_angle_T2 = atand(m2);

% Display Ti+1 points
Tooth_num = ['2-6'; '2-5'; '2-4'; '2-3'; '2-2'; '2-1'; '1-1'; '1-2'; '1-3'; '1-4'; '1-5'; '1-6'];
translation = table(Tooth_num, M_X2, M_Y2, M_Z2, P1_X2, P1_Y2, P1_Z2, P2_X2, P2_Y2, P2_Z2);
translation.Properties.VariableNames = {'Tooth', 'Mid X', 'Mid Y', 'Mid Z', 'P1 X', 'P1 Y', 'P1 Z', 'P2 X', 'P2 Y', 'P2 Z'};
disp('Time 2 Points')
disp(translation)

%% Measure Translation Movements
% Global Differences
% X-DIRECTION
% Solve for global difference in X Direction
delta_X = M_X2 - M_X1;
% Y-DIRECTION
% Solve for global difference in Y Direction
delta_Y = M_Y2 - M_Y1;

% OSIM cantilever angles
theta = [-9, -18, -25, -33, -56, -79, -102, -130, -148, -156, -164, -169];

```

```

% Local Differences
K = 1;
Num_teeth = 12;
while K <= Num_teeth
    % Solve for local difference in tooth's mesio-distal direction
    delta_MD(K) = delta_X(K)*cosd(theta(K)) + delta_Y(K)*sind(theta(K));

    % Solve for local difference in tooth's bucco-lingual direction
    delta_BL(K) = -delta_X(K)*sind(theta(K)) + delta_Y(K)*cosd(theta(K));
    K = K + 1;
end

% Z-DIRECTION
% Solve for global difference = occlusal-gingival difference in Z Direction
delta_OG = MZ2 - MZ1;

%% Measure Rotation Movements (not used for thesis work)
% Rotation about Z-axis
% Find difference between angle at Ti+1 and Ti
rotation = rot_angle_T2 - rot_angle_T1_v1;

%% Display final calculations
% Put each column of Delta values back into table for display
Tooth_num = ['2-6'; '2-5'; '2-4'; '2-3'; '2-2'; '2-1'; '1-1'; '1-2'; '1-3'; '1-4'; '1-5'; '1-6'];
translation = table(Tooth_num, transpose(delta_MD), transpose(delta_BL), delta_OG, rotation)
;
translation.Properties.VariableNames = {'Tooth', 'Mesio-distal', 'Buccal-lingual', 'Occlusal-gingival', '1st Order Rotation'};
disp('Translation & Rotation in specific local tooth directions')
disp(translation)

```

# Appendix B: Jig Design & Bracket Position Preparation for Experiments

## B.1 Default Jig Configuration Design in SolidWorks

The jigs used for experimentation, as presented in Chapter 3, were designed in SolidWorks. A default configuration was built with generic dimensions later modified using an integrated Excel design table for patient-specific jig sets. The jig base was first sketched as a 5 mm x 11 mm rectangle on the Top Plane and extruded by 2 mm using the Extruded Boss/Base feature (Figure B.1).

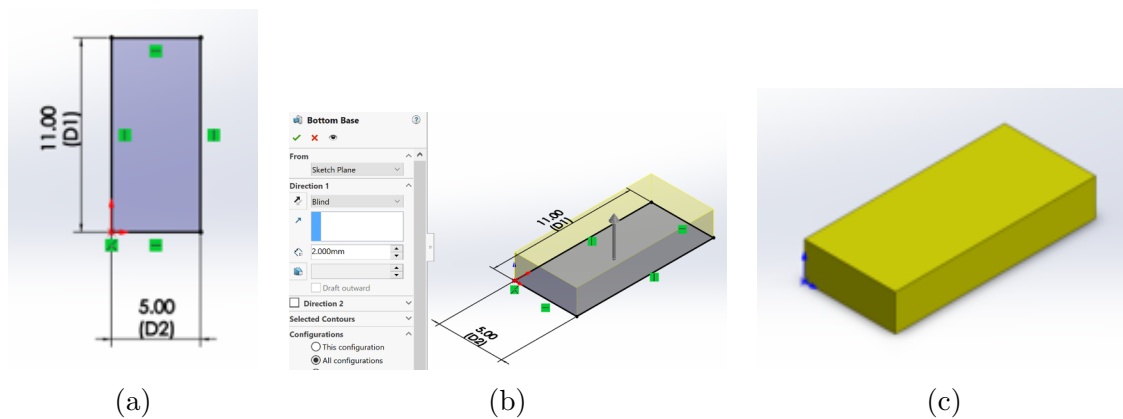


Figure B.1: Construction of jig bottom base in SolidWorks; a). Sketch, b). Extruded sketch, c). Completed bottom base part

Next, sketches were created for side walls extending upwards from the bottom base (Figure B.2). The space between the walls was dimensioned as 4 mm to hold a nut (for mounting purposes). The Extruded Boss/Base feature was used to extrude the two rectangles by 3 mm.

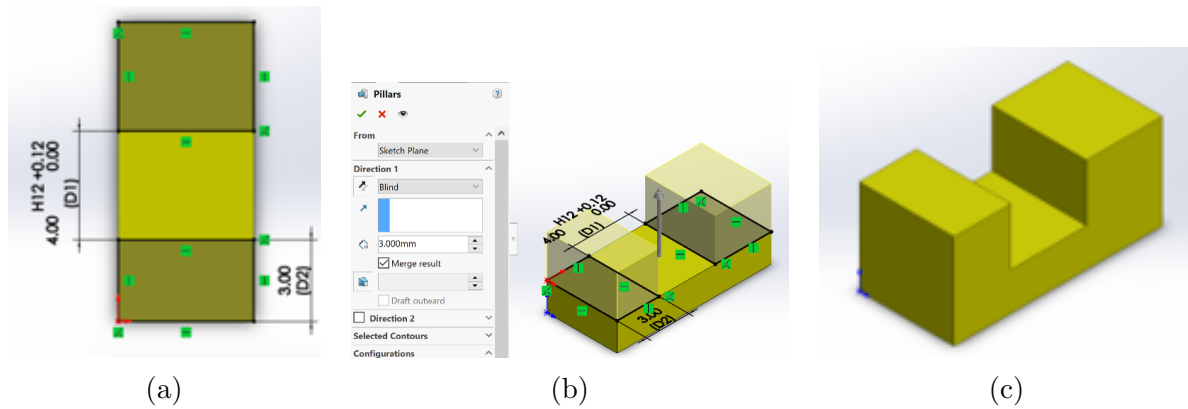


Figure B.2: Construction of jig side walls in SolidWorks; a). Sketch, b). Extruded sketch, c). Completed side walls

A new sketch with a 4 mm extension in comparison to the bottom base was created on the top surface of the side walls to create the top base (Figure B.3). The sketch was then extruded by 2 mm using the Extruded Boss/Base feature.

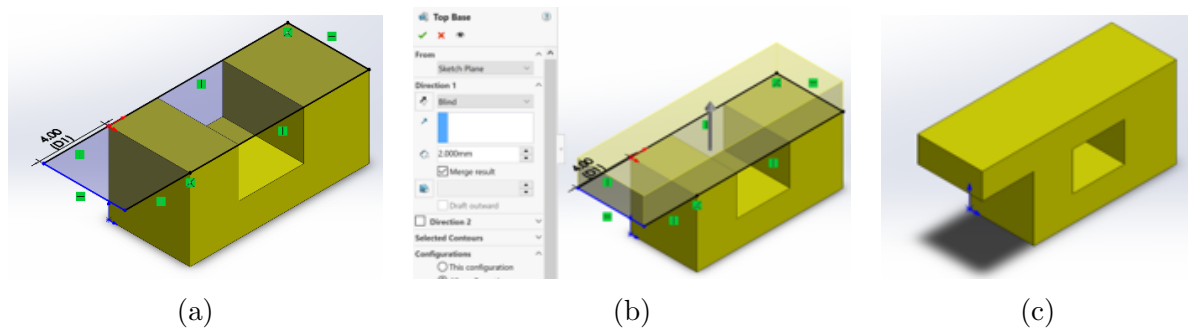


Figure B.3: Construction of jig top base in SolidWorks; a). Sketch, b). Extruded sketch, c). Completed top base part

To later accommodate a hole in the bottom base of the jig, a sketch with construction lines was established to indicate the center of the hole between the jig walls (Figure B.4).

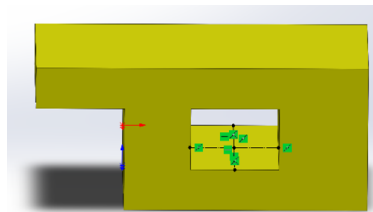


Figure B.4: Construction lines for mounting jig hole

For the jig to be mounted securely onto the OSIM, orientation pieces were created (Figure B.5) extending downwards from the bottom base to sit on either side of the OSIM cantilever. Additionally, these pieces rotate the jigs to accommodate any positional requirements in the local X-Direction, which is uncontrollable by the micrometers. Starting a new sketch on the bottom surface of the jig, two 1 mm x 15 mm rectangles centered about the jig hole sketch, were sketched 5 mm apart, extruded downwards by 3 mm, and kept parallel to each other (Figure B.5a, B.5b). An extension was included for better connection of the orientation pieces to the bottom base (Figure B.5c). This was created by sketching a rectangle on the top surface of the orientation pieces and then extruding it upwards by 2 mm.

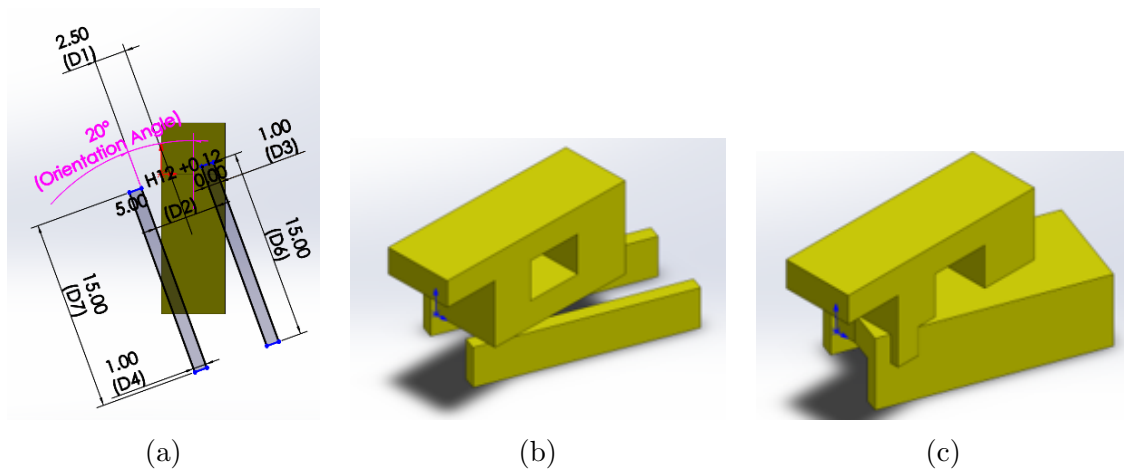


Figure B.5: Construction of jig orientation pieces in SolidWorks; a). Sketch, b). Extruded sketch, c). Base Extension

A few cleanup steps were included to minimize model material and rebuild errors when using custom dimensions. Cleanup included the trimming of the orientation pieces (Figure B.6a), and the front and back portion of the jig extension pieces (Figure B.6b, B.6c).

A tooth feature was created to hold the bracket (Figure B.7). It sits on the top base, has a rotation on the jig base (first order rotation), customizable height, and a slant on top. The position of the tooth on the top base depends on two factors: its buccal lingual position and bracket thickness. Using the central point of the jig top base as the reference for the buccal lingual position, a perpendicular construction line was built from this point to the tooth center and the length of this line was dimensioned to be the bracket thickness

as measured by digital calipers (Figure B.7a). These dimensions steps were completed so that when the bracket is bonded on the tooth, its slot midpoint lined up at the desired position. A tooth slant was also incorporated to shorten the tooth to the correct height and accommodate second order rotation of the bracket (Figure B.7b). Using the dimensions calculated in MATLAB, the tooth height was determined and the Cut Extrude feature was applied to remove the remaining tooth material.

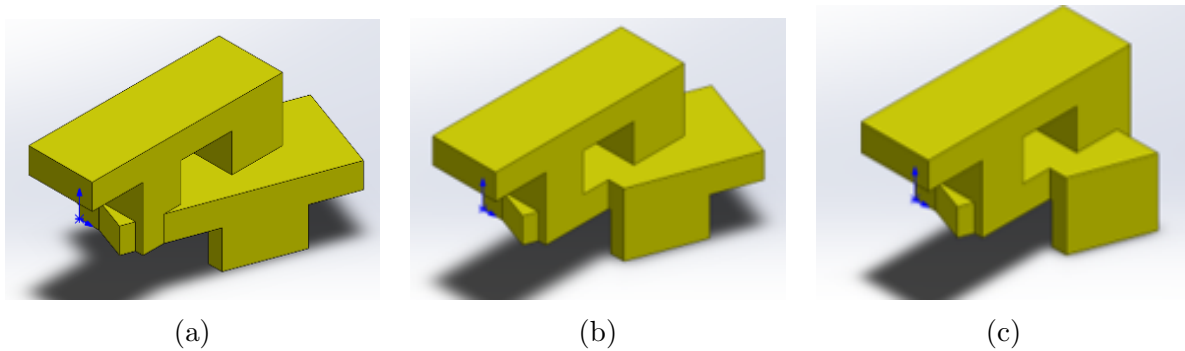


Figure B.6: Jig cleanup to remove unwanted material; a) Step 1, b). Step 2, c). Step 3

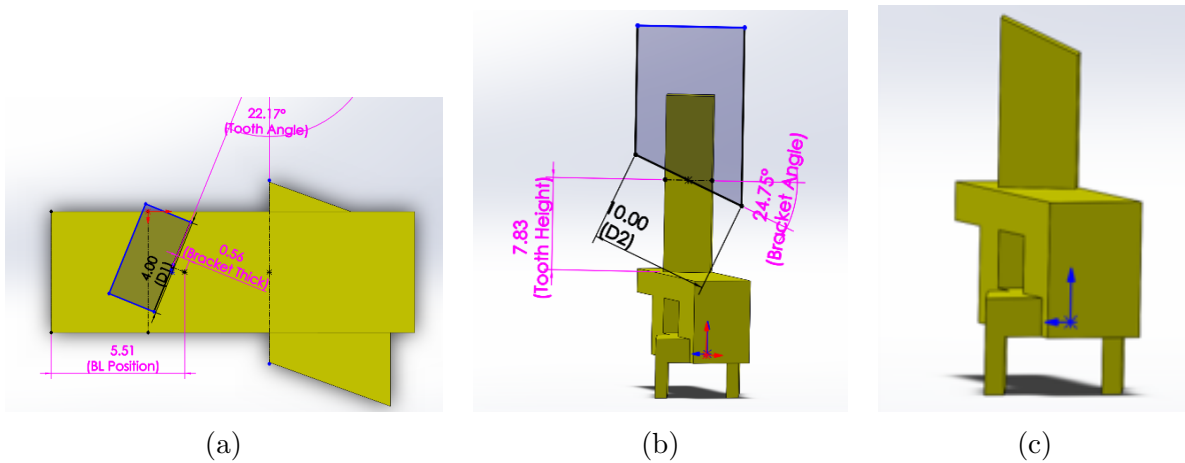


Figure B.7: Construction of jig tooth in SolidWorks; a). Tooth sketch, b). Tooth slant sketch, c). Completed tooth feature

To secure the jig onto the OSIM cantilevers, a bolt hole with diameter of 2 mm was created through the bottom portion of the jig body (Figure B.8). Once the jig was printed, M2 x 10 mm screws were inserted through the cantilever hole and the jig bolt hole and screwed into the M2-sized nut already placed inside of the jig.

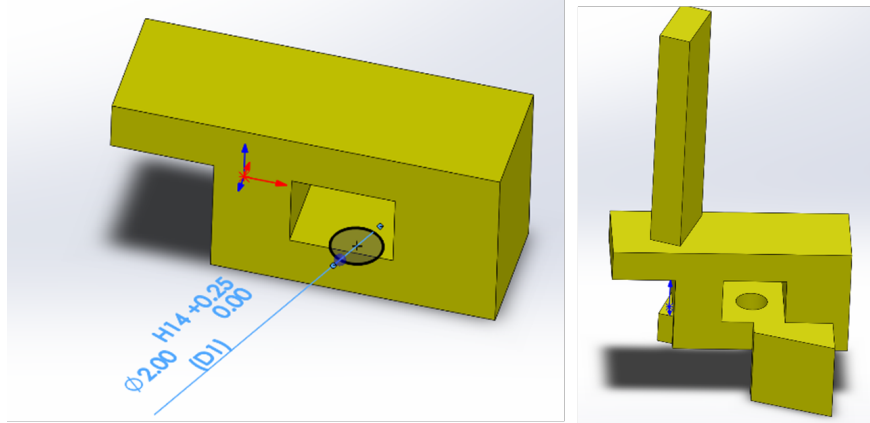


Figure B.8: Addition of bolt hole in jig design for mounting onto OSIM

One of the final additions to the jig design were bracket placement guides (Figure B.9, B.10). These were vertical and horizontal protrusions on the tooth's front surface to serve as a guide for bonding the bracket to the tooth center. The guides were unique to the measured bracket dimensions and were the only jig dimension calculations completed in Excel after running the MATLAB code. The top thickness of the bracket (with half the slot height included) was used to calculate the vertical guide dimensions and the width of the bracket was used to calculate the horizontal guide dimensions (Figure B.9). For the generic jig guide sketch (Figure B.10a), a construction line across the tooth slant was drawn and another line 2 mm in length was added to the left of the slant. Three 5 mm construction lines were drawn perpendicular to the tooth slant. The middle construction line was dimensioned away from the 2 mm line based on the side thickness calculated, whereas the left most construction line represented the guide side height to be calculated. Both these lines were dimensioned to be 0.4 mm apart to represent the default thickness of the side guide. All other lines were used as connections for the sketch and were not specified dimensions. Lastly, a Boss Extrude of 0.8 mm was applied to the jig guide sketch (Figure B.10b).

To ensure created jig sets were organized for experiments, identification labels were added to the front face of the jig body to recognize which jig corresponds to which tooth based on the OSIM naming convention (Tooth 2-6 to 1-6). The identification label was created using the Sketch Text feature and was composed of bolded lettering of the tooth and jig

set number (Figure B.11a), followed by the patient arch underneath (Figure B.11b). As an example, “11 1 P1L” corresponds to Tooth 1-1 of the Time 1 jig set for Patient 1’s lower arch. The label was etched into the jig by applying a 0.5 mm Cut Extrude to the sketch. A fully constructed jig is provided in Figure B.12.

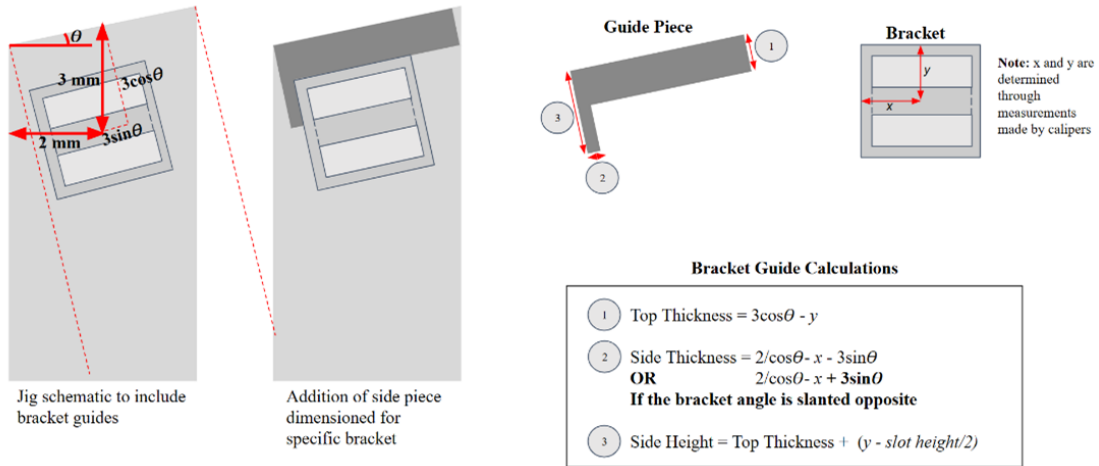


Figure B.9: Jig bracket placement guide schematic for calculating dimensions

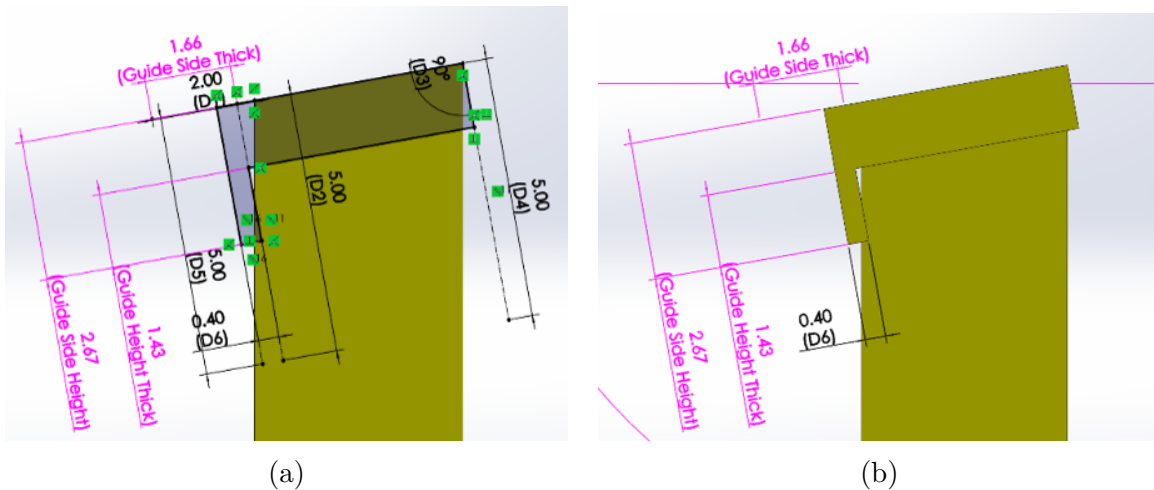


Figure B.10: Constructing jig bracket placement guides in SolidWorks; a). Jig bracket placement guide sketch, b). Extruded bracket placement guide sketch

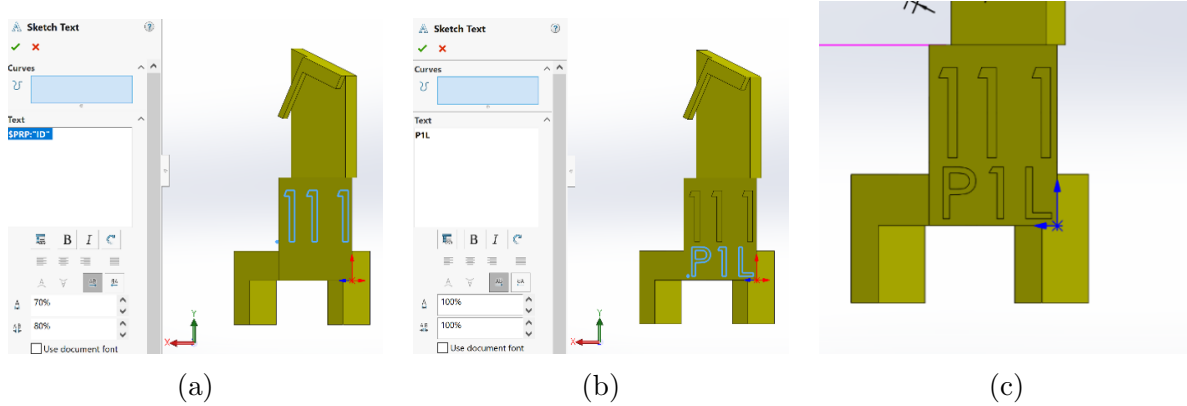


Figure B.11: Jig patient arch identification label; a). Tooth and jig set number sketch, b). Patient arch number sketch, c). Final label etched into jig

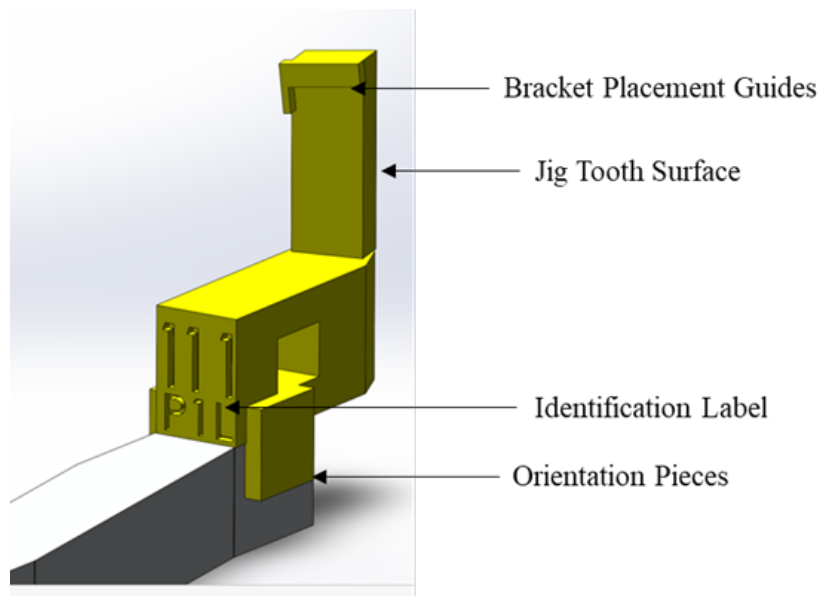


Figure B.12: Final jig design with main features labelled

## B.2 Patient-Specific Jig Set Creation

### *Jig Set Creation Procedure*

Using the ‘Jig Dimensions’ MATLAB code presented in the next section of Appendix B.2, the custom jig dimensions were calculated for each patient scan using the previously exported bracket endpoint positions from Slicer. Using the Jig Dimensions Excel file, the endpoint coordinates were pasted into the first sheet for use in MATLAB. Prior to running the code,

there were three modifiable elements: the specific patient Excel file, the OSIM micrometer positions, and an x-translation variable applied to the patient positions to move them closer to the OSIM’s cantilever hole positions. At neutral position, the actual OSIM micrometer cantilever hole positions and angles were measured (Table B.1) and used to mathematically determine other micrometer positions used in the code.

Table B.1: Measured OSIM cantilever angles and mounting hole positions using FaroArm measurement device

<b>Tooth</b>	<b>X-Coordinate [mm]</b>	<b>Y-Coordinate [mm]</b>	<b>Z-Coordinate [mm]</b>	<b>Cantilever Angle [°]</b>
2-6	-24.28	24.27	128.39	-9
2-5	-16.23	22.82	128.24	-18
2-4	-10.07	21.38	129.67	-25
2-3	-2.60	16.94	128.91	-33
2-2	1.86	11.79	128.87	-56
2-1	5.32	4.46	129.89	-79
1-1	5.44	-3.28	128.56	-102
1-2	3.10	-9.99	129.18	-130
1-3	-1.33	-15.8	129.36	-148
1-4	-8.95	-20.48	127.57	-156
1-5	-16.17	-23.35	128.96	-164
1-6	-23.51	-25.1	129.21	-169

Besides defining the patient file, the other elements required trial and error to determine the optimal combination that would output jig dimensions (specifically the jig orientation angle and buccal-lingual position) within an appropriate range to avoid rebuild errors in SolidWorks. Therefore, multiple combinations were tested using the ‘Jig Dimensions’ code until the most ideal settings were retrieved to accommodate the patient-specific arch form, which was achieved by repeating calculations for a range of values based on the initially

defined micrometer position and x-translation. Figure B.13 shows an example of the different outputs retrieved for two different combinations tested. Table B.2 provides the summary of combinations used for the jig sets presented in Chapter 3.

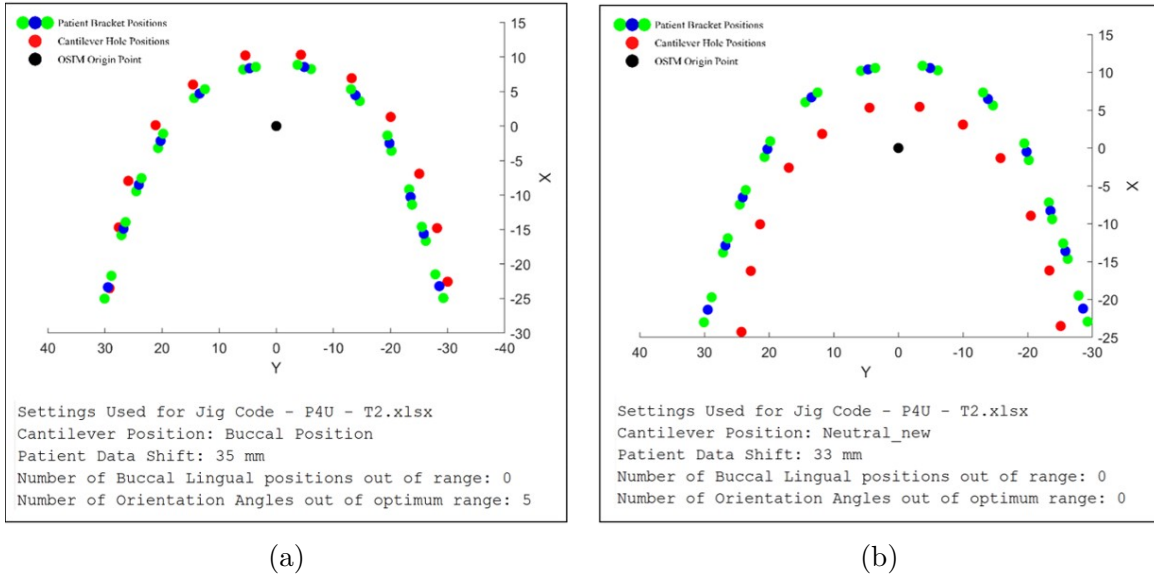


Figure B.13: Testing different position combinations for OSIM cantilever holes and patient data shift in Jig Dimensions code; a). Example combination with values out of optimal range, b). Example combination with all values within optimal range

Table B.2: Summary of setting combinations used for retrieving patient jig set dimensions

Patient	Arch	Position Direction (OSIM Micrometer Setting)	X-Translation
Patient 1	Maxillary	-	-
	Mandibular	Buccal (2 mm)	30 mm
Patient 2	Maxillary	Neutral (5 mm)	37 mm
	Mandibular	Buccal (0 mm)	36 mm
Patient 3	Maxillary	Buccal (3 mm)	30 mm
	Mandibular	Buccal (1 mm)	25 mm
Patient 4	Maxillary	Neutral (5 mm)	33 mm
	Mandibular	Buccal (2 mm)	35 mm

A design table was utilized to create unique jig configurations from the default design

presented in Section B.1. This was created for the following dimensions of the SolidWorks jig part: Buccal-Lingual Position, Tooth Height, Orientation Angle, Tooth Angle, Bracket Angle, and Jig Guide Dimensions. In the SolidWorks interface, the dimensions of interest were first isolated as “Feature Dimensions” (Figure B.14a) and individually double-clicked to appear in the design table (Figure B.14b). Next, the calculated jig dimensions were copied from the Excel sheet and pasted into the design table. The jig configurations were automatically generated based on the patient-specific dimensions (Figure B.14c).

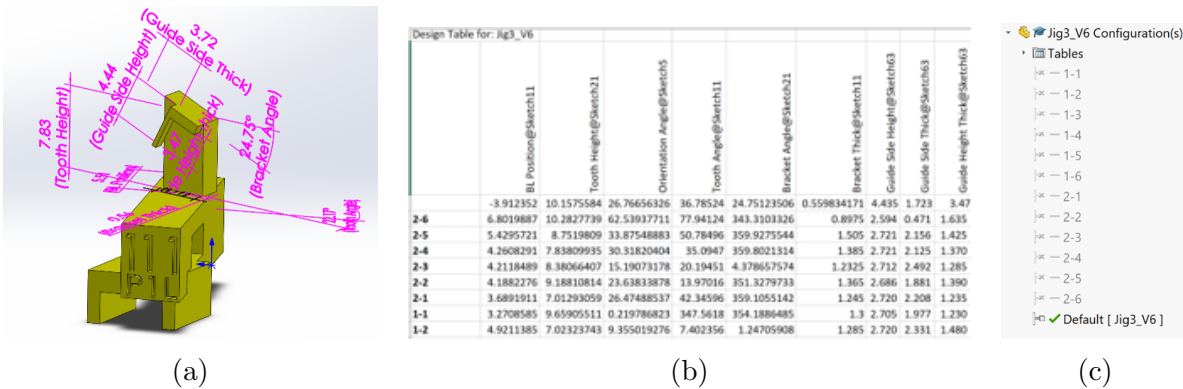


Figure B.14: SolidWorks design table to create jig configurations; a). Jig feature dimensions, b). Design table interface for pasting jig dimensions calculated in MATLAB, c). Jig configurations created based on design table

All configurations were mounted on the OSIM model within the SolidWorks Assembly (Figure B.15). Each jig configuration was mounted to the respective micrometer hole using three mates: Coincident mate to line up the jig’s inner surface of side piece to the cantilever side, coincident mate to line up the bottom jig surface with the cantilever’s top surface, and a concentric mate to align the cantilever hole with the jig’s bolt hole. The micrometer positions were updated using distance mates according to the position used in the MATLAB code. The SolidWorks assembly was used as final check prior to printing to locate areas of interference between adjacent jigs (Figure B.16). Existing interference was eliminated by applying the Cut Extrude feature to manually remove jig material. In the cases where the jig tooth was positioned near the jig base edge, additional material was added.

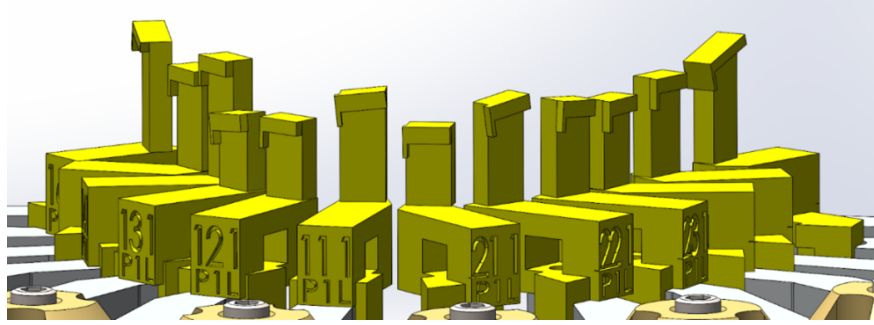
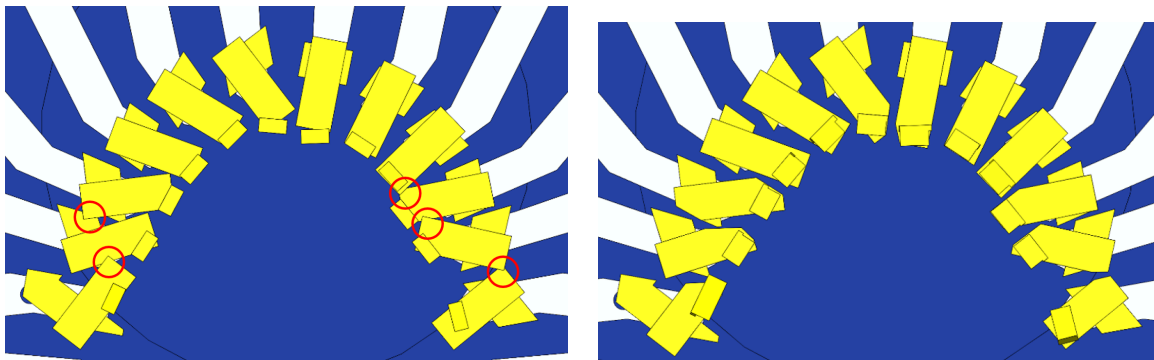


Figure B.15: Example jig set mounted on OSIM model in SolidWorks assembly



(a)

(b)

Figure B.16: Minimizing jig interference in SolidWorks assembly prior to printing jig models; a). Before manual trimming with areas of interference identified, b). Minimal interference after manual trimming

### *Jig Dimensions Code*

This MATLAB script was created to calculate the unique jig dimensions based on the collected bracket positions from a patient's scan. The dimensions were then saved within an Excel file for use in SolidWorks.

```

%% Jig Dimensions Code
% Code will take bracket position information and calculate jig dimensions
% Final output will be required jig dimensions to be inputted into Solidworks
% All final dimensions will be positive to avoid errors in design table
clf
clear
clc

%% PLOTTING 3D POINTS FROM EXCEL FILE: BRACKET MIDPOINTS
% Import patient arch excel file data
JigData = 'Jig Code - P4U - T2.xlsx'; % USER DEFINED
T0 = readtable(JigData, 'Sheet', 'Slot Endpoints RAS', 'PreserveVariableNames', true);

```

```

for i = 5 % Define specific sheet or define as i = 1:5 to loop through different OSIM
positions

% Import OSIM excel file data
T2 = readtable('OSIM Data.xlsx','Sheet',i); % USER DEFINED
sheetname = sheetnames('OSIM Data.xlsx'); % Create vector of OSIM excel file names
tooth_names = table2array(T2(1:12,1)); %Tooth names for data tips
Tooth_num = ['2-6'; '2-5'; '2-4'; '2-3'; '2-2'; '2-1'; '1-1'; '1-2'; '1-3'; '1-4'; '1-5'; '
1-6'];

% x-translate is the distance that we want to move all patient points in X direction
x = 33; % USER DEFINED

% Either define 1 value or use range to loop through options
% for x_translate = 33;
for x_translate = (x-3):(x+3)
clf
% z min is minimum jig height to prevent bracket gate hitting jig base
z_min = 7; % USER DEFINED

% Calculate slot midpoint between slot endpoints
% First put RAS coordinates into XYZ
[R1_R, R1_A, R1_S] = deal(table2array(T0(1:12,2)),table2array(T0(1:12,3)),table2array(T0
(1:12,4)));
[R2_R, R2_A, R2_S] = deal(table2array(T0(1:12,5)),table2array(T0(1:12,6)),table2array(T0
(1:12,7)));

% L is the midpoint between slot endpoints
L_R = (R1_R + R2_R)/2;
L_A = (R1_A + R2_A)/2;
L_S = (R1_S + R2_S)/2;

% Convert RAS to XYZ System
L_X = L_A;
L_Y = L_R*-1;
L_Z = L_S;

% Save values in the same excel file but different sheets
A = [L_R, L_A, L_S]; % Saving Midpoints in RAS CS
writematrix(A,JigData,'sheet','Landmark RAS','range','B2:D2')
B = [L_X, L_Y, L_Z]; % Saving Midpoints in XYZ CS
writematrix(B,JigData,'sheet','Landmark XYZ','range','B2:D2')

% Display Patient Data as Table
T1 = readtable(JigData,'Sheet','Landmark XYZ','PreserveVariableNames',true);
disp('Bracket Midpoints in Global XYZ CS')
disp(T1)

% Level the Z-Coordinates of patient data with OSIM data
% Find minimum Z-Coord in patient data
min(L_Z);
% Subtract all Z-Coord with minimum Z-Coord
L_Z_inter = L_Z - min(L_Z);
% Add value that is larger than OSIM hole height to all Z-Coord to
% avoid negative dimensions
L_Z_final = L_Z_inter + 130;

% translate patient data in X-direction only
L_X_final = L_X - x_translate;
L_Y_final = L_Y;

% Plot Patient Points in figure
point1 = plot3(L_X_final, L_Y_final, L_Z_final, '.', 'Color', 'b', 'MarkerSize', 25);
row = dataTipTextRow(" Midpoint - Tooth",tooth_names);
point1.DataTipTemplate.DataTipRows(end+1) = row;
hold on

```

```

% Save imported OSIM excel file data as table
% Convert the text to array values so that it can be plotted
[O_X_final, O_Y_final, O_Z_final] = deal(table2array(T2(:,2)),table2array(T2(:,3)),
    table2array(T2(:,4)));

% Plot OSIM Points on same figure as Patient Points
point2 = plot3(O_X_final,O_Y_final,O_Z_final, '.', 'Color', 'r', 'MarkerSize', 25);
row = dataTipTextRow("OSIM - Tooth",tooth_names);
point2.DataTipTemplate.DataTipRows(end+1) = row;

% Display OSIM Data as Table
disp('OSIM Coordinate Points Global CS')
disp(T2)

% Plot a 3D origin point for reference
point3 = plot3(0,0,0, '.', 'Color', 'black', 'MarkerSize', 25);

% Find difference between patient point and OSIM cantilever holes relative to
% global system
L_Delta_X = L_X_final - O_X_final;
L_Delta_Y = L_Y_final - O_Y_final;
L_Delta_Z = L_Z_final - O_Z_final;

% Define angles (in degrees) of individual bracket coordinate systems
theta = [-9,-18,-25,-33,-56,-79,-102,-130,-148,-156,-164,-169]; % Measured Angles

% Initialize variable K and empty vectors for local X and Y direction
K = 1;
L_Vec_X = [];
L_Vec_Y = [];
% Define how many teeth are considered (12 per arch)
Num_teeth = 12;

% While loop to solve for X and Y changes with respect to local OSIM
% coordinate systems
while K <= Num_teeth
    % Solving for changes in X-dirn
    % Assign to empty vector
    L_Vec_X(K) = L_Delta_X(K)*cosd(theta(K)) + L_Delta_Y(K)*sind(theta(K));

    % Solving for changes in Y-dirn
    % Assign to empty vector
    L_Vec_Y(K) = -L_Delta_X(K)*sind(theta(K)) + L_Delta_Y(K)*cosd(theta(K));

    K = K + 1;
end

% Transpose vectors to be vertical for putting into table below
L_T_Delta_X_new = transpose(L_Vec_X);
L_T_Delta_Y_new = transpose(L_Vec_Y);

% Put transposed values back into table for display
A1 = table(tooth_names, L_T_Delta_X_new, L_T_Delta_Y_new, L_Delta_Z);
A1.Properties.VariableNames = {'Tooth', 'Delta X', 'Delta Y', 'Delta Z'};
% disp('Bracket Landmarks Local CS')
% disp(A1)

%Export the table to the same Excel file that contained the initial
%Slicer data
writetable(A1,JigData, 'sheet', 'Landmark Delta Translations', 'range', 'A1')

%% PLOTTING 3D POINTS FROM EXCEL FILE: BRACKET ENDPOINTS
% Plot bracket slot endpoints for angle-based dimension calculations
% R1 is slot endpoint 1, R2 is slot endpoint 2
% convert RAS to XYZ coordinate system
R1_X = (R1_A);
R1_Y = (R1_R*-1);
R1_Z = (R1_S);

```

```

R2_X = (R2_A);
R2_Y = (R2_R*-1);
R2_Z = (R2_S);

% Export XYZ slot endpoint coordinates to Excel file
A = [R1_X, R1_Y, R1_Z]; % Saving Endpoint 1 coordinates
writematrix(A,JigData,'sheet','Rotation XYZ','range','B2:D2')
B = [R2_X, R2_Y, R2_Z]; % Saving Endpoint 2 coordinates
writematrix(B,JigData,'sheet','Rotation XYZ','range','E2:G2')

% Read endpoint coordinates and display as table
T4 = readtable(JigData,'Sheet','Rotation XYZ','PreserveVariableNames',true);
disp('Bracket Endpoints Coordinates Global CS')
disp(T4)

% Level the data in the z-dirn like done with the slot midpoints
R1_Z_inter = R1_Z - min(L_S);
R2_Z_inter = R2_Z - min(L_S);
R1_Z_final = R1_Z_inter + 130;
R2_Z_final = R2_Z_inter + 130;

% Subtract x-translation value
R1_X_final = R1_X - x_translate;
R2_X_final = R2_X - x_translate;
R1_Y_final = R1_Y;
R2_Y_final = R2_Y;

% Plot the endpoints on the same figure as before
point4 = plot3(R1_X_final,R1_Y_final,R1_Z_final, '.', 'Color','g','MarkerSize',25);
row = dataTipTextRow("Endpoint - Tooth",tooth_names);
point4.DataTipTemplate.DataTipRows(end+1) = row;

point5 = plot3(R2_X_final,R2_Y_final,R2_Z_final, '.', 'Color','g','MarkerSize',25);
row = dataTipTextRow("Endpoint - Tooth",tooth_names);
point5.DataTipTemplate.DataTipRows(end+1) = row;

% Find global difference between endpoints and OSIM cantilever holes
R1_Delta_X = R1_X_final - O_X_final;
R1_Delta_Y = R1_Y_final - O_Y_final;
R1_Delta_Z = R1_Z_final - O_Z_final;

R2_Delta_X = R2_X_final - O_X_final;
R2_Delta_Y = R2_Y_final - O_Y_final;
R2_Delta_Z = R2_Z_final - O_Z_final;

% Initialize variable K and make empty vectors for X and Y direction
K = 1;
R1_Vec_X = [];
R1_Vec_Y = [];
R2_Vec_X = [];
R2_Vec_Y = [];

% Define how many teeth are considered
Num_teeth = 12;

% While loop to solve for X and Y changes with respect to local OSIM
% coordinate systems
while K <= Num_teeth
    % Solving for changes in X & Y-dirn - R1
    R1_Vec_X(K) = R1_Delta_X(K)*cosd(theta(K)) + R1_Delta_Y(K)*sind(theta(K));
    R1_Vec_Y(K) = -R1_Delta_X(K)*sind(theta(K)) + R1_Delta_Y(K)*cosd(theta(K));

    % Solving for changes in X & Y-dirn - R2
    R2_Vec_X(K) = R2_Delta_X(K)*cosd(theta(K)) + R2_Delta_Y(K)*sind(theta(K));
    R2_Vec_Y(K) = -R2_Delta_X(K)*sind(theta(K)) + R2_Delta_Y(K)*cosd(theta(K));

    K = K + 1;

```

```

end

% Transpose vectors to be vertical for putting into table below
R1_T_Delta_X_new = transpose(R1_Vec_X);
R1_T_Delta_Y_new = transpose(R1_Vec_Y);
R2_T_Delta_X_new = transpose(R2_Vec_X);
R2_T_Delta_Y_new = transpose(R2_Vec_Y);

% Put each column of values back into table for display
R1_A1 = table(tooth_names, R1_T_Delta_X_new, R1_T_Delta_Y_new, R1_Delta_Z);
R1_A1.Properties.VariableNames = {'Tooth', 'X', 'Y', 'Z'};
% disp('Bracket Endpoint 1 in Local CS')
% disp(R1_A1)
R2_A1 = table(tooth_names, R2_T_Delta_X_new, R2_T_Delta_Y_new, R2_Delta_Z);
R2_A1.Properties.VariableNames = {'Tooth', 'X', 'Y', 'Z'};
% disp('Bracket Endpoint 2 in Local CS')
% disp(R2_A1)

%Export the Delta table to the same Excel file but different sheets
writetable(R1_A1, JigData, 'Sheet', 'Rotation Local CS', 'Range', 'A1');
writetable(R2_A1, JigData, 'Sheet', 'Rotation Local CS', 'Range', 'E1');

%% JIG DIMENSIONS: TOOTH & BRACKET ROTATION
% Find slope between endpoints of each bracket
% Then find angle with respect to the positive local X axis on XY plane
% (+) is CW and (-) is CCW

% Rotation angle is the angle of the line between the two bracket endpoints
% Tooth angle refers to first order rotation
% Bracket angle refers to second order rotation
[rotation_angle, tooth_angle, translation_angle] = deal(zeros(Num_teeth,1));

K = 1;
% Calculate first order tooth rotation
% This will be the angle that the tooth needs to be rotated on the jig to
% be parallel with the bracket endpoints
while K <= Num_teeth
    % Endpoint 1 & Endpoint 2
    % Values with respect to cantilever hole centers
    R1X = R1_T_Delta_X_new(K);
    R1Y = R1_T_Delta_Y_new(K);
    R2X = R2_T_Delta_X_new(K);
    R2Y = R2_T_Delta_Y_new(K);

    % local values again for bracket midpoint
    % Values with respect to cantilever hole centers
    X1 = L_T_Delta_X_new(K);
    Y1 = L_T_Delta_Y_new(K);

    % m1 is the real bracket slope
    m1 = (R2Y - R1Y)/(R2X - R1X);
    % Solve for angle w.r.t local cantilever x-axis
    rotation_angle(K) = atand(m1);

    % m2 is parallel with tooth face before rotation (will be perpendicular
    % to orientation angle)
    m2 = -X1/Y1;

    % We want m2 and m1 to be the same
    % Translation angle is the angle of m2
    % This will be the angle diff b/w the cantilever hole and bracket
    % midpoint
    translation_angle(K) = atand(m2);
    % Take difference of angles to find the amount of tooth rotation
    tooth_angle(K) = translation_angle(K) - rotation_angle(K);
    % If the angle is negative, add 360 degrees to it
    if tooth_angle(K) < 0
        tooth_angle(K) = 360 + tooth_angle(K);
    end
end

```

```

        end
        K=K+1;
    end

% Find second order bracket rotation
[R1Xnew, R1Ynew, R2Xnew, R2Ynew] = deal(zeros(Num.teeth,1));

% Find coordinates of bracket endpoints in new Local bracket CS
% Rotate CS (X and Y) so that the bracket face (measured) is parallel with X axis
% First use while loop for converting coordinates
K=1;
while K <= Num.teeth
    % local delta values again for each bracket endpoint
    R1X = R1_T_Delta_X_new(K);
    R1Y = R1_T_Delta_Y_new(K);
    R2X = R2_T_Delta_X_new(K);
    R2Y = R2_T_Delta_Y_new(K);

    % Solving for local changes in X-dirn & Y-dirn - R1
    R1Xnew(K) = R1X*cosd(rotation_angle(K)) + R1Y*sind(rotation_angle(K));
    R1Ynew(K) = -R1X*sind(rotation_angle(K)) + R1Y*cosd(rotation_angle(K));

    % Solving for local changes in X-dirn & Y-dirn - R2
    R2Xnew(K) = R2X*cosd(rotation_angle(K)) + R2Y*sind(rotation_angle(K));
    R2Ynew(K) = -R2X*sind(rotation_angle(K)) + R2Y*cosd(rotation_angle(K));

    K=K+1;
end

% Now find bracket angle
% Need to use z-dirn values (unchanged with cs transformation)
% Bracket angle will be the angle for the tooth slant at top
K=1;
bracket_angle = zeros(Num.teeth,1);
while K <= Num.teeth
    R1X = R1Xnew(K);
    R1Z = R1_Delta_Z(K);
    R2X = R2Xnew(K);
    R2Z = R2_Delta_Z(K);

    % find bracket slope (on XZ plane, or tooth face) wrt new CS
    m =(R2Z - R1Z)/(R2X - R1X);

    % CW is + and CCW is -
    bracket_angle(K) = atand(m);

    % if the angle is negative, add 360 degrees to it
    if bracket_angle(K) < 0
        bracket_angle(K) = 360 + bracket_angle(K);
    end
end
K=K+1;
end

% Export rotational jig dimensions to excel sheet
writematrix(tooth_angle, JigData, 'Sheet', 'Jig Dimensions', 'Range', 'E3')
writematrix(bracket_angle, JigData, 'Sheet', 'Jig Dimensions', 'Range', 'F3')

%% Jig Dimensions: BL POSITION, ORIENTATION ANGLE, SLOT HEIGHT
% Using: L_T_Delta_X_new, L_T_Delta_Y_new, L_Delta_Z
% Allocate empty vectors for buccal-lingual position and orientation angle
[BL_position, Orientation_angle] = deal(zeros(12,1));

K = 1;
% Find tooth's buccolingual position along jig base
% Uses while-loop to first determine direction of the patient midpoint
% w.r.t to the center of the jig hole
% The distance between the jig hole and jig end (9mm) is then used for addition
% or subtraction for finding net distance from the jig end

```

```

while K <= Num_teeth
    if L_T_Delta_Y_new(K) >= 0
        BL_position(K) = 9 + (sqrt(L_T_Delta_X_new(K)^2 + L_T_Delta_Y_new(K)^2));
    else
        BL_position(K) = 9 - (sqrt(L_T_Delta_X_new(K)^2 + L_T_Delta_Y_new(K)^2));
    end
    K = K+1;
end
% Export buccal-lingual position dimensions to excel sheet
writematrix(BL_position, JigData, 'Sheet', 'Jig Dimensions', 'Range', 'B3')

% Check if BL Position within range of 0 to 15 (length of top base)
% This is part of determining optimal dimension combination
K = 1;
count_BL = 0;
while K <= Num_teeth
    if (0 <= BL_position(K)) && (BL_position(K) <= 15)
        count_BL = count_BL + 1;
    else
        count_BL = count_BL + 1;
    end
    K = K+1;
end

% Find orientation angle and keep all angles positive
K = 1;
while K <= Num_teeth
    X = L_T_Delta_X_new(K);
    Y = L_T_Delta_Y_new(K);
    % Taking tan inverse to find angle
    % This angle is measured w.r.t the y-axis of the cantilever hole
    Orientation_angle(K) = -(atand(X/Y));

    % if the angle is negative, add 360 degrees to it
    if Orientation_angle(K) < 0
        Orientation_angle(K) = 360 + Orientation_angle(K);
    end
    K = K+1;
end

% Check whether Orientation Angle is within range of 0 to 30 or 330 to
% 360
% This is part of determining optimal dimension combination
K = 1;
count_OA = 0;
while K <= Num_teeth
    if ((0 <= Orientation_angle(K)) && (Orientation_angle(K) <= 30)) || ((330 <=
        Orientation_angle(K)) && (Orientation_angle(K) <= 360))
        count_OA = count_OA + 1;
    else
        count_OA = count_OA + 1;
    end
    K = K+1;
end
% Export orientation angle dimensions to excel sheet
writematrix(Orientation_angle, JigData, 'Sheet', 'Jig Dimensions', 'Range', 'D3')
A3 = table(Tooth_num, tooth_angle, bracket_angle);
A3.Properties.VariableNames = {'Tooth', 'Tooth Angle (first order rotation)', 'Bracket
    Guide Angle (second order rotation)'};
disp('Jig Rotational Dimensions')
disp(A3)

% Find bracket slot height
% Minimum height is z_min as defined at the start of code
% Measured relative to bottom of jig tooth
slot_height = z_min + L_Delta_Z;
writematrix(slot_height, JigData, 'Sheet', 'Jig Dimensions', 'Range', 'C3')

```

```

% Create table for displaying final jig dimensions
A4 = table(Tooth_num, BL_position, Orientation_angle, slot_height);
A4.Properties.VariableNames = {'Tooth', 'Tooth Buccolingual position', 'Jig Orientation
    Angle', 'Tooth Height'};
disp('Jig Dimensions')
disp(A4)

%% Format Figure
% Format Figure with labels and title
xlabel('X'); ylabel('Y'); zlabel('Z')
title([JigData, sheetname(i) 'and' x_translate])

% Print information for user regarding combination used after each loop
fprintf(" Settings Used for %s \n", JigData)
fprintf(" Cantilever Position: %s \nPatient Data Shift: %d mm\n", sheetname(i),
    x_translate)
fprintf("Number of Buccal Lingual positions out of range: %d \n", count_BL)
fprintf("Number of Orientation Angles out of optimum range: %d \n", count_OA)
end
end

```

## B.3 Evaluating Replication Errors

### *Establishing OSIM Coordinate System & Bracket Endpoint Selection with FaroArm*

Errors in bracket position replication were evaluated for each jig set used in this work, and the summarized results were presented in Chapter 3. To calculate errors, 3D coordinates of the physical bracket endpoints were measured using a FaroArm measurement device and compared with the scanned positions. The OSIM was first secured on the FaroArm cart and a global coordinate system was manually constructed using the CAM2 Measure 10 software by measuring a plane, line, and central origin point feature (Figure B.17). The plane feature was first created by recording at least three points on the OSIM top plate surface. Next, the line feature was created by selecting at least two points on the edge of OSIM's bottom plate. To establish an origin point, a cylindrical feature was first measured. The OSIM micrometers were set to its maximum buccal position to maximize room around the OSIM's upper plate cylindrical hole region. At least six points were selected around the cylindrical region, and this process was repeated if the output cylinder was tilted. The origin point was then constructed by intersecting the measured cylinder and top plane using the Construct feature. The coordinate system was created by inputting the plane, line, and origin point

and defining the plane to represent the positive Z-direction and the line to represent the positive Y-direction (Figure B.18).

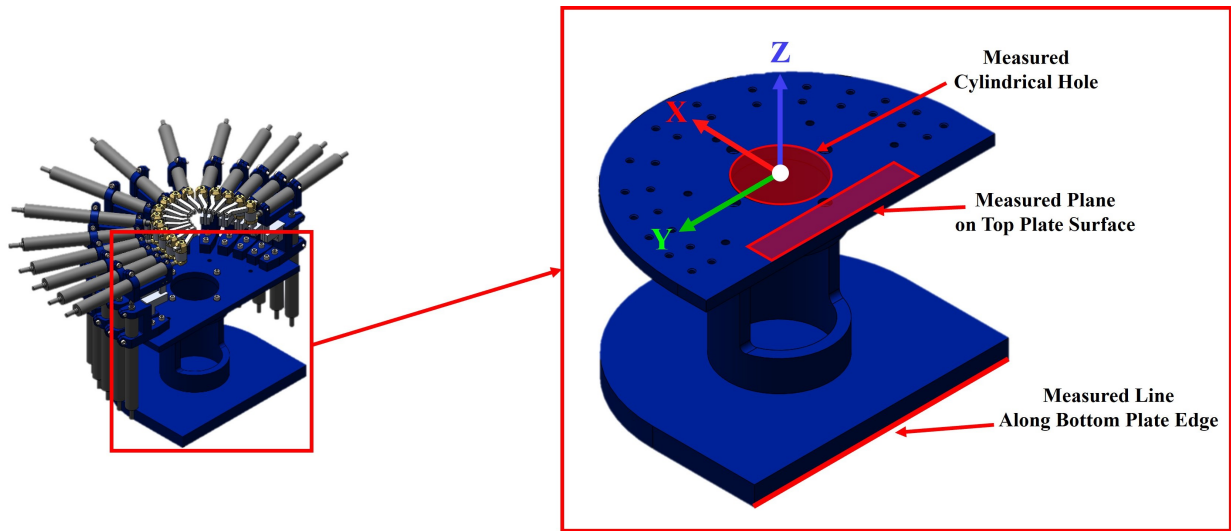


Figure B.17: Summary of features selected for OSIM global coordinate system construction with FaroArm measurement device

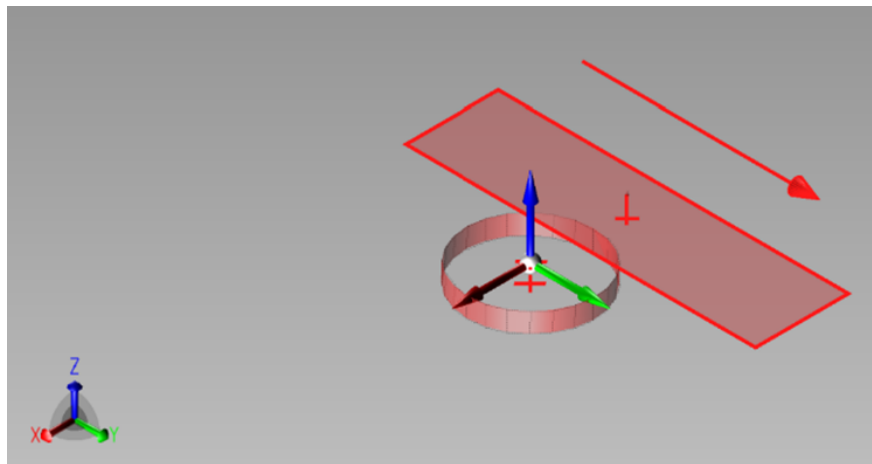


Figure B.18: OSIM global coordinate system creation in FaroArm CAM2 Measure 10 software

Bracket endpoint positions were next measured in a consistent order for easy export starting from Tooth 2-6 to Tooth 1-6. The tooth to be measured was moved to the maximum occlusal position (10 mm), while the other teeth were kept at 0 mm to overcome difficulties of measuring in the tight space between jigs. Going from right endpoint to left endpoint, the individual bracket positions were measured, and the micrometer positions were changed for

the subsequent teeth. When all the necessary endpoint measurements were completed, the 3D coordinates of all points were exported as a .txt file. The positions were measured twice per jig set and the average positions were used for further analysis in MATLAB. Figure B.19 provides an example of an exported .txt file for a measurement trial.

```

Units: mm
Decimal Indicator: .
Date: 5/29/2023 3:19:07 PM
Feature Name;Geometry Type;M.Center.x;M.Center.y;M.Center.z

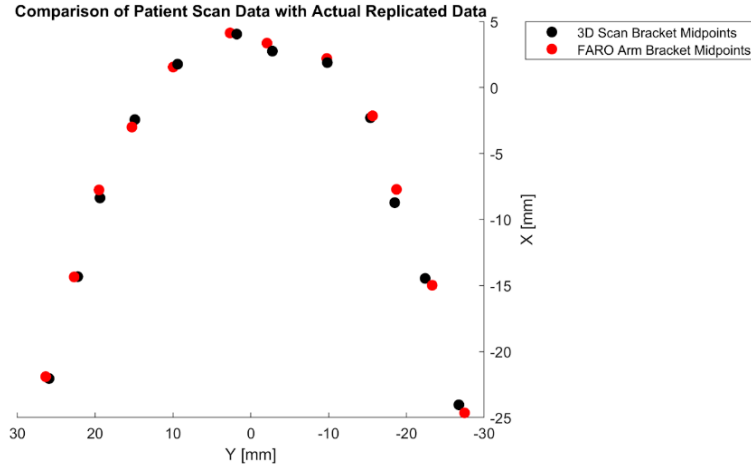
2-6-P1T1 - Actual;Point;-24.6594516733506;27.2075232675122;149.341535936776
2-6-P2T1 - Actual;Point;-19.2567092277621;25.516;147.650
2-5-P1T1 - Actual;Point;-15.9433;24.0614912;146.545066624394
2-5-P2T1 - Actual;Point;-12.49413;21.5851;146.34907
2-4-P1T1 - Actual;Point;-9.89276868387181;20.1947780916457;147.251289341589
2-4-P2T1 - Actual;Point;-5.57113417321237;18.827589088;147.04192665
2-3-P1T1 - Actual;Point;-4.90894662241935;16.6070683528283;146.5184
2-3-P2T1 - Actual;Point;-1.0434223292;13.9092107;146.883189473124
2-2-P1T1 - Actual;Point;-0.0988;11.45253;147.6960743
2-2-P2T1 - Actual;Point;3.251;8.43325946652854;146.481759247884
2-1-P1T1 - Actual;Point;4.5535386356;5.0663;146.108627213086
2-1-P2T1 - Actual;Point;3.6392277;0.2477245;146.01051
1-1-P1T1 - Actual;Point;3.206155;0.426413487553161;147.70954643455
1-1-P2T1 - Actual;Point;3.455;-4.525637153216;147.116622578278
1-2-P1T1 - Actual;Point;3.709;-7.9553807;145.026
1-2-P2T1 - Actual;Point;0.46857853549;-11.500744;145.401
1-3-P1T1 - Actual;Point;-0.5470745578;-14.264;145.373724092514
1-3-P2T1 - Actual;Point;-3.5409106;-17.3127851;145.403369413943
1-4-P1T1 - Actual;Point;-5.9168562826906;-17.1116;147.2502
1-4-P2T1 - Actual;Point;-9.42588381267925;-20.2936055573392;147.860
1-5-P1T1 - Actual;Point;-13.2853;-21.7255207484523;147.1793
1-5-P2T1 - Actual;Point;-16.601386;-25.0318253625348;147.286945435347
1-6-P2T1 - Actual;Point;-27.8585488862645;-28.2835786;149.563854159348
1-6-P1T1 - Actual;Point;-21.4511194588829;-26.48152307943;148.3377

```

Figure B.19: Sample .txt file of measured bracket endpoint coordinates exported from FaroArm CAM2 software

## *Calculating Replication Errors*

As described in Chapter 3, replication errors for each jig set were assessed by comparing the FaroArm measured positions and those initially selected on the patient scan. The ‘Replication Error’ MATLAB code presented in the next section of Appendix B.3 was used to measure the positional differences in bracket midpoints with respect to the local cantilever coordinate systems. The output of the code included a figure with both sets of points plotted for visual comparison (Figure B.20a), along with two tables of error results (Figure B.20b, B.20c).



(a)

Tooth	Global Delta X	Global Delta Y	Local Delta X	Local Delta Y	Tooth	Delta Z
2-6	0.14193	0.43028	0.072872	0.44719	2-6 to 2-5	-0.43003
2-5	-0.021301	0.46538	-0.16407	0.43602	2-5 to 2-4	0.23899
2-4	0.60645	0.12503	0.49679	0.36961	2-4 to 2-3	-0.1774
2-3	-0.56544	0.37706	-0.67958	0.0082692	2-3 to 2-2	-0.386
2-2	-0.21918	0.56756	-0.59309	0.13567	2-2 to 2-1	0.13423
2-1	0.085683	0.85847	-0.82635	0.24791	2-1 to 1-1	0.017652
1-1	0.60863	0.69724	-0.80855	0.45037	1-1 to 1-2	-0.1322
1-2	0.31126	0.063199	-0.24849	0.19781	1-2 to 1-3	0.18858
1-3	0.14673	-0.27355	0.020523	0.30974	1-3 to 1-4	0.15755
1-4	1.0054	-0.23122	-0.82446	0.62017	1-4 to 1-5	0.038024
1-5	-0.5191	-0.90267	0.7478	0.72461	1-5 to 1-6	0.13447
1-6	-0.61058	-0.7348	0.73956	0.6048		

(b)

(c)

Figure B.20: MATLAB output for bracket position replication errors; a). Plot visually comparing scanned and FaroArm measured bracket slot midpoint positions, b). In-plane global and local discrepancies for each tooth, c). Vertical discrepancies between adjacent teeth

Translation errors were solved the same way tooth movements were calculated, and rotational errors were solved in Excel using the bracket endpoints (P1 and P2) and solving for bracket and tooth rotations using Equations B.1 and B.2:

$$Bracket\ Rotation = \sin^{-1} \left( \frac{P2_z - P1_z}{\sqrt{(P2_x - P1_x)^2 + (P2_y - P1_y)^2 + (P2_z - P1_z)^2}} \right) \quad (B.1)$$

$$Tooth\ Rotation = \tan^{-1} \left( \frac{P2_x - P1_x}{P2_y - P1_y} \right) \quad (B.2)$$

The detailed replication error results for each patient arch analyzed in Chapter 3 is provided in Table B.3-Table B.9.

Table B.3: Translation and rotation replication errors for Patient 1 mandibular jig sets

<b>Replication Errors</b>		<b>Time 1</b>	<b>Time 2</b>	<b>Time 3</b>	<b>Time 4</b>
<b>Local X Dirn</b>	Range [mm]	0.01 - 0.82	0.00 - 1.05	0.02 - 0.87	0.10 - 1.27
	Avg $\pm$ Std.	0.52 $\pm$ 0.31	0.55 $\pm$ 0.33	0.53 $\pm$ 0.29	0.56 $\pm$ 0.37
	Dev [mm]				
<b>Local Y Dirn</b>	Range [mm]	0.01 - 0.72	0.04 - 0.57	0.05 - 0.68	0.01 - 0.88
	Avg $\pm$ Std.	0.38 $\pm$ 0.21	0.26 $\pm$ 0.21	0.42 $\pm$ 0.20	0.32 $\pm$ 0.26
	Dev [mm]				
<b>Local Z Dirn</b>	Range [mm]	0.02 - 0.43	0.01 - 0.42	0.00 - 0.42	0.00 - 0.51
	Avg $\pm$ Std.	0.19 $\pm$ 0.13	0.18 $\pm$ 0.16	0.13 $\pm$ 0.15	0.19 $\pm$ 0.20
	Dev [mm]				
<b>Bracket Rot</b>	Range [°]	0.05 - 6.53	0.19 - 4.25	0.39 - 5.55	0.18 - 7.27
	Avg $\pm$ Std.	2.51 $\pm$ 2.41	2.69 $\pm$ 1.43	2.10 $\pm$ 1.67	3.45 $\pm$ 2.24
	Dev [°]				
<b>Tooth Rot</b>	Range [°]	0.00 - 12.33	0.22 - 10.54	0.15 - 11.27	1.11 - 13.35
	Avg $\pm$ Std.	3.73 $\pm$ 3.47	3.70 $\pm$ 2.87	2.67 $\pm$ 2.91	4.78 $\pm$ 3.42
	Dev [°]				

Table B.4: Translation and rotation replication errors for Patient 2 mandibular jig sets

<b>Replication Errors</b>		<b>Time 1</b>	<b>Time 2</b>	<b>Time 3</b>
<b>Local X Dirn</b>	Range [mm]	0.23 – 1.07	0.13 – 0.83	0.00 – 0.96
	Avg ± Std. Dev [mm]	0.63 ± 0.26	0.55 ± 0.25	0.55 ± 0.30
<b>Local Y Dirn</b>	Range [mm]	0.06 – 0.94	0.01 – 0.89	0.04 – 0.92
	Avg ± Std. Dev [mm]	0.48 ± 0.29	0.43 ± 0.33	0.35 ± 0.35
<b>Local Z Dirn</b>	Range [mm]	0.02 – 0.45	0.01 – 0.51	0.00 – 0.33
	Avg ± Std. Dev [mm]	0.13 ± 0.12	0.17 ± 0.14	0.17 ± 0.12
<b>Bracket Rot</b>	Range [°]	0.10 – 15.69	0.01 – 7.60	0.91 – 7.68
	Avg ± Std. Dev [°]	4.51 ± 4.35	4.10 ± 2.50	3.84 ± 2.21
<b>Tooth Rot</b>	Range [°]	0.40 – 12.78	0.76 – 12.96	0.04 – 13.47
	Avg ± Std. Dev [°]	6.15 ± 3.46	5.16 ± 3.79	4.20 ± 3.93

Table B.5: Translation and rotation replication errors for Patient 2 maxillary jig sets

<b>Replication Errors</b>		<b>Time 1</b>	<b>Time 2</b>	<b>Time 3</b>	<b>Time 4</b>
<b>Local X Dirn</b>	Range [mm]	0.00 - 1.27	0.05 - 1.48	0.10 - 1.45	0.07 - 1.73
	Avg $\pm$ Std.	$0.64 \pm 0.42$	$0.65 \pm 0.53$	$0.70 \pm 0.45$	$0.61 \pm 0.52$
	Dev [mm]				
<b>Local Y Dirn</b>	Range [mm]	0.09 - 1.37	0.00 - 1.05	0.07 - 0.95	0.01 - 1.15
	Avg $\pm$ Std.	$0.66 \pm 0.33$	$0.36 \pm 0.32$	$0.39 \pm 0.33$	$0.71 \pm 0.39$
	Dev [mm]				
<b>Local Z Dirn</b>	Range [mm]	0.04 - 0.45	0.05 - 0.62	0.01 - 0.66	0.06 - 0.52
	Avg $\pm$ Std.	$0.23 \pm 0.14$	$0.25 \pm 0.16$	$0.25 \pm 0.19$	$0.29 \pm 0.14$
	Dev [mm]				
<b>Bracket Rot</b>	Range [°]	0.64 - 7.30	0.11 - 4.08	0.03 - 6.60	0.23 - 7.71
	Avg $\pm$ Std.	$3.97 \pm 2.32$	$2.54 \pm 1.28$	$3.11 \pm 2.26$	$3.21 \pm 2.37$
	Dev [°]				
<b>Tooth Rot</b>	Range [°]	4.00 - 12.31	4.66 - 12.70	4.50 - 13.19	0.49 - 17.04
	Avg $\pm$ Std.	$8.41 \pm 2.50$	$8.63 \pm 2.91$	$8.76 \pm 3.11$	$8.29 \pm 4.92$
	Dev [°]				

Table B.6: Translation and rotation replication errors for Patient 3 mandibular jig sets

<b>Replication Errors</b>		<b>Time 1</b>	<b>Time 2</b>	<b>Time 3</b>	<b>Time 4</b>
<b>Local X Dirn</b>	Range [mm]	0.30 - 1.44	0.19 - 1.35	0.08 - 1.18	0.09 - 1.14
	Avg $\pm$ Std.	$0.61 \pm 0.36$	$0.62 \pm 0.37$	$0.58 \pm 0.34$	$0.62 \pm 0.38$
	Dev [mm]				
<b>Local Y Dirn</b>	Range [mm]	0.01 - 0.82	0.25 - 0.87	0.07 - 0.74	0.07 - 1.02
	Avg $\pm$ Std.	$0.44 \pm 0.28$	$0.52 \pm 0.24$	$0.42 \pm 0.22$	$0.50 \pm 0.32$
	Dev [mm]				
<b>Local Z Dirn</b>	Range [mm]	0.00 - 0.56	0.05 - 0.60	0.03 - 0.60	0.04 - 0.60
	Avg $\pm$ Std.	$0.24 \pm 0.19$	$0.24 \pm 0.16$	$0.25 \pm 0.18$	$0.28 \pm 0.20$
	Dev [mm]				
<b>Bracket Rot</b>	Range [°]	0.41 - 6.61	0.10 - 8.03	0.24 - 5.77	0.03 - 7.19
	Avg $\pm$ Std.	$3.40 \pm 2.01$	$2.69 \pm 2.46$	$2.11 \pm 1.62$	$3.03 \pm 1.65$
	Dev [°]				
<b>Tooth Rot</b>	Range [°]	0.34 - 14.96	0.10 - 13.45	0.41 - 15.29	0.29 - 14.04
	Avg $\pm$ Std.	$6.31 \pm 4.85$	$5.95 \pm 5.10$	$6.59 \pm 4.60$	$6.34 \pm 4.92$
	Dev [°]				

Table B.7: Translation and rotation replication errors for Patient 3 maxillary jig sets

<b>Replication Errors</b>		<b>Time 1</b>	<b>Time 2</b>	<b>Time 3</b>	<b>Time 4</b>
<b>Local X Dirn</b>	Range [mm]	0.03 - 1.38	0.04 - 1.45	0.02 - 1.47	0.05 - 1.18
	Avg $\pm$ Std.	$0.65 \pm 0.38$	$0.64 \pm 0.41$	$0.58 \pm 0.40$	$0.62 \pm 0.39$
	Dev [mm]				
<b>Local Y Dirn</b>	Range [mm]	0.04 - 0.95	0.04 - 0.92	0.04 - 0.95	0.15 - 0.82
	Avg $\pm$ Std.	$0.40 \pm 0.25$	$0.48 \pm 0.29$	$0.47 \pm 0.30$	$0.45 \pm 0.23$
	Dev [mm]				
<b>Local Z Dirn</b>	Range [mm]	0.04 - 0.51	0.01 - 0.28	0.00 - 0.36	0.02 - 1.47
	Avg $\pm$ Std.	$0.19 \pm 0.16$	$0.14 \pm 0.09$	$0.16 \pm 0.11$	$0.15 \pm 0.09$
	Dev [mm]				
<b>Bracket Rot</b>	Range [°]	0.35 - 6.85	0.15 - 4.15	0.19 - 5.52	0.51 - 7.39
	Avg $\pm$ Std.	$2.58 \pm 2.39$	$2.27 \pm 1.18$	$2.54 \pm 1.90$	$2.68 \pm 2.06$
	Dev [°]				
<b>Tooth Rot</b>	Range [°]	0.76 - 13.91	0.42 - 19.42	1.02 - 11.00	0.48 - 14.17
	Avg $\pm$ Std.	$6.99 \pm 4.93$	$7.24 \pm 5.28$	$5.18 \pm 3.06$	$6.85 \pm 4.04$
	Dev [°]				

Table B.8: Translation and rotation replication errors for Patient 4 mandibular jig sets

<b>Replication Errors</b>		<b>Time 1</b>	<b>Time 2</b>	<b>Time 3</b>	<b>Time 4</b>
<b>Local X Dirn</b>	Range [mm]	0.25 - 1.27	0.02 - 1.22	0.05 - 1.30	0.03 - 1.16
	Avg $\pm$ Std. Dev [mm]	$0.70 \pm 0.33$	$0.68 \pm 0.34$	$0.56 \pm 0.41$	$0.57 \pm 0.45$
<b>Local Y Dirn</b>	Range [mm]	0.02 - 0.94	0.19 - 0.93	0.02 - 0.91	0.29 - 0.97
	Avg $\pm$ Std. Dev [mm]	$0.39 \pm 0.28$	$0.44 \pm 0.23$	$0.45 \pm 0.30$	$0.53 \pm 0.21$
<b>Local Z Dirn</b>	Range [mm]	0.07 - 0.40	0.01 - 0.60	0.00 - 0.35	0.02 - 0.40
	Avg $\pm$ Std. Dev [mm]	$0.25 \pm 0.12$	$0.20 \pm 0.16$	$0.18 \pm 0.11$	$0.16 \pm 0.12$
<b>Bracket Rot</b>	Range [°]	0.02 - 12.89	0.44 - 11.23	0.46 - 11.50	0.06 - 11.77
	Avg $\pm$ Std. Dev [°]	$4.51 \pm 4.35$	$4.28 \pm 3.16$	$3.25 \pm 3.08$	$3.56 \pm 3.36$
<b>Tooth Rot</b>	Range [°]	0.56 - 10.56	0.01 - 12.11	0.47 - 10.55	0.26 - 14.01
	Avg $\pm$ Std. Dev [°]	$4.34 \pm 4.92$	$3.98 \pm 3.98$	$4.11 \pm 3.54$	$4.01 \pm 4.50$

Table B.9: Translation and rotation replication errors for Patient 4 maxillary jig sets

<b>Replication Errors</b>		<b>Time 1</b>	<b>Time 2</b>	<b>Time 3</b>	<b>Time 4</b>
<b>Local X Dirn</b>	Range [mm]	0.08 - 1.05	0.02 - 0.99	0.03 - 0.89	0.04 - 1.16
	Avg $\pm$ Std. Dev [mm]	$0.55 \pm 0.29$	$0.59 \pm 0.29$	$0.61 \pm 0.39$	$0.56 \pm 0.35$
<b>Local Y Dirn</b>	Range [mm]	0.01 - 0.88	0.03 - 0.91	0.00 - 0.90	0.01 - 0.98
	Avg $\pm$ Std. Dev [mm]	$0.45 \pm 0.35$	$0.47 \pm 0.28$	$0.40 \pm 0.33$	$0.39 \pm 0.30$
<b>Local Z Dirn</b>	Range [mm]	0.00 - 0.45	0.02 - 0.28	0.01 - 0.23	0.00 - 0.31
	Avg $\pm$ Std. Dev [mm]	$0.19 \pm 0.16$	$0.14 \pm 0.10$	$0.12 \pm 0.07$	$0.12 \pm 0.09$
<b>Bracket Rot</b>	Range [°]	1.28 - 7.04	0.48 - 6.59	1.75 - 5.29	3.88 - 10.92
	Avg $\pm$ Std. Dev [°]	$3.33 \pm 1.84$	$3.85 \pm 1.93$	$3.53 \pm 1.24$	$3.01 \pm 1.54$
<b>Tooth Rot</b>	Range [°]	0.23 - 14.26	0.43 - 11.79	1.07 - 17.7	1.08 - 6.19
	Avg $\pm$ Std. Dev [°]	$7.21 \pm 3.74$	$5.43 \pm 3.37$	$6.90 \pm 4.28$	$6.84 \pm 2.74$

## Replication Error Code

This MATLAB script was created to evaluate translation errors in bracket position replication by comparing scanned positions with the FaroArm coordinate measurements. Results are provided with respect to the OSIM cantilever coordinate systems.

```
%% Replication Error Code
% Compares FaroArm measurements with the scanned patient positions
% Outputs errors in each direction and provided avg and Std Dev results
clf
clear
clc

%% PLOTTING 3D POINTS FROM EXCEL FILE
% Import patient excel file data
JigData = 'Jig Code - P4U - T4.xlsx'; %%CHANGE
T0 = readtable(JigData, 'Sheet', 'Slot Endpoints RAS', 'PreserveVariableNames', true);

% Import OSIM excel file data
T2 = readtable('OSIM Data.xlsx', 'Sheet', 'Neutral_new');
tooth_names = table2array(T2(1:12,1)); %Tooth names for data tips
Tooth_num = ['2-6'; '2-5'; '2-4'; '2-3'; '2-2'; '2-1'; '1-1'; '1-2'; '1-3'; '1-4'; '1-5'; '1-6'];

% x_translate is the distance that we want to move all patient points in X direction
x_translate = 33; % USER DEFINED

%z_min is the minimum bracket slot height
z_min = 7; % USER DEFINED

% Calculate bracket slot midpoint with endpoint values
% First put RAS coordinates into XYZ
[R1.R, R1.A, R1.S] = deal(table2array(T0(1:12,2)), table2array(T0(1:12,3)), table2array(T0(1:12,4)));
[R2.R, R2.A, R2.S] = deal(table2array(T0(1:12,5)), table2array(T0(1:12,6)), table2array(T0(1:12,7)));

% L is the midpoint between slot poixdnts, use for landmark
L.R = (R1.R + R2.R)/2;
L.A = (R1.A + R2.A)/2;
L.S = (R1.S + R2.S)/2;

% Convert RAS to XYZ System
L.X = L.A;
L.Y = L.R*-1;
L.Z = L.S;

% Level the Z-Coordinates of patient data with OSIM data
% Find minimum Z-Coord in patient data
min(L.Z)
% Subtract all Z-Coord with minimum Z-Coord
L.Z_inter = L.Z - min(L.Z);
% L.Z_inter = L.Z - 1.11812055303403; P3U T1
% Add the height of the bracket midpoint to all Z-Coord
L.Z_final = L.Z_inter + 128.5;
%L.Z_final = L.Z_inter + 130;

% trasnslate patient data in X direction
L.X_final = L.X - x_translate;
L.Y_final = L.Y;
```

```

% Plot Patient Points
point1 = plot3(L_X_final, L_Y_final, L_Z_final, '.', 'Color', 'black', 'MarkerSize', 25);
row = dataTipTextRow("Midpoint - Tooth", tooth_names);
point1.DataTipTemplate.DataTipRows(end+1) = row;
hold on

% Dealing with the bracket endpoints
R1_X = (R1.A);
R1_Y = (R1.R*-1);
R1_Z = (R1.S);

R2_X = (R2.A);
R2_Y = (R2.R*-1);
R2_Z = (R2.S);

% Level the data in the z-dirn
R1_Z_inter = R1_Z - min(L.S);
R2_Z_inter = R2_Z - min(L.S);
R1_Z_final = R1_Z_inter + 130;
R2_Z_final = R2_Z_inter + 130;

% Add x-translation
R1_X_final = R1_X - x_translate;
R2_X_final = R2_X - x_translate;

R1_Y_final = R1_Y;
R2_Y_final = R2_Y;

%% FARO Arm measurements
FaroCheck = 'P4U_T4_FaroArm_Msmts_Aug10.xlsx'; %% CHANGEEEEE
T7 = readtable(FaroCheck, 'Sheet', 'bracketmidpoint');
[F1_X, F1_Y, F1_Z] = deal(table2array(T7(1:12,2)), table2array(T7(1:12,3)), table2array(T7
(1:12,4)));
F1_Z_inter = F1_Z - min(F1_Z);
% F1_Z_inter = F1_Z - 145.393370379873; P3U T1
F1_Z_final = F1_Z_inter + 128.5;
%F1_Z_final = F1_Z_inter + 130;
point2 = plot3(F1_X, F1_Y, F1_Z_final, '.', 'Color', 'red', 'MarkerSize', 25);

%% Format Figure
% Format Figure with labels and title
xlabel('X [mm]'); ylabel('Y [mm]'); zlabel('Z [mm]')
title('Comparison of Patient Scan Data with Actual Replicated Data')
% Use vector to avoid all plotted points having legend entry
h = [point1(1); point2(1)];
% Label names according to order of plotting
legend(h, '3D Scan Bracket Midpoints', 'FARO Arm Bracket Midpoints')
zlim([100 150])
figure(2)
% Plot the endpoints on the same figure
point4 = plot3(R1_X_final, R1_Y_final, R1_Z_final, '.', 'Color', 'black', 'MarkerSize', 25);
hold on
point5 = plot3(R2_X_final, R2_Y_final, R2_Z_final, '.', 'Color', 'black', 'MarkerSize', 25);

T8 = readtable(FaroCheck, 'Sheet', 'Endpoints');
[End_X, End_Y, End_Z] = deal(table2array(T8(1:24,1)), table2array(T8(1:24,2)), table2array(T8
(1:24,3)));
point6 = plot3(End_X, End_Y, End_Z, '.', 'Color', 'red', 'MarkerSize', 25);

g = [point4(1); point6(1)];
% Label names according to order of plotting
legend(g, '3D Scan Bracket Endpoints', 'FARO Arm Bracket Endpoints')
xlabel('X [mm]'); ylabel('Y [mm]'); zlabel('Z [mm]')
title('Comparison of Patient Scan and Actual Replicated Endpoints')

%% CHECK DELTA X AND Y ERRORS (w.r.t global system)
Delta_x = F1_X - L_X_final;
Delta_y = F1_Y - L_Y_final;

```

```

A = table(tooth_names, Delta_x, Delta_y);
A.Properties.VariableNames = {'Tooth', 'Delta X', 'Delta Y'};
disp('Delta X & Y in the Global Coordinate System')
disp(A)

%% CHECK DELTA X AND Y ERRORS(w.r.t Local system)
theta = [-9,-18,-25,-33,-56,-79,-102,-130,-148,-156,-164,-169];
% Initialize variable K and 2 empty vectors for X and Y direction
K = 1;
L_Vec_X = [];
L_Vec_Y = [];
% Define how many teeth are considered
Num_teeth = 12;

% While loop to solve for X and Y changes with respect to local bracket
% coordinate systems
while K <= Num_teeth
    % Solving for changes in X-dirn
    % Assign to empty vector
    L_Vec_X(K) = Delta_x(K)*cosd(theta(K)) + Delta_y(K)*sind(theta(K));

    % Solving for changes in Y-dirn
    % Assign to empty vector
    L_Vec_Y(K) = -Delta_x(K)*sind(theta(K)) + Delta_y(K)*cosd(theta(K));

    K = K + 1;
end

% Transpose vectors to be vertical for putting into table below
L_T_Delta_X_new = transpose(L_Vec_X);
L_T_Delta_Y_new = transpose(L_Vec_Y);

% Put each column of Delta values back into table for display
A1 = table(tooth_names, L_T_Delta_X_new, L_T_Delta_Y_new);
A1.Properties.VariableNames = {'Tooth', 'Delta X', 'Delta Y'};
disp('Delta X & Y in Local Coordinate System')
disp(A1)

%% Solve for magnitude of error
Mag = sqrt(L_Vec_X.^2 + L_Vec_Y.^2);

%% CHECK DELTA Z ERRORS
% First find the difference in heights between adjacent points for both the
% scan and FaroArm measurements separately
for i = 1:11
    Z_scan(i) = L_Z_final(i) - L_Z_final(i+1)
    Z_faro(i) = F1_Z_final(i) - F1_Z_final(i+1)
end

Delta_Z = Z_scan - Z_faro;

%% Display final results in table
A2 = table(Tooth_num, Delta_x, Delta_y, L_T_Delta_X_new, L_T_Delta_Y_new, transpose(Mag));
A2.Properties.VariableNames = {'Tooth', 'Global Delta X', 'Global Delta Y', 'Local Delta X',
    'Local Delta Y', 'Magnitude'};
disp(A2)

Tooth_num_Z = ['2-6 to 2-5'; '2-5 to 2-4'; '2-4 to 2-3'; '2-3 to 2-2'; '2-2 to 2-1'; '2-1 to
    1-1'; '1-1 to 1-2'; '1-2 to 1-3'; '1-3 to 1-4'; '1-4 to 1-5'; '1-5 to 1-6'];
A3 = table(Tooth_num_Z, transpose(Delta_Z));
A3.Properties.VariableNames = {'Tooth', 'Delta Z'};
disp(A3)

% Scale of figure
zlim([100 150])

%% Average & Std Deviation calculations for the in-plane and out-of-plane errors
inplane_avg = mean(abs(Mag))

```

```
inplane_stdev = std(abs(Mag))

outplane_avg = mean(abs(Delta_Z))
outplane_stdev = std(abs(Delta_Z))

disp(" average & st.dev x-dirn error")
x_avg = mean(abs(L_T_Delta_X_new))
x_stdev = std(abs(L_T_Delta_X_new))

disp(" average & st.dev y-dirn error")
y_avg = mean(abs(L_T_Delta_Y_new))
y_stdev = std(abs(L_T_Delta_Y_new))
```

## B.4 Rectifying Jig Position Errors

### *Sensitivity Analysis*

Prior to the experimentation presented in Chapter 3, a sensitivity analysis was completed with the objective of understanding the changes in measured forces when a tooth was positioned out of alignment. In relation to the experiments conducted in Chapter 3, this analysis helped clarify how the force results would be affected by replication errors. The analysis was carried out with a set of mandibular metal teeth with Carrick SLX brackets (already bonded on the available metal teeth) and 0.014" and 0.016" sized Damon CuNiTi archwires (Figure B.21).

The canine (1-3), incisor (2-1), and second premolar (2-5) were individually displaced 0.5 mm in the buccal direction from the neutral position in 0.1 mm increments, and then moved back lingually to the neutral position using the same increments. For efficiency purposes, the outlined tooth movements were achieved within a single experiment in randomized order for each sample wire. A total of five sample wires were tested per size, and five experiments were performed for each wire. The average force (Y-Direction) experienced by the three teeth during the maximum displacement is provided in Table B.10 for each wire size. Additionally, the Y-directional force during all phases of movement was plotted for the three teeth as provided in Figure B.22.

Table B.10: Average measured force in Y-direction at 0.5 mm buccal displacement of canine, central incisor, and second premolar teeth during use of 0.014" and 0.016" archwire

Tooth	0.014" Wire	0.016" Wire
<b>Tooth 1-3 (Canine)</b>	0.589 N $\pm$ 0.153 N	1.043 N $\pm$ 0.085 N
<b>Tooth 2-1 (Central Incisor)</b>	0.353 N $\pm$ 0.031 N	0.594 N $\pm$ 0.084 N
<b>Tooth 2-5 (2nd Premolar)</b>	1.014 N $\pm$ 0.151 N	1.460 N $\pm$ 0.110 N

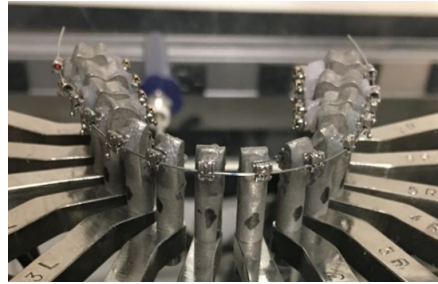


Figure B.21: Metal mandibular teeth used in sensitivity analysis experiments with wire inserted through brackets

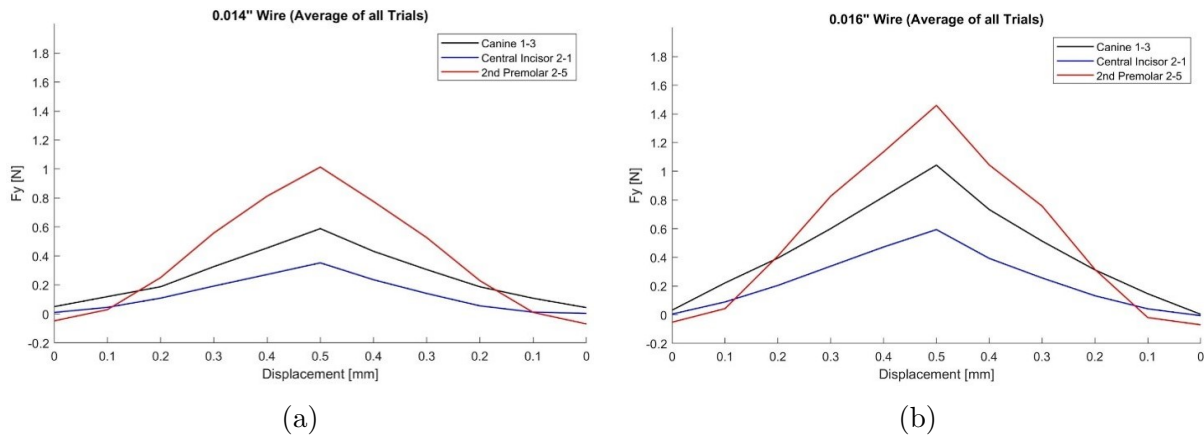


Figure B.22: Average Y-directional force results at each 0.1 mm displacement increment for canine, central incisor, and second premolar teeth; a). Results for 0.014" archwires, b). Results for 0.016" archwires

Based on the results, the force magnitudes retrieved for the 0.016" archwire were larger than that collected for the 0.014" archwire. For both archwire sizes, the second premolar experienced the greatest lingual force when displaced, followed by the canine, and then the central incisor. When a tooth was displaced in the buccal direction while keeping all

other teeth in the neutral position, there was also an observable and clinically relevant force generated. This was observed at roughly 0.2 mm displacement for the 0.014” archwire and roughly 0.1 mm displacement for the 0.016” archwire. In the larger context of the experimental work, the sensitivity analysis results show the need to manually fix bracket position discrepancies with the micrometers where possible, as small displacements clearly affect the measured force.

### ***Updating Micrometer Positions before Experimentation***

Before performing experiments for each jig set, the micrometers were used to adjust the jig positions to help mitigate errors in the local Y-direction and the vertical direction. Calculated replication discrepancies from MATLAB were pasted into an Excel file and added to the original micrometer positions to update vertical and horizontal micrometers positions (Figure B.23). These updated positions were copied into the “Current Micrometers” section of the OSIM software to move the micrometers (Figure B.24). Remaining interference between the mounted jigs was eliminated by filing the jigs.

Updated Vertical  
Micrometer Positions

Updated Horizontal  
Micrometer Positions

Vertical				Horizontal			
All measurements in mm							
Tooth	OG	MVMT	NEW	Tooth	OG	MVMT	NEW
2-6	5	-0.546	4.454	2-6	2	0.447	2.447
2-5	5	-0.116	4.884	2-5	2	0.436	2.436
2-4	5	-0.355	4.645	2-4	2	0.370	2.370
2-3	5	-0.178	4.822	2-3	2	0.008	2.008
2-2	5	0.208	5.208	2-2	2	0.136	2.136
2-1	5	0.074	5.074	2-1	2	0.248	2.248
1-1	5	0.056	5.056	1-1	2	0.450	2.450
1-2	5	0.189	5.189	1-2	2	0.198	2.198
1-3	5	0.000	5.000	1-3	2	0.310	2.310
1-4	5	-0.158	4.842	1-4	2	0.620	2.620
1-5	5	-0.196	4.804	1-5	2	0.725	2.725
1-6	5	-0.330	4.670	1-6	2	0.605	2.605

INPUTS OF USER		Z_Scan	Z_Faro	Vertical Discrepancy (ZDirn)	Horizontal Discrepancy (YDirn)	For the OG position:
OG Vertical position	5	131.173	131.719	-0.546	0.4471882854	
OG Horizontal position	2	129.492	129.608	-0.116	0.4360189743	
		130.008	130.363	-0.355	0.3696097109	
		129.791	129.968	-0.178	0.008269249754	
		130.558	130.350	0.208	0.1356673834	
		129.403	129.329	0.074	0.2479128758	
		130.719	130.663	0.056	0.4503653231	
		128.703	128.515	0.189	0.1978148662	
		128.500	128.500	0.000	0.30973769	

Pasted MATLAB Results

Figure B.23: Excel sheet for calculating updated micrometer positions for a patient jig set

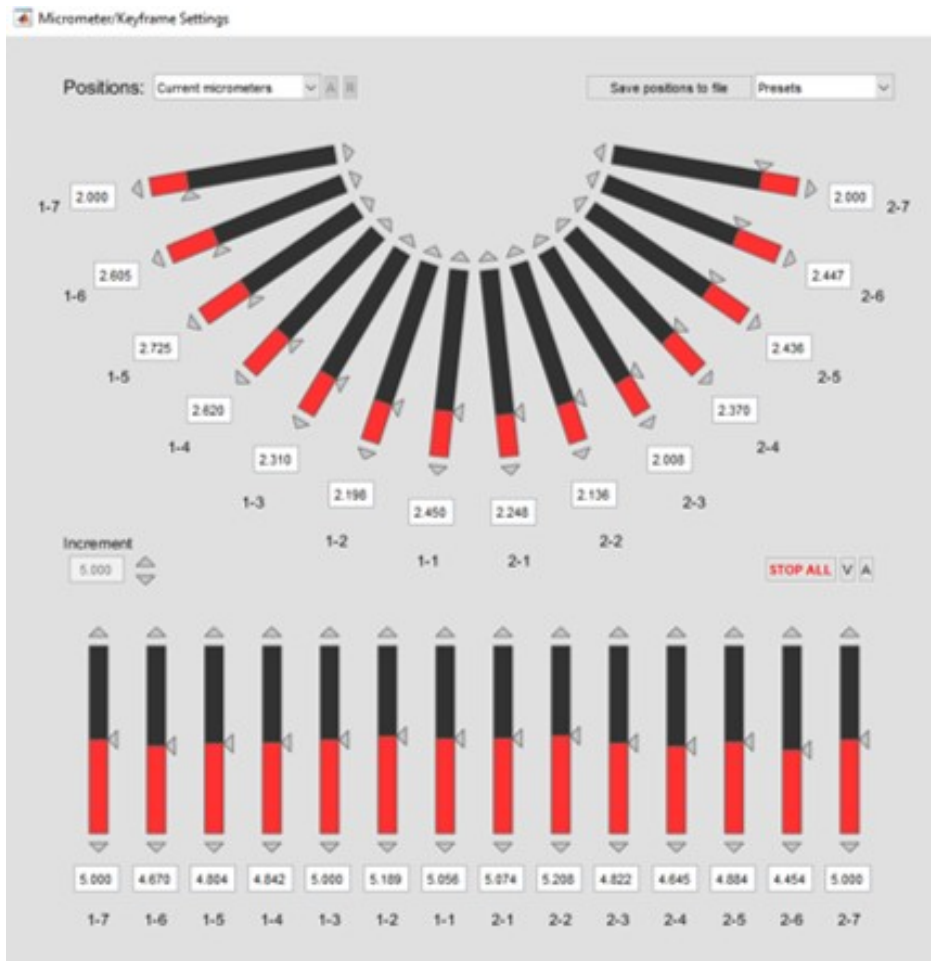


Figure B.24: Micrometer setting user interface in OSIM software for manually updating micrometer positions prior to experimentation